

Abstracta

Ano XVI - N. 06

Dez-12



Número Especial Comemorativo de 15 anos!

Trabalhos Publicados

Outubro à Dezembro 2012 - [P169-12](#) à [P210-12](#)

Proceedings

Outubro à Dezembro 2012 - [P211-12](#)

Os dez trabalhos mais citados por ano nos últimos 15 anos.

Gráfico com número de artigos e citações da produção IFGW nos últimos 15 anos.

Gráfico com a média do Fator de Impacto - JCR das publicações IFGW de 2000 a 2011.

Trabalhos Publicados

[P169-12] “a-SiOx < Er > active photonic crystal resonator membrane fabricated by focused Ga⁺ ion beam”

Figueira, D. S. L.*; Barea, L. A. M.*; Vallini, F.*; Jarschel, P. F.*; Lang, R.*; Frateschi, N. C.*

We have fabricated thin erbium-doped amorphous silicon suboxide (a-SiOx < Er >) photonic crystal membrane using focused gallium ion beam (FIB). The photonic crystal is composed of a hexagonal lattice with a H1 defect supporting two quasi-doubly degenerate second order dipole states. 2-D simulation was used for the design of the structure and full 3-D FDTD (Finite-Difference Time-Domain) numerical simulations were performed for a complete analysis of the structure. The simulation predicted a quality factor for the structure of $Q = 350$ with a spontaneous emission enhancement of 7. Micro photoluminescence measurements showed an integrated emission intensity enhancement of similar to 2 times with a $Q = 130$. We show that the discrepancy between simulation and measurement is due to the conical shape of the photonic crystal holes and the optical losses induced by FIB milling.

Optics Express 20[17], 18772-18783, 2012.

[P170-12] “Accretion of Nonminimally Coupled Generalized Chaplygin gas into Black Holes”

Rodrigues, M. G.*; Bernardini, A. E.

The mass evolution of Schwarzschild black holes by the absorption of scalar fields is investigated in the scenario of the generalized Chaplygin gas (GCG). The GCG works as a unification picture of dark matter plus dark energy that naturally accelerates the expansion of the Universe. Through elements of the quasi-stationary approach, we consider the mass evolution of Schwarzschild black holes accreted by nonminimally coupled cosmological scalar fields reproducing the dynamics of the GCG. As a scalar field nonminimally coupled to the metrics, such an exotic content has been interconnected with accreting black holes. The black hole increasing masses by the absorption of the gas reflects some consistence of the accretion mechanism with the hypothesis of the primordial origin of supermassive black holes. Our results effectively show that the nonminimal coupling with the GCG dark sector accelerates the increasing of black hole masses. Meanwhile some exotic features can also be depicted for specific ranges of the nonminimal coupling in which the GCG dynamics is substantially modified.

International Journal of Modern Physics D 21[9], 1250075, 2012.

[P171-12] “Activation of HMDSO Thin Films With Low Pressure Argon Plasma and Vacuum Ultraviolet Radiation”

Garcia-Perez, T.; Rodriguez, E.*; Bittencourt, E.; Jova, Z.

Polymeric surfaces obtained by chemical vapor deposition of HMDSO on aluminum plates using plasma were modified by means of low pressure Argon plasma and vacuum ultraviolet radiation (VUV). The polymeric surface was directly exposed to the plasma -which also acted as a vacuum ultraviolet radiation source- at different conditions. An important contribution of the VUV radiation component in surface modification was observed. The surface free-energy, the chemical composition, and the morphology of the films were determined by contact angle measurement, FTIR spectroscopy, and SEM. It was observed that the action of VUV radiation inside de Argon plasma was responsible for more than 45% of the increase of surface freeenergy, and that the influence of VUV radiation on surface free-energy varied significantly as consequence of different exposure times.

Latin American Appied Research 42[1], 19-25, 2012.

[P172-12] “Anomalous metamagnetic-like transition in a FeRh/Fe3Pt interface occurring at T approximate to 120 K in the field-cooled-cooling curves for low magnetic fields”

Salem-Sugui, S.; Alvarenga, A. D.; Noce, R. D.; Guimaraes, R. B.; Mejia, C. S.; Salim, H.; Gandra, F. G.*

We report on the magnetic properties of a special configuration of a FeRh thin film. An anomalous behavior on the magnetisation vs. temperature was observed when low magnetic fields are applied in the plane of a thin layer of FeRh deposited on ordered Fe3Pt. The anomalous effect resembles a metamagnetic transition and occur only in the field-cooled-cooling magnetisation curve at temperatures near 120 K in samples without any heat treatment.

AIP Advances 2[3], 032168, 2012.

[P173-12] “Chemistry and Atomic Distortion at the Surface of an Epitaxial BaTiO3 Thin Film after Dissociative Adsorption of Water”

Wang, J. L.; Gaillard, F.; Pancotti, A.*; Gautier, B.; Niu, G.; Vilquin, B.; Pillard, V.; Rodrigues, G. L. M. P.; Barrett, N.

We present a study of the atomic and chemical structure of the surface of a fully strained, TiO2-terminated, ferroelectric BaTiO3 (BTO) (001) epitaxial film on a SrTiO3 substrate after controlled exposure to water. The epitaxial quality was checked by atomic force microscopy and X-ray diffraction. Quantitative low-energy electron diffraction compared with multiple scattering simulations was used to measure the structure of the first few atomic layers of BTO surface. The surface chemistry was investigated using high-resolution X-ray photoelectron spectroscopy. Finally, temperature-programmed desorption measured the desorption energies. We find that water undergoes mainly dissociative adsorption on the polarized BTO(001) surface. There are two competing sites for dissociative adsorption: oxygen vacancies and on-top Ti surface lattice atoms. The Ti on-top site is the dominant site for OH- chemisorption. One fifth of the surface Ti atoms bind to OH-. The concentration of surface oxygen vacancies acts mainly to favor initial physisorption. Before exposure to water, the outward pointing polarization in the BTO film is stabilized by atomic rumpling in the TiO2 termination layer. After exposure to water, the chemisorbed OH- species provide the screening, inverting the surface dipole layer and stabilizing the bulk polarization. Molecular adsorption is observed only for high water coverage.

Journal of Physical Chemistry C 116[41], 21802-21809, 2012.

[P174-12] “Colossal intrinsic magnetoelectric effect in Pb(Fe2/3W1/3)(0.83)Ti0.17O3”

Fraygola, B.; Coelho, A. A.*; Garcia, D.; Eiras, J. A.

Dielectric and magnetic properties were investigated in Pb(Fe2/3W1/3)(0.83)Ti0.17O3 ceramics. The dielectric constant in these samples exhibits colossal changes at the magnetic ordering temperature under the presence of bias external electric fields, which presents a close connection with magnetoelectrics effects (ME), confirming the possibility to control magnetic proprieties with electric fields. The ferroelectromagnetoelastic coefficient was determined from the dielectric response as a function of the electric field. The analysis of magnetic and dielectric susceptibilities based on the Landau-Devonshire thermodynamic formalisms indicates that the ME effects is a contribution of intrinsic ME coupling and a field dependent term.

Applied Physics Letters 101[9], 092903, 2012.

[P175-12] “Effect of a GaAsP Shell on the Optical Properties of Self-Catalyzed GaAs Nanowires Grown on Silicon”

Couto, O. D. D.*; Sercombe, D.; Puebla, J.; Otubo, L.; Luxmoore, I. J.; Sich, M.; Elliott, T. J.; Chekhovich, E. A.; Wilson, L. R.; Skolnick, M. S.; Liu, H. Y.; Tartakovskii, A. I.

We realize the growth of self-catalyzed core-shell GaAs/GaAsP nanowires (NWs) on Si substrates using molecular-beam epitaxy. Transmission electron microscopy of single GaAs/GaAsP NWs demonstrates their high crystal quality and shows domination of the GaAs zinc-blende phase. Using continuous-wave and time-resolved photoluminescence (PL), we make a detailed comparison with uncapped GaAs NWs to emphasize the effect of the GaAsP capping in suppressing the nonradiative surface states. Significant PL enhancement in the core-shell structures exceeding 3 orders of magnitude at 10 K is observed; in uncapped NWs PL is quenched at 60 K, whereas single core-shell GaAs/GaAsP structures exhibit bright emission even at room temperature. From analysis of the PL temperature dependence in both types of NW we are able to determine the main carrier escape mechanisms leading to the PL quench.

Nano Letters 12[10], 5269-5274, 2012.

[P176-12] “Evolution of Eu²⁺ spin dynamics in Ba_{1-x}Eu_xFe₂As₂”

Rosa, P. F. S.*; Adriano, C.*; Iwamoto, W.*; Garitezi, T. M.*; Grant, T.; Fisk, Z.; Pagliuso, P. G.*

Single crystals of Ba_{1-x}Eu_xFe₂As₂ were studied by magnetic susceptibility, heat capacity, resistivity, and electron spin resonance (ESR) measurements. Spin-density wave (at T-SDW) and antiferromagnetic (at T-N) phase transitions were mapped as a function of x. For x >= 0.2, we found a single Eu²⁺ ESR Dysonian line that presents an isotropic linear increase (Korringa) of its linewidth (ΔH) above T-SDW which systematically decreases with decreasing x. In contrast, for a critical concentration x(c) (0.10 < x(c) < 0.20), ΔH decreases with increasing T, suggesting a distinct relaxation process that we associate with a Eu²⁺ Kondo single impurity regime. The Korringa rate suppression towards the Ba-rich compounds is claimed to be due to the reduction of the q-dependent exchange interaction between the Eu²⁺ f electrons and the conduction electrons, which is likely associated with an increasing of localization of Fe d electrons. This result may help the understanding of the SDW phase suppression (that can lead to superconductivity) in this class of materials.

Physical Review B 86[16], 165131, 2012.

[P177-12] “Exact dynamics of single-qubit-gate fidelities under the measurement-based quantum computation scheme”

Arruda, L. G. E.; Fanchini, F. F.; Napolitano, R. D. J.; Hornos, J. E. M.; Caldeira, A. O.*

Measurement-based quantum computation is an efficient model to perform universal computation. Nevertheless, theoretical questions have been raised, mainly with respect to realistic noise conditions. In order to shed some light on this issue, we evaluate the exact dynamics of some single-qubit-gate fidelities using the measurement-based quantum computation scheme when the qubits which are used as a resource interact with a common dephasing environment. We report a necessary condition for the fidelity dynamics of a general pure N-qubit state, interacting with this type of error channel, to present an oscillatory behavior, and we show that for the initial canonical cluster state, the fidelity oscillates as a function of time. This state fidelity oscillatory behavior brings significant variations to the values of the computational results of a generic gate acting on that state depending on the instants we choose to apply our set of projective measurements.

As we shall see, considering some specific gates that are frequently found in the literature, the fast application of the set of projective measurements does not necessarily imply high gate fidelity, and likewise the slow application thereof does not necessarily imply low gate fidelity. Our condition for the occurrence of the fidelity oscillatory behavior shows that the oscillation presented by the cluster state is due exclusively to its initial geometry. Other states that can be used as resources for measurement-based quantum computation can present the same initial geometrical condition. Therefore, it is very important for the present scheme to know when the fidelity of a particular resource state will oscillate in time and, if this is the case, what are the best times to perform the measurements.

Physical Review A 86[4], 042326, 2012.

[P178-12] “Finite-momentum condensate of magnetic excitons in a bilayer quantum Hall system”

Doretto, R. L.; Smith, C. M.; Caldeira, A. O.*

We study the bilayer quantum Hall system at total filling factor $\nu(T) = 1$ within a bosonization formalism which allows us to approximately treat the magnetic exciton as a boson. We show that in the region where the distance between the two layers is comparable to the magnetic length, the ground state of the system can be seen as a finite-momentum condensate of magnetic excitons provided that the excitation spectrum is gapped. We analyze the stability of such a phase within the Bogoliubov approximation first assuming that only one momentum Q is macroscopically occupied and later we consider the same situation for two modes $\pm Q$. We find strong evidences that a first-order quantum phase transition at small interlayer separation takes place from a zero-momentum condensate phase, which corresponds to Halperin 111 state, to a finite-momentum condensate of magnetic excitons.

Physical Review B 86[3], 035326, 2012.

[P179-12] “Fröhlich Condensate: Emergence of Synergetic Dissipative Structures in Information Processing Biological and Condensed Matter Systems”

Vasconcellos, A. R.*; Vannucchi, F. S.; Mascarenhas, S.; Luzzi, R.*

We consider the case of a peculiar complex behavior in open boson systems sufficiently away from equilibrium, having relevance in the functioning of information-processing biological and condensed matter systems. This is the so-called Fröhlich-Bose-Einstein condensation, a self-organizing-synergetic dissipative structure, a phenomenon apparently working in biological processes and present in several cases of systems of boson-like quasi-particles in condensed inorganic matter. Emphasis is centered on the quantum-mechanical-statistical irreversible thermodynamics of these open systems, and the informational characteristics of the phenomena.

Information 3[4], 601-620, 2012.

[P180-12] “General derivation of the Green’s functions for the atomic approach of the Anderson model: application to a single electron transistor (SET)”

Foglio, M. E.*; Lobo, T.; Figueira, M. S.

We consider the cumulant expansion of the periodic Anderson model (PAM) in the case of a finite electronic correlation U,

employing the hybridization as perturbation, and obtain a formal expression of the exact one-electron Green's function (GF). This expression contains effective cumulants that are as difficult to calculate as the original GF, and the atomic approach consists in substituting the effective cumulants by the ones that correspond to the atomic case, namely by taking a conduction band of zeroth width and local hybridization. In a previous work (T. Lobo, M. S. Figueira, and M. E. Foglio, *Nanotechnology* 21, 274007 (2010)) we developed the atomic approach by considering only one variational parameter that is used to adjust the correct height of the Kondo peak by imposing the satisfaction of the Friedel sum rule. To obtain the correct width of the Kondo peak in the present work, we consider an additional variational parameter that guarantees this quantity. The two constraints now imposed on the formalism are the satisfaction of the Friedel sum rule and the correct Kondo temperature. In the first part of the work, we present a general derivation of the method for the single impurity Anderson model (SIAM), and we calculate several density of states representative of the Kondo regime for finite correlation U , including the symmetrical case. In the second part, we apply the method to study the electronic transport through a quantum dot (QD) embedded in a quantum wire (QW), which is realized experimentally by a single electron transistor (SET). We calculate the conductance of the SET and obtain a good agreement with available experimental and theoretical results.

AIP Advances 2[3], 032139, 2012.

[P181-12] "Generation of quaternary-amplitude microwave signals by using a new optical heterodyne technique"

Villena, A. T. P.; Cerqueira, S. A.; Abbade, M. L.; Hernandez-Figueroa, H. E.; Fragnito, H. L.*

We propose and experimentally investigate a new technique, based on optical heterodyne generation, which converts two optical binary amplitude-shift keyed (2-ASK) into a single microwave quaternary ASK (4-ASK) one. Results show that 4-ASK signals are properly generated even when the 2-ASK signals are propagated through 40 km optical links from a geographically distributed optical network under real conditions of temperature, pressure, humidity, and wind.

Microwave and Optical Technology Letters 54[12], 2738-2743, 2012.

[P182-12] "High energy sideband on the magnetic polaron related luminescence in EuTe"

Heredia, E.; Motisuke, P.; Rappl, P. H. D.; Brasil, M. J. S. P.*; Iikawa, F.*

We investigated the near band gap luminescence of EuTe thin films grown by molecular beam epitaxy, using excitation intensities up to 2×10^5 W/cm². Besides the previously reported high energy emissions MX1 and MX2, we observed an additional emission band at higher energies. This higher-energy band is only detected when high excitation intensities, over 2 kW/cm², are used. With increasing externally applied magnetic field, this additional emission band shifts to lower energies at a rate even higher than the MX1. The two bands, however, have different temperature dependences and decay times, suggesting that distinct electronic states are involved in their emission.

Applied Physics Letters 101[9], 092108, 2012.

[P183-12] "High-temperature superconductivity from realistic Coulomb and Frohlich interactions"

Alexandrov, A. S.*; Samson, J. H.; Sica, G.

In recent years ample experimental evidence has shown that charge carriers in high-temperature superconductors are strongly correlated but also coupled with lattice vibrations (phonons), signalling that the true origin of high-T_c superconductivity can only be found in a proper combination of Coulomb and electron-phonon interactions. On this basis, we propose and study a model for high-T_c superconductivity which accounts for realistic Coulomb repulsion, strong electron-phonon (Frohlich) interaction and residual on-site (Hubbard-(U) over tilde) correlations without any ad hoc assumptions on their relative strength and interaction range. In the framework of this model, which exhibits a phase transition to a superconducting state with a critical temperature T_c well in excess of 100 K, we emphasize the role of (U) over tilde as the driving parameter for a BEC/BCS crossover. Our model lays a microscopic foundation for the polaron-bipolaron theory of superconductivity. We argue that the high-T_c phenomenon originates in competing Coulomb and Frohlich interactions beyond the conventional BCS description.

EPL 100[1], 17011, 2012.

[P184-12] "Host-parasitoid persistence over variable spatio-temporally susceptible habitats: bottom-up effects of ephemeral resources"

Reigada, C.*; de Aguiar, M. A. M.*

We experimentally and theoretically investigated the persistence of hosts and parasitoids interacting in a metapopulation structure consisting of ephemeral local patches (MELPs). We used a hostparasitoid system consisting of necrophagous Diptera species and their pupal parasitoids. The basal resources used by the host species were assumed to be ephemeral, supporting only one generation of individuals before completely disappearing from the environment. We experimentally measured the hostparasitoid persistence and the effects of local demographic processes in two scenarios: 1) constant occurrence of basal resources at a single site (no dispersion or colonization of other sites) and 2) variable occurrence of basal resources between two sites (colonization of a new patch requiring species dispersal). The experimental setup and findings were then formalized into a mathematical model describing the interaction dynamics in a MELP structure. We evaluated the contribution of several factors to the hostparasitoid coexistence, such as resource allocation probability (probability of resource appearance in a site), variation in resource size and number of sites available to receive resources in the MELP. We found that demographic fluctuations and environmental stochasticity affected the density of migrants, patch habitat connectivity, persistence and spatial distribution of interacting species.

Oikos 121[10], 1665-1679, 2012.

[P185-12] "Implementation and performance investigation of radio-over-fiber systems in wireless sensor networks"

Lona, D. G.*; Assumpcao, R. M.; Branquinho, O. C.; Abbade, M. L. F.; Hernandez-Figueroa, H. E.*; Sodre, A. C.

We report the performance investigation and implementation of four different radio-over-fiber (ROF) systems as backhaul for wireless sensor networks based on frequency shift keying modulation at 915 MHz. Its applicability was experimentally verified as a function of packet error rate, received signal strength indicator, and system reach. Furthermore, a performance noise analysis was carried out by taking into account the optical transmitter and receiver parameters,

This is a preliminary study in which we evaluated NAA and NAAG changes during a visual stimulation experiment using functional MRS. The paradigm used consisted of a rest period (5 min and 20 s), followed by a stimulation period (10 min and 40 s) and another rest period (10 min and 40 s). MRS from 17 healthy subjects were acquired at 3T with TR/TE = 2000/288 ms. Spectra were averaged over subjects and quantified with LCModel. The main outcomes were that NAA concentration decreased by about 20% with the stimulus, while the concentration of NAAG concomitantly increased by about 200%. Such variations fall into models for the energy metabolism underlying neuronal activation that point to NAAG as being responsible for the hyperemic vascular response that causes the BOLD signal. They also agree with the fact that NAAG and NAA are present in the brain at a ratio of about 1: 10, and with the fact that the only known metabolic pathway for NAAG synthesis is from NAA and glutamate.

Brazilian Journal of Medical and Biological Research 45[11], 1031-1036, 2012.

[P191-12] “Nanosized precipitates in H13 tool steel low temperature plasma nitriding”

Zagonel, L. F.*; Bettini, J.; Basso, R. L. O.*; Paredez, P.*; Pinto, H.; Lepienski, C. M.; Alvarez, F.*

A comprehensive study of pulsed nitriding in AISI H13 tool steel at low temperature (400 degrees C) is reported for several durations. X-ray diffraction results reveal that a nitrogen enriched compound (epsilon-Fe₂-3N, iron nitride) builds up on the surface within the first process hour despite the low process temperature. Beneath the surface, X-ray Wavelength Dispersive Spectroscopy (WDS) in a Scanning Electron Microscope (SEM) indicates relatively higher nitrogen concentrations (up to 12 at.%) within the diffusion layer while microscopic nitrides are not formed and existing carbides are not dissolved. Moreover, in the diffusion layer, nitrogen is found to be dispersed in the matrix and forming nanosized precipitates. The small coherent precipitates are observed by High-Resolution Transmission Electron Microscopy (HR-TEM) while the presence of nitrogen is confirmed by electron energy loss spectroscopy (EELS). Hardness tests show that the material hardness increases linearly with the nitrogen concentration, reaching up to 14.5 GPa in the surface while the Young Modulus remains essentially unaffected. Indeed, the original steel microstructure is well preserved even in the nitrogen diffusion layer. Nitrogen profiles show a case depth of about similar to 43 μm after nine hours of nitriding process. These results indicate that pulsed plasma nitriding is highly efficient even at such low temperatures and that at this process temperature it is possible to form thick and hard nitrided layers with satisfactory mechanical properties. This process can be particularly interesting to enhance the surface hardness of tool steels without exposing the workpiece to high temperatures and altering its bulk microstructure.

Surface & Coatings Technology 207, 72-78, 2012.

[P192-12] “Numerical and experimental analysis of polarization properties from hybrid PCFs across different photonic bandgaps”

Cerqueira, S. A.; do Nascimento, A. R.; Franco, M. A. R.; de Oliveira, I.; Serrao, V. A.; Fragnito, H. L.*

This work presents a numerical and experimental characterization of polarization properties from hybrid photonic crystal fibers (hybrid PCFs or HPCFs) across different bandgaps. Very high extinction ratio over at least three wide bands and single-mode and single-polarization operation over more than 320 nm have been obtained by using only one fiber. Furthermore, it is reported, for the first time, a multi- and broadband fiber-based optical polarizer.

Numerical simulations and experiments of modal, birefringence and polarization properties have been carried out to demonstrate the remarkable performance of the proposed device.

Optical Fiber Technology 18[6], 462-469, 2012.

[P193-12] “Optical Biomarkers of Serous and Mucinous Human Ovarian Tumor Assessed with Nonlinear Optics Microscopies”

Adur, J.*; Pelegati, V. B.*; de Thomaz, A. A.*; Baratti, M. O.*; Almeida, D. B.*; Andrade, L. A. L. A.; Bottcher-Luiz, F.; Carvalho, H. F.; Cesar, C. L.*

Background: Nonlinear optical (NLO) microscopy techniques have potential to improve the early detection of epithelial ovarian cancer. In this study we showed that multimodal NLO microscopies, including two-photon excitation fluorescence (TPEF), second-harmonic generation (SHG), third-harmonic generation (THG) and fluorescence lifetime imaging microscopy (FLIM) can detect morphological and metabolic changes associated with ovarian cancer progression. Methodology/ Principal Findings: We obtained strong TPEF + SHG + THG signals from fixed samples stained with Hematoxylin & Eosin (H&E) and robust FLIM signal from fixed unstained samples. Particularly, we imaged 34 ovarian biopsies from different patients (median age, 49 years) including 5 normal ovarian tissue, 18 serous tumors and 11 mucinous tumors with the multimodal NLO platform developed in our laboratory. We have been able to distinguish adenomas, borderline, and adenocarcinomas specimens. Using a complete set of scoring methods we found significant differences in the content, distribution and organization of collagen fibrils in the stroma as well as in the morphology and fluorescence lifetime from epithelial ovarian cells. Conclusions/Significance: NLO microscopes provide complementary information about tissue microstructure, showing distinctive patterns for serous and mucinous ovarian tumors. The results provide a basis to interpret future NLO images of ovarian tissue and lay the foundation for future in vivo optical evaluation of premature ovarian lesions.

Plos One 7[10], e47007, 2012.

[P194-12] “Optical emission of InAs nanowires”

Moller, M.; de Lima, M. M.; Cantarero, A.; Chiamonte, T.*; Cotta, M. A.*; Iikawa, F.*

Wurtzite InAs nanowire samples grown by chemical beam epitaxy have been analyzed by photoluminescence spectroscopy. The nanowires exhibit two main optical emission bands at low temperatures. They are attributed to the recombination of carriers in quantum well structures, formed by zincblende-wurtzite alternating layers, and to the donor-acceptor pair. The blue-shift observed in the former emission band when the excitation power is increased is in good agreement with the type-II band alignment between the wurtzite and zincblende sections predicted by previous theoretical works. When increasing the temperature and the excitation power successively, an additional band attributed to the band-to-band recombination from wurtzite InAs appears. We estimated a lower bound for the wurtzite band gap energy of approximately 0.46 eV at low temperature.

Nanotechnology 23[37], 375704, 2012.

[P195-12] “Probing the localized to itinerant behavior of the 4f electron in CeIn₃-xSn_x by Gd³⁺ electron spin resonance”

Bittar, E. M.*; Adriano, C.*; Giles, C.*; Rettori, C.*; Fisk, Z.; Pagliuso, P. G.*

The CeIn₃-xSn_x cubic heavy fermion system presents an antiferromagnetic transition at T-N = 10 K, for x = 0, that decreases continuously down to 0 K upon Sn substitution at a critical concentration of x(c) approximate to 0.65. In the vicinity of T-N → 0 the system shows non-Fermi liquid behavior due to antiferromagnetic critical fluctuations. For a high Sn content, x greater than or similar to 2.2, intermediate valence effects are present. In this work we show that Gd³⁺-doped electron spin resonance (ESR) probes a change in the character of the Ce 4f electron, as a function of Sn substitution. The Gd³⁺ ESR results indicate a transition of the Ce 4f spin behavior from localized to itinerant. Near the quantum critical point, on the antiferromagnetic side of the magnetic phase diagram, both localized and itinerant behaviors coexist.

Physical Review B 86[12], 125108, 2012.

[P196-12] “Production of Muons from Heavy Flavor Decays at Forward Rapidity in pp and Pb-Pb Collisions at root s(NN)=2.76 TeV”

Abelev, B.; Adam, J.; Adamova, D.; Adare, A. M.; Aggarwal, M. M.; Rinella, G. A.; Chinellato, D. D.*; Dash, A.*; Takahashi, J.*; et al.

ALICE Collaboration

The ALICE Collaboration has measured the inclusive production of muons from heavy-flavor decays at forward rapidity, $2.5 < y < 4$, in pp and Pb-Pb collisions at $\sqrt{s(NN)} = 2.76$ TeV. The p(t)-differential inclusive cross section of muons from heavy-flavor decays in pp collisions is compared to perturbative QCD calculations. The nuclear modification factor is studied as a function of p(t) and collision centrality. A weak suppression is measured in peripheral collisions. In the most central collisions, a suppression of a factor of about 3-4 is observed in $6 < p(t) < 10$ GeV/c. The suppression shows no significant p(t) dependence.

Physical Review Letters 109[11], 112301, 2012.

[P197-12] “Projected length annealing of etched Sm-152 ion tracks in apatite”

Alencar, I.*; Guedes, S.*; Jonckheere, R.; Trautmann, C.; Soares, C. J.*; Moreira, P. A. F. P.*; Curvo, E. A. C.; Tello, C. A.; Nakasuga, W. M.; Dias, A. N. C.; Hadler, J. C.*

Slices of apatite (cut similar to 45 degrees apart from c-axis) were irradiated with Sm-152 ions and heated at different steps in order to investigate the thermal annealing property of tracks generated by these ions. The ions were impinged with 45 degrees and similar to 150 MeV at apatite surface. Samples were etched with diluted nitric acid. Results of annealed projected lengths are presented for isochronal 10, 100 and 1000 h thermal treatments (runs) for samples with and without pre-annealing preparation. For low annealing temperatures, a distinct behavior of these samples was observed: pre-annealed samples presented a faster annealing rate. At elevated temperatures, the behavior seems to be equal. A single activation energy model was fitted to data and the energy obtained is in agreement with literature. Finally, despite the different trend in comparison with annealing rates of confined fission tracks, extrapolation to geological timescales presents reasonable estimates, indicating small influence of surface effects and, in principle, the possibility to employ ion tracks as proxies for annealing kinetics.

Nuclear Instruments & Methods in Physics Research Section B-beam interactions with materials and atoms 288, 48-52, 2012.

[P198-12] “Properties of faujasite zeolites containing methyl-substituted ammonium cations”

Almeida, K. A.; Landers, R.*; Cardoso, D.

This paper describes the properties of new X zeolite catalysts, whose anions are compensated by different methylammonium cations. The properties of these catalysts, with varying degrees of exchange, are compared with those of Y zeolites containing the same cations. For steric reasons, cation exchange was restricted to the faujasite supercavity, and the degree of ion exchange decreased with the radius of the organic cation. The basicity of the catalysts was analyzed using X-ray photoelectron spectroscopy (XPS) and the Knoevenagel condensation reaction, with good correlation obtained between the results of the two methods. The best catalytic activity was observed for the faujasite with the highest aluminum content (X zeolite), exchanged using the monomethylammonium cation. The better performance of this catalyst was attributed to its basicity, as well as the available micropore volume.

Journal of Catalysis 294, 151-160, 2012.

[P199-12] “Quantitative changes in human epithelial cancers and osteogenesis imperfecta disease detected using nonlinear multicontrast microscopy”

Adur, J.*; Pelegati, V. B.*; de Thomaz, A. A.*; D’Souza-Li, L.; Assuncao, M. D.; Bottcher-Luiz, F.; Andrade, L. A. L. A.; Cesar, C. L.*

We show that combined multimodal nonlinear optical (NLO) microscopies, including two-photon excitation fluorescence, second-harmonic generation (SHG), third harmonic generation, and fluorescence lifetime imaging microscopy (FLIM) can be used to detect morphological and metabolic changes associated with stroma and epithelial transformation during the progression of cancer and osteogenesis imperfecta (OI) disease. NLO microscopes provide complementary information about tissue microstructure, showing distinctive patterns for different types of human breast cancer, mucinous ovarian tumors, and skin dermis of patients with OI. Using a set of scoring methods (anisotropy, correlation, uniformity, entropy, and lifetime components), we found significant differences in the content, distribution and organization of collagen fibrils in the stroma of breast and ovary as well as in the dermis of skin. We suggest that our results provide a framework for using NLO techniques as a clinical diagnostic tool for human cancer and OI. We further suggest that the SHG and FLIM metrics described could be applied to other connective or epithelial tissue disorders that are characterized by abnormal cells proliferation and collagen assembly.

Journal of Biomedical Optics 17[8], 081407, 2012.

[P200-12] “Quantum bit encoding and information processing with field superposition states in a circuit”

Neto, O. P. D.*; de Oliveira, M. C.*

Solid-state superconducting devices coupled to coplanar transmission lines offer an exquisite architecture for quantum optical phenomena probing as well as for quantum computation implementation, which is the object of intense theoretical and experimental investigation lately. Under appropriate conditions, the transmission line radiation modes can become strongly coupled to a superconducting device with only two levels-for that reason called an artificial atom or qubit. Employing this system, we propose a two-quantum bit gate encoding, involving quantum electromagnetic field qubit states prepared in a coplanar transmission line capacitively coupled to a single charge qubit.

Since dissipative effects are more drastic in the solid-state qubit than in the field one, it can be employed for the storage of information, whose efficiency against the action of an ohmic bath shows that this encoding can be readily implemented with present-day technology. We extend the investigation to generate entanglement between several solid-state qubits and the field qubit through the action of external classical magnetic pulses.

Journal of Physics B-Atomic Molecular and Optical Physics 45[18], 185505, 2012.

[P201-12] “Reactor (ν)over-bar(e) disappearance in the Double Chooz experiment”

Abe, Y.; Aberle, C.; dos Anjos, J. C.; Barriere, J. C.; Bergevin, M.; Bernstein, A.; Bezerra, T. J. C.; Gonzalez, L. F. G.*; Kemp, E.*; et al.

Double Chooz Collaboration

The Double Chooz experiment has observed 8249 candidate electron antineutrino events in 227.93 live days with 33.71 GW-ton-years (reactor power X detector mass X live time) exposure using a 10.3 m³ fiducial volume detector located at 1050 m from the reactor cores of the Chooz nuclear power plant in France. The expectation in case of $\theta(13) = 0$ is 8937 events. The deficit is interpreted as evidence of electron antineutrino disappearance. From a rate plus spectral shape analysis we find $\sin^2(2\theta(13)) = 0.109 \pm 0.030(\text{stat}) \pm 0.025(\text{syst})$. The data exclude the no-oscillation hypothesis at 99.8% CL (2.9 sigma).

Physical Review D 86[5], 052008, 2012.

[P202-12] “Solar induced chemical vapor deposition of carbon from ethanol”

Lunazzi, F.; Peterlevitz, A. C.; Ceragioli, H. J.; Lunazzi, J. J.*; Baranauskas, V.

Solar induced chemical vapor deposition (S-CVD) process using the concentrated solar radiation flux provided at the focus of a Fresnel lens (diameter 40 cm, focal length 40 cm) has been investigated. Carbon deposits on silicon and on silica have been produced using ethanol as the carbon precursor, highly diluted in hydrogen. A simple optical modeling results in a spot of 0.36 cm diameter with maximum radiation flux of 0.388 kW cm⁻². The deposited spots morphology observed by Scanning Electron Microscopy (SEM) are round shaped with dimensions smaller than 500 x 500 μm^2 . Several flakes and holes of diameters around 2 μm are easily seen on both substrates. Raman results suggest that the deposits may be composed of complex structured carbon.

Vacuum 86[12], 2126-2128, 2012.

[P203-12] “Robust signatures in the current-voltage characteristics of DNA molecules oriented between two graphene nanoribbon electrodes”

Paez, C. J.*; Schulz, P. A.*; Wilson, N. R.; Romer, R. A.

In this work, we numerically calculate the electric current through three kinds of DNA sequences (telomeric, lambda-DNA and p53-DNA) described by different heuristic models. A bias voltage is applied between two zigzag edged graphene contacts attached to the DNA segments, while a gate terminal modulates the conductance of the molecule. Calculation of the current is performed by integrating the transmission function (calculated using the lattice Green's function) over the range of energies allowed by the chemical potentials.

We show that a telomeric DNA sequence, when treated as a quantum wire in the fully coherent low-temperature regime, works as an excellent semiconductor. Clear steps are apparent in the current-voltage curves of telomeric sequences and are present independent of length and sequence initialization at the contacts. We also find that the molecule-electrode coupling can drastically influence the magnitude of the current. The difference between telomeric DNA and other DNAs, such as lambda-DNA and DNA for the tumour suppressor p53, is particularly visible in the length dependence of the current.

New Journal of Physics 14, 093049, 2012.

[P204-12] “Robustness against extinction by stochastic sex determination in small populations”

Schneider, D. M.*; do Carmo, E.*; Bar-Yam, Y.; de Aguiar, M. A. M.*

Sexually reproducing populations with a small number of individuals may go extinct by stochastic fluctuations in sex determination, causing all their members to become male or female in a generation. In this work we calculate the time to extinction of isolated populations with fixed number N of individuals that are updated according to the Moran birth and death process. At each time step, one individual is randomly selected and replaced by its offspring resulting from mating with another individual of the opposite sex; the offspring can be male or female with equal probability. A set of N time steps is called a generation, the average time it takes for the entire population to be replaced. The number k of females fluctuates in time, similarly to a random walk, and extinction, which is the only asymptotic possibility, occurs when k = 0 or k = N. We show that it takes only one generation for an arbitrary initial distribution of males and females to approach the binomial distribution. This distribution, however, is unstable and the population eventually goes extinct in $2(N) / N$ generations. We also discuss the robustness of these results against bias in the determination of the sex of the offspring, a characteristic promoted by infection by the bacteria Wolbachia in some arthropod species or by temperature in reptiles.

Physical Review E 86[4], 041104, Part 1, 2012.

[P205-12] “Strain dependent stabilization of metallic paramagnetic state in epitaxial NdNiO3 thin films”

Kumar, Y.; Choudhary, R. J.; Sharma, S. K.*; Knobel, M.*; Kumar, R.

We report here the strain dependent study of epitaxial NdNiO3 films deposited on LaAlO3 and SrTiO3 substrates using pulsed laser deposition. Electrical transport and magnetic properties of films are found to be controlled by the substrate induced strain. NdNiO3 film on SrTiO3 substrate exhibits behaviour similar to that of bulk NdNiO3, while stabilization of low temperature metallic paramagnetic phase has been observed for film deposited on LaAlO3 substrate. Invariance of Raman spectra, with temperature, of the film on LaAlO3 reveals that the melting of charge ordering under compressive strain is responsible for the stabilization of metallic phase at lower temperature.

Applied Physics Letters 101[13], 132101, 2012.

[P206-12] “Structure and Magnetism of Hybrid Fe and Co Nanoclusters up to N <= 7 Atoms”

Faccin, G. M.; da Silva, E. Z.*

The structural and magnetic properties of small gas-phase Fe (m) Co (n) clusters with $m + n$ ranging between 2 and 7 atoms are investigated using spin-polarized density functional theory. For a given cluster size possible compositions are subject to optimization using a variety of initial structures. The geometry, bond lengths, binding energies and magnetization are reported for the lowest energy structures. The results show that a magnetization peak occurs for Fe-4, while for hybrid clusters, switching a cobalt atom with an iron atom increases the cluster's total magnetization by 1 μ_B . Our structural predictions are generally in agreement with other theoretical results; the origin of the discrepancies arising in some cases is discussed.

Journal of Cluster Science 23[4], 953-966, 2012.

[P207-12] "Synchronization of Micromechanical Oscillators Using Light"

Zhang, M.; Wiederhecker G. S.*; Manipatruni, S.; Barnard, A.; McEuen, P.; Lipson, M.

Synchronization, the emergence of spontaneous order in coupled systems, is of fundamental importance in both physical and biological systems. We demonstrate the synchronization of two dissimilar silicon nitride micromechanical oscillators, that are spaced apart by a few hundred nanometers and are coupled through an optical cavity radiation field. The tunability of the optical coupling between the oscillators enables one to externally control the dynamics and switch between coupled and individual oscillation states. These results pave a path toward reconfigurable synchronized oscillator networks.

Physical Review Letters 109[23], 233906, 2012 (Artigo Destaque de Capa)

[P208-12] "The rule of synchrotron radiation in the prebiotic evolution"

de Brito, A. N.*; da Silva, A. M.; Mocellin, A.

Synchrotron radiation-based spectroscopic techniques are discussed. Their relevance to obtain information regarding the prebiotic evolution problem is pointed out. We present photoelectron-photoion coincidence (PEPICO) spectra of adenine and glycine obtained using 12 and 21 eV photons. The fragmentation pattern belonging to these molecules was found to present striking differences, which are discussed. Adenine partial ion yield in the energy region 12-21 eV is also presented. The neutral fragments were found to have very simple assignment. The importance of hydrogen cyanide (HCN) as a building block of these molecules is confirmed. A special instrumentation allowing precise comparisons between photon-induced desorption and energetic ion bombardment desorption is described. As an example, we show, for the first time, the frozen CO₂ ice mass spectra bombarded by photons and energetic ions, under the same experimental conditions. The comparison shows that prebiotic evolution may only be properly understood if more than one particle, as energy source, is considered.

International Journal of Astrobiology 11[4], SI, 235-241, 2012.

[P209-12] "Transverse single-spin asymmetry and cross section for pi(0) and eta mesons at large Feynman x in p(up arrow) + p collisions at root s=200 GeV"

Adamczyk, L.; Agakishiev, G.; Aggarwal, M. M.; Ahammed, Z.; Alakhverdyants, A. V.; Alekseev, I.; de Souza, R. D.*; Takahashi, J.*; Vasconcelos, G. M. S.*; et al.

STAR Collaboration

Measurements of the differential cross section and the transverse single-spin asymmetry, $A(N)$, vs $x(F)$ for $\pi(0)$ and η mesons are reported for $0.4 < x(F) < 0.75$ at an average pseudorapidity of 3.68. A data sample of approximately 6.3 pb⁻¹ was analyzed, which was recorded during p(up arrow) + p collisions at root $s = 200$ GeV by the STAR experiment at RHIC. The average transverse beam polarization was 56%. The cross section for $\pi(0)$, including the previously unmeasured region of $x(F) > 0.55$, is consistent with a perturbative QCD prediction, and the $\eta/\pi(0)$ cross-section ratio agrees with existing midrapidity measurements. For $0.55 < x(F) < 0.75$, the average $A(N)$ for η is 0.210 ± 0.056 , and that for $\pi(0)$ is 0.081 ± 0.016 . The probability that these two asymmetries are equal is similar to 3%.

Physical Review D 86[5], 051101, 2012.

[P210-12] "Underlying Event measurements in pp collisions at root s=0.9 and 7 TeV with the ALICE experiment at the LHC"

Abelev, B.; Quintana, A. A.; Adamova, D.; Adare, A. M.; Aggarwal, M.; Rinella, G. A.; Cheshkov, C.; Cheynis, B.; Ducroux, L.; Grossiord, J. Y.; Guilbaud, M. R. J.; Massacrier, L. M.; Takahashi, J.*; Tieulent, R. N.; Uras, A.; Zoccarato, Y. D.; et al.

ALICE Collaboration

We present measurements of Underlying Event observables in pp collisions at root $s = 0.9$ and 7 TeV. The analysis is performed as a function of the highest charged-particle transverse momentum $p(T)$, L-T in the event. Different regions are defined with respect to the azimuthal direction of the leading (highest transverse momentum) track: Toward, Transverse and Away. The Toward and Away regions collect the fragmentation products of the hardest partonic interaction. The Transverse region is expected to be most sensitive to the Underlying Event activity. The study is performed with charged particles above three different $p(T)$ thresholds: 0.15, 0.5 and 1.0 GeV/c. In the Transverse region we observe an increase in the multiplicity of a factor 2-3 between the lower and higher collision energies, depending on the track $p(T)$ threshold considered. Data are compared to PYTHIA 6.4, PYTHIA 8.1 and PHOJET. On average, all models considered underestimate the multiplicity and summed $p(T)$ in the Transverse region by about 10-30%.

Journal of High Energy Physics [7], 116, 2012.

Proceedings

[P211-12] "A fitting formula for the effects of massive neutrinos in the nonlinear regime"

Boriero, D.*; Oberauer L. (editor); Raffelt G.(editor); Wagner R.(editor)

The distribution of matter on small scales will be much better known in the next few years through upcoming surveys. To accomplish the measurement of parameters such as the neutrino mass, the accuracy of theoretical predictions must improve accordingly. We present an improved fitting formula for the matter power spectrum taking into account the effect of massive neutrinos in the nonlinear regime. The method used is a modified version of HALOFIT calibrated against N-body simulations with massive neutrinos.

International Conference on Topics in Astroparticle and Underground Physics (TAUP). XII. Journal of Physics Conference Series. V. 375, 032002, Pts 1-6, 2012 - International Conference on Topics in Astroparticle and Underground Physics XII, SEP 05-09, 2011, Munich, Germany.

*Autores do Instituto de Física "Gleb Wataghin".

Especial Comemorativo de 15 anos!

Criado em 1966 e iniciando suas atividades em 1967 o Instituto de Física “Gleb Watahin” contou desde os seus primórdios com a atuação de cientistas de alto nível, a maioria deles com experiência internacional. O conhecimento desses cientistas em Ciência e Tecnologias de ponta em nível mundial favoreceu o desenvolvimento do instituto desde cedo, garantindo assim a captação de recursos para implantação de laboratórios avançados. A estrutura do instituto aliada à experiência desses cientistas teve como resultado o estabelecimento de mais um importante centro de excelência em Física no Brasil, contando com uma estrutura altamente profissional e competitiva.

A importância do instituto é refletida na qualidade do ensino, pesquisa e extensão nele desenvolvidos até hoje. Nos últimos anos o IFGW recebeu a colocação de “Cinco estrelas” no ranking das “Melhores Universidades” do Guia Abril. O Programa de Pós-graduação possui conceito 7 na avaliação da Capes. Com cientistas atuantes, o IFGW desenvolve pesquisas de ponta, capacitando recursos humanos e gerando conhecimentos científicos e tecnológicos significativos. A atuação e cooperação dos docentes e pesquisadores do IFGW com outras instituições brasileiras e no exterior permitem aos seus estudantes oportunidades diferenciadas e com acesso ao conhecimento de fronteira em Física.

Nesse contexto, surge em 1997 o Abstracta com o objetivo de divulgar e compartilhar a produção científica do IFGW entre pesquisadores e instituições da área de Física. A principal finalidade era suscitar o debate, a discussão e a cooperação a partir dos conhecimentos gerados no instituto. Em 2012, o boletim Abstracta migrou do seu formato eletrônico tradicional para o Sistema Eletrônico de Editoração de Revistas - SEER do Instituto Brasileiro de Ciência e Tecnologia - IBICT. A migração do Boletim para o formato revista possibilitou aos leitores maior facilidade de acesso e acompanhamento às publicações do IFGW através da sua versão on-line. Todos os volumes, desde janeiro de 1997, estão disponíveis para download em: <<http://abstracta.ifi.unicamp.br>>. Caso tenha interesse, realize o seu cadastro no portal como “Leitor” e receba todas as novidades de cada número publicado.

Completando 15 anos de publicação esta edição especial apresenta além das publicações do ano corrente, outras informações que delineiam e refletem a evolução do Instituto no que se refere a sua produção científica. Para tanto, apresentamos seleção dos 10 artigos mais citados por ano ao longo desses 15 anos. Além disso, será possível ao leitor observar a evolução da produção científica do IFGW a partir de gráficos sobre número de artigos indexados na Web of Science e o número de citações recebidas da produção anual ao longo dos últimos anos. São apresentados também a média do Fator Impacto dos periódicos que receberam artigos de autores do IFGW nos últimos anos.

Esperamos que façam uma boa leitura!

Trabalhos mais citados - 1997

[E001-1997] "Giant magnetoimpedance effect in soft magnetic wires for sensor applications"

Vazquez, M.; Knobel, M.; Sanchez, M.L.; Valenzuela, R.; Zhukov, A.P.

The giant magneto-impedance effect (GMI) consists of the large relative change of the impedance (up to around 300%) observed in magnetically very soft ribbon and wire alloys under the application of de magnetic fields (units of kA m(-1)), The phenomenology of the GMI effect is firstly described including a discussion about its origin which mainly lies in the classical skin-effect. An alternative approach to GMI phenomena considering equivalent circuits is also introduced. The main requirements to detect GMI is to count on a sample with very large circular susceptibility and reduced resistivity provided the frequency of the ac current flowing along the sample (necessary to evaluate the impedance) is high enough (roughly above 0.1 MHz for most samples here considered). The dependence on de magnetic field, mechanical stresses and particularly on thermal treatments resulting in the induced magnetic anisotropies or in the devitrification of amorphous samples into a nanocrystalline structure are reviewed. First results on GMI in glass-coated amorphous microwires are also reported. The use of the GMI as a tool for studying the inner circular magnetization process or for evaluating the magnetostriction is introduced. Finally, a description on various aspects regarding the development of magnetic field, current, proximity and stress sensor applications is presented.

SENSORS AND ACTUATORS A-PHYSICAL 59[1-3], 20-29, 1997

Número de citações na Web of Science: 136

[E002-1997] "Influence of the distribution of magnetic moments on the magnetization and magnetoresistance in granular alloys"

Ferrari, E.F.; daSilva, F.C.S; Knobel, M.

In granular solids, the magnetoresistance is directly related to the macroscopic magnetization, but this relationship is extremely complex due to the distribution of grain sizes and the intergranular magnetic interactions. The dependence of the magnetoresistance on the magnetization is here investigated by means of a theoretical. model that is developed taking explicitly into account the magnetic moment distribution and the spin-dependent electron-impurity scattering within magnetic grains and at the interface between the grains and the metallic matrix. Using this model, one can explain large experimental deviations from the parabolic behavior of the magnetoresistance vs magnetization curves that are typically expected for equal noninteracting superparamagnetic grains. The expressions for the magnetization and magnetoresistance, obtained for general distribution functions, are tested considering a log-normal-type distribution function by fitting on data obtained from melt-spun Cu90Co10 ribbons after annealing by de Joule heating. The experimental data are well traced using just three parameters that determine the particle size distribution, the particle density, and the ratio of the scattering cross section at the boundaries of the grains to the scattering cross section within the grains.

PHYSICAL REVIEW B 56[10], 6086-6093, 1997

Número de citações na Web of Science: 116

[E003-1997] "The small-angle X-ray scattering beamline of the Brazilian Synchrotron Light Laboratory"

Kellermann, G.; Vicentin, F.; Tamura, E.; Rocha, M.; Tolentino, H.; Barbosa, A.; Craievich, A.; Torriani, I.

This paper describes the small-angle scattering beamline built at the Brazilian Synchrotron Light Laboratory (LNLS). Vertical focusing of the synchrotron beam is achieved by an elastically bent gold-plated cylindrical mirror. An asymmetric cut curved triangle-shaped silicon single crystal (111 reflection) is used for monochromatization and horizontal focusing. The mirror, monochromator optics and 2 theta arm were designed to cover the spectral range between 1.0 and 2.0 Angstrom. Three slit sets, a secondary photon shutter, two beam monitors, filters and absorbers, a multi-sample holder, a vacuum path, a beam-stopper and a set of detectors are the basic components of the workstation. The stepping motors are equipped with specially designed encoders. All mechanical and pneumatic movements and detectors can be remotely controlled using a direct panel or a PC.

JOURNAL OF APPLIED CRYSTALLOGRAPHY 30[2], 880-883, 1997

Número de citações na Web of Science:96

[E004-1997] "The role of hydrogen in nitrogen-containing diamondlike films studied by photoelectron spectroscopy"

Souto, S.; Alvarez, F.

The influence of H on the local structure of N-containing amorphous diamondlike films (a-CN_x:H) is reported. The samples were prepared by rf sputtering of graphite in a N-2, Ar, and H-2 atmosphere. The chemical bonding of C and N atoms was inferred by analyzing the C 1s and N 1s electronic core-level by x-ray photoelectron spectroscopy. Hydrogen free films present N 1s peaks with a "doublet", located at 398.2-400.5 eV. When H is introduced in the preparation chamber, the doublet evolves to a single wider band located at 399.1 eV. This new band becomes dominant when increasing H-2 partial pressure, completely hiding the original structure. High H-2 partial pressure interrupts the growing network formed by N and C due to the attachment of H to N and/or C. Furthermore, the experimental results suggest that the possibility of formation of the C₃N₄ phaselike is inhibited by the presence of hydrogen.

APPLIED PHYSICS LETTERS 70[12], 1539-1541, 1997

Número de citações na Web of Science:64

[E005-1997] "Erbium luminescence from hydrogenated amorphous silicon-erbium prepared by cosputtering"

Zanatta, A.R.; Nunes, L.A.O; Tessler, L.R.

Hydrogenated amorphous silicon with small amounts of erbium (Er/Si concentration similar to 5 at.%) was prepared by radio frequency sputtering from a Si target partially covered by tiny metallic Er chunks. Four sets of samples were studied: nonintentionally contaminated hydrogenated and nonhydrogenated amorphous silicon-erbium (a-SiEr:H and a-SiEr); nitrogen doped a-SiEr(N):H and oxygen contaminated a-SiEr(O):H. Samples from the first two sets present only faint 1.54 mu m photoluminescence characteristic from Er³⁺ ions even at 77 K. Samples from the other sets show this luminescence at 77 K as deposited, without any further annealing step. Thermal annealing up to 500 degrees C increases the photoluminescence intensity, and room temperature emissions become strong enough to be easily detected. These results indicate that in an amorphous silicon environment the chemical neighborhood of the Er³⁺ ions is crucial for efficient 1.54 mu m emission. Raman scattering from both as-deposited and annealed samples showed that network disorder relaxation by annealing is not determinant for efficient Er³⁺ luminescence.

APPLIED PHYSICS LETTERS 70[4], 511-513, 1997

Número de citações na Web of Science:58

[E006-1997] "Electrochromism and photochromism in amorphous molybdenum oxide films"

Scarminio, J.; Lourenco, A.; Gorenstein, A.

In this paper, we present a study of the influence of the oxygen flow rate (ϕ) during r.f. sputtering of molybdenum metal targets on the resulting MoOx thin films. The optical behavior upon Li⁺ electrochemical intercalation (electrochromic effect) or UV irradiation (photochromic effect) is analyzed. At low ϕ , blue substoichiometric molybdenum oxide films are formed. At high ϕ , the composition of the oxide films approaches that of transparent, stoichiometric MoO₃. The optical gap for the as-grown films increases with the increase of ϕ , in the range 2.8 eV for low ϕ to 3.2 eV at high ϕ . Lithium intercalation or UV irradiation promoted transmittance changes. The highest electrochemical and photochemical transmittance change was obtained for the sample deposited at low ϕ .

THIN SOLID FILMS 302[1-2], 66-70, 1997

Número de citações na Web of Science:55

[E007-1997] "Chemical (dis)order in a-Si_{1-x}C_x:H for x<0.6"

Rovira, P.I.; Alvarez, F.

We studied the local bonding structure of the hydrogenated amorphous silicon-carbon alloy system (a-Si_{1-x}C_x:H). The chemistry of the carbon incorporation in the alloys for 0<x<0.6 was analyzed by infrared and visible spectroscopies. The material was deposited in a controlled atmosphere of argon and hydrogen by rf cosputtering of Si and C targets. We found that up to x approximate to 0.2 the carbon atom prefers to bond in a chemically disordered configuration, i.e., homonuclear bonds are favored. Between 0.2<x<0.6 a tendency to chemical ordering is apparent. These results are consistent with the behavior of the optical gap, the Urbach energy, and the density of defects of the material as a function of x.

PHYSICAL REVIEW B 55[7], 4426-4434, 1997

Número de citações na Web of Science:54

[E008-1997] "Photorefractive saturable Kerr-type nonlinearity in photovoltaic crystals"

Bian, S.; Frejlich, J.; Ringhofer, K.H.

We deduce the equation describing the refractive index perturbation in photovoltaic photorefractive crystals produced by the incidence of a focused laser beam and an incoherent uniform illumination. Under short-circuit conditions the equation shows a saturable Kerr-type nonlinearity that can be controlled by the intensity of the uniform background illumination. Z-scan experiments in an iron doped lithium niobate crystal are carried out using a 532 nm wavelength laser line to evaluate its self-lensing properties and to measure its photovoltaic field.

PHYSICAL REVIEW LETTERS 78[21], 4035-4038, 1997

Número de citações na Web of Science:50

[E009-1997] "Chilling stress leads to increased cell membrane rigidity in roots of coffee (Coffea arabica L) seedlings"

Alonso, A.; Queiroz, C.S.; Magalhaes, A.C.

Tropical and sub-tropical higher plant species show marked growth inhibition when exposed to chilling temperatures. In root tip segments of coffee seedlings which were subjected for 6 days to temperatures of 10, 15, 20 and 25 degrees C, in darkness, we have detected an increased amount of malondialdehyde formed in the 10 degrees C treatment, accompanied by higher electrolyte leakage. The electron paramagnetic resonance (EPR) technique and the fatty acid spin probes 5-, 12- and 16-doxylstearic acid were used to assess cellular membrane fluidity. At the depth of the 5th and 16th carbon atom of the alkyl chains the nitroxide radical detected more rigid membranes in seedlings subjected to 10 degrees C compared with 15 and 25 degrees C. At the C-12 position of the chains the probe showed very restricted motion and was insensitive to chilling induced membrane alterations. EPR parameters for intact tissues and microsome preparations from root tips showed that the fluidity was essentially the same when evaluated at C-5 and C-16 positions of the chains, and was considerably more fluid for microsomal membranes in the region of the C-12 position of the bilayers. The rotational motion of the nitroxide at C-16 position of the chains experienced a phase transition at about 15 degrees C. The calculated energy barriers for reorientational motion of the probe 16-doxylstearic acid were higher at temperatures of 5-15 degrees C than in the interval of 15-25 degrees C, suggesting that below the phase transition the membrane lipids assume a more ordered and compacted array. Membrane rigidity induced by chilling was interpreted as due to lipid peroxidation that could have been facilitated by higher density of peroxidizable chains below the membrane phase transition.

BIOCHIMICA ET BIOPHYSICA ACTA-BIOMEMBRANES 1323[1], 75-84, 1997

Número de citações na Web of Science:43

[E010-1997] "Retrieval of optical constants and thickness of thin films from transmission spectra"

Chambouleyron, I.; Martinez, J.M.; Moretti, A.C.; Mulato, M.

We discuss a new method to estimate the absorption coefficient, the index of refraction, and the thickness of thin films using optical transmission data only. To solve the problem we used a pointwise constrained optimization approach, defining a nonlinear programming problem, the unknowns of which are the coefficients to be estimated, with linear constraints that represent prior knowledge about the physical solution. The method applies to all kinds of transmission spectra and does not rely on the existence of fringe patterns or transparency. Results on amorphous semiconductor thin films and gedanken films are reported. They show that the new method is highly reliable.

APPLIED OPTICS 36[31], 8238-8247, 1997

Número de citações na Web of Science:42

Trabalhos mais citados - 1998

[E001-1998] "Electronic structure of nitrogen-carbon alloys (a-CN_x) determined by photoelectron spectroscopy"

Souto, S.; Pickholz, M.; dos Santos, M.C.; Alvarez, F.

The electronic structure of nitrogen-containing diamondlike films prepared by sputtering was determined by photoelectron spectroscopy. The N 1s core-level spectra are constituted by two peaks at 400.5 and 398.2 eV associated with substitutional N sp² in aromatic rings and N bonded to C sp³, respectively. On increasing N, the top of the valence band suffers profound changes.

The new features are identified by a comparison of the experimental spectra with theoretically calculated density of states of nitrogen-containing graphite and C₃N₄ structures.

PHYSICAL REVIEW B 57[4], 2536-2540, 1998

Número de citações na Web of Science: 151

[E002-1998] "Quantum dynamical manifestation of chaotic behavior in the process of entanglement"

Furuya, K.; Nemes, M.C.; Pellegrino, G.Q.

Manifestation of chaotic behavior is found in an intrinsically quantum property. The entanglement process, quantitatively expressed in terms of the reduced density linear entropy, is studied for the N-atom Jaynes-Cummings model. For a given energy, initial conditions are prepared as minimum uncertainty wave packets centered at regular and chaotic regions of the classical phase space. We find for short times a faster increase in decoherence for the chaotic initial conditions as compared to regular ones, which have oscillatory increase.

PHYSICAL REVIEW LETTERS 80[25], 5524-5527, 1998

Número de citações na Web of Science: 122

[E003-1998] "Electronic structure of hydrogenated carbon nitride films"

Hammer, P.; Victoria, N.M.; Alvarez, F.

Hydrogen-induced changes on the electronic and structural properties of amorphous carbon nitride (a-CN(x):H) prepared by ion beam assisted deposition are investigated by x-ray photoelectron, ultraviolet photoelectron, infrared, and Raman spectroscopies. Two series of specimen are studied: films with a constant nitrogen content (C/N = 26%) grown at 150 degrees C using different hydrogen partial pressures between 0% and 70% and samples deposited at different substrate temperatures (150-500 degrees C) with fixed Hz partial pressure of 60%. The pronounced changes of the N 1s and C 1s core level spectra on increasing hydrogen incorporation (up to 17 at. %) are interpreted as due to the formation of terminating NH and CH bonds accompanied by modifications of the local C-N bonding structure. Corresponding changes are observed in the He II valence band spectra showing a recession of the leading edge of more than 0.9 eV while the optical band gap widens from 0 to more than 1 eV. Consistent with these results, the information obtained from the infrared and Raman spectra suggests a hydrogen induced transformation of the disordered sp(2)/sp(3) network into a polymerlike structure. With increasing substrate temperature a reversed process takes place. At 700 degrees C an increasing graphitization of the films is observed, but the effect of hydrogen on the structure influencing the growth kinetics is still present at this temperature. The nitrogen concentration (N/C) of about 30% indicates high thermal stability of the CN material.

JOURNAL OF VACUUM SCIENCE & TECHNOLOGY A 16[5], 2941-2949, 1998

Número de citações na Web of Science: 121

[E004-1998] "Phonon Raman scattering in R(1-x)A(x)MnO(3+delta) (R = La,Pr; A = Ca,Sr)"

Granado, E.; Moreno, N.O.; Garcia, A.; Sanjurjo, J.A.; Rettori, C.; Torriani, I.; Oseroff, S.B.; Neumeier, J.J.; McClellan, K.J.; Cheong, S.W.; Tokura, Y.

Polarized Raman spectra of single and polycrystalline R(1-x)A(x)MnO(3) (R = La,Pr; A = Ca,Sr) ceramic samples were studied as a function of temperature. For the rhombohedral LaMnO_{3.1} and La_{0.7}Sr_{0.3}MnO₃, the observed Raman peaks were associated with modes arising from the folding of the Brillouin zone under lattice deformation. For the orthorhombic LaMnO_{3.0}, the Raman spectra are consistent with the Pnma structure and show an anomalous softening of the 494 and 604 cm⁻¹ modes below the antiferromagnetic ordering temperature T_N similar or equal to 140 K. Polycrystalline samples of La_{0.5}Ca_{0.5}MnO₃ show a dramatic change of the Raman spectra between 100 and 160 K, which was associated with the increase of the orthorhombic distortion observed by others for T less than or similar to 240 K. Other R(1-x)A(x)MnO(3) single crystals, with small orthorhombic distortions, show Raman spectra which are similar to those observed in the rhombohedral samples.

PHYSICAL REVIEW B 58[17], 11435-11440, 1998

Número de citações na Web of Science: 117

[E005-1998] "Nitrogen substitution of carbon in graphite: Structure evolution toward molecular forms"

dos Santos, M.C.; Alvarez, F.

A series of randomly nitrogen-substituted carbon clusters in graphitelike structures, containing up to 96 carbon atoms, is theoretically investigated through semiempirical pseudopotential techniques. The evolution of conformation and electronic structure is obtained as a function of nitrogen content. Results from semiempirical geometry optimizations reveal that the clusters are planar for nitrogen concentrations up to [N]/[C] similar to 20%. Above this concentration, buckling develops in the clusters. One of the characteristics of these corrugated clusters is the presence of carbon dangling bonds. Chemical stabilization imposes that these structures evolve to either a three-dimensional, fully covalent carbon nitride network, or to molecular forms. Among the well-defined molecular structures that could develop in amorphous carbon nitride, we found nanotubules and a molecular cage of elemental compositions CN and C₃N₄, respectively.

PHYSICAL REVIEW B 58[20], 13918-13924, 1998

Número de citações na Web of Science: 107

[E006-1998] "Absolute thermal lens method to determine fluorescence quantum efficiency and concentration quenching of solids"

Baesso, M.L.; Bento, A.C.; Andrade, A.A.; Sampaio, J.A.; Pecoraro, E.; Nunes, L.A.O.; Catunda, T.; Gama, S.

An absolute thermal lens method to determine fluorescence quantum efficiency and concentration quenching of solids is described in this work. The quantum efficiency of low silica calcium aluminate glasses doped with different concentrations of neodymium dioxide and melted under vacuum conditions to remove water has been measured by using mode-mismatched thermal lens spectrometry. It has been shown that the thermal lens signal amplitude is linearly dependent on neodymium concentrations up to 4.0 wt %, changing significantly from 4.5 to 5.0 wt %, indicating that there was quenching of the fluorescence only above 4.0 wt % neodymium dioxide. The quantitative treatment for the thermal lens effect provided the absolute value of the sample's fluorescence quantum efficiency. The technique is simple to perform and can be applied for a wide range of fluorescent materials.

PHYSICAL REVIEW B 57[17], 10545-10549, 1998

Número de citações na Web of Science:99

[E007-1998] "Optical characterization of dielectric and semiconductor thin films by use of transmission data"

Cisneros, J.I.

A method to calculate the optical functions $n(\lambda)$ and $k(\lambda)$ by use of the transmission spectrum of a dielectric or semiconducting thin film measured at normal incidence is described. The spect-nun should include the low-absorption region and the absorption edge to yield the relevant optical characteristics of the material. The formulas are derived from electromagnetic theory with no simplifying assumptions. Transparent films are considered as a particular case for which a simple method of calculation is proposed. In the general case of absorbing films the method takes advantage of some properties of the transmittance $T(\lambda)$ to permit the parameters in the two regions mentioned above to be calculated separately. The interference fringes and the optical path at the extrema of $T(\lambda)$ are exploited for determining with precision the refractive index and the film thickness. The absorption coefficient is computed at the absorption edge by an efficient iterative method. At the transition zone between the interference region and the absorption edge artifacts in the absorption curve are avoided. A small amount of absorption of the substrate is allowed for in the theory by means of a factor determined from an independent measurement, thus improving the quality of the results. Application of the method to a transmission spectrum of an α -SixN1-x:H film is illustrated in detail. Refractive index, dispersion parameters, film thickness, absorption coefficient, and optical gap are given with the help of tables and graphs.

APPLIED OPTICS 37[22], 5262-5270, 1998

Número de citações na Web of Science:97

[E008-1998] "Ruthenium nitrosyl complexes with N-heterocyclic ligands"

Borges, S.D.S.; Davanzo, C.U.; Castellano, E.E.; Z-Schpector, J.; Silva, S.C.; Franco, D.W.

A new route was developed for preparing a series of trans nitrosyl complexes of general formula $\text{trans-}[\text{Ru}(\text{NH}_3)_4(\text{L})(\text{NO})](\text{BF}_4)_3$, where L = imidazole: L-histidine, pyridine, or nicotinamide. The complexes have been characterized by elemental analysis, molar conductance measurements, UV-visible, infrared, proton nuclear magnetic, and electron paramagnetic resonance spectroscopies, and electrochemical techniques. The compounds possess relatively high $\nu(\text{NO})$ stretching frequencies indicating that a high degree of positive charge resides on the coordinated nitrosyl group. The nitrosyl complexes react with OH- according to the equation $\text{trans-}[\text{Ru}(\text{NH}_3)_4(\text{L})(\text{NO})]^{3+} + 2\text{OH}^- \rightleftharpoons \text{trans-}[\text{Ru}(\text{NH}_3)_4(\text{L})(\text{NO}_2)]^+ + \text{H}_2\text{O}$, with a K_{eq} (at 25.0 degrees C in 1.0 mol/L NaCl) of 2.2×10^5 , 5.9×10^7 , 9.7×10^{10} , and 4.6×10^{13} L-2 mol(-2) for the py, nic, imN, and L-hist complexes, respectively. Only one redox process attributed to the reaction $[\text{Ru-II}(\text{NH}_3)_4(\text{L})(\text{NO}^+)]^{3+} + e^- \rightleftharpoons [\text{Ru-II}(\text{NH}_3)_4(\text{L})(\text{NO})]^{2+}$ was observed in the range -0.45 to 1.20 V for all the nitrosyl complexes. Linear correlations are observed in plots of $\nu(\text{NO})$ versus $E^{-1/2}$ and of $E^{-1/2}$ versus $\Sigma E-L$ showing that the oxidizing strength of the coordinated NO increases with increase in L pi-acidity. The crystal structure analysis of $\text{trans-}[\text{Ru}(\text{NH}_3)_4(\text{nicNO})_2(\text{SiF}_6)_3]$ shows that the mean Ru-N-O angle is very close to 180 degrees (177 ± 1 degrees) and the mean N-O distance is 1.17 ± 0.02 Angstrom, thus confirming the presence of the Ru-II-NO+ moiety in the nitrosyl complexes studied.

INORGANIC CHEMISTRY 37[11], 2670-2677, 1998

Número de citações na Web of Science:92

[E009-1998] "Hard hydrogenated carbon films with low stress"

Lacerda, R.G.; Marques, F.C.

Analysis of hard a-C:H films with low stress prepared by methane plasma decomposition is reported. Films with hardness as high as 14 GPa and stress as low as 0.5 GPa were obtained. These films have a high Raman I-d/I-g ratio (similar to 1.0), and small Tauc's band gap (similar to 0.4 eV). This letter also supplies strong evidence that the subimplantation deposition model, used to explain the formation of la-C and ta-C:H films, is also valid for a-C:H films deposited by methane plasma decomposition. It is proposed that the rigidity of the films is basically provided by a matrix of dispersed cross-linked sp(2) sites, in addition to the contribution of the sp(3) sites.

APPLIED PHYSICS LETTERS 73[5], 617-619, 1998

Número de citações na Web of Science:72

[E010-1998] "Infrared analysis of deuterated carbon-nitrogen films obtained by dual-ion-beam-assisted-deposition"

Alvarez, F.; Victoria, N.M.; Hammer, P.; Freire, F.L.; dos Santos, M.C.

The isotopic effect on the infrared spectra is used to determine the existence of nitrogen-hydrogen bonds in amorphous carbon-nitrogen alloys (a-CN_x) prepared by dual-ion-beam-assisted deposition. The deuteration experiments and the evolution of the infrared spectra upon atmospheric exposure show that hydroxyls are incorporated from atmospheric moisture.

APPLIED PHYSICS LETTERS 73[8], 1065-1067, 1998

Número de citações na Web of Science:60

Trabalhos mais citados - 1999

[E001-1999] "Laser ablation inductively coupled plasma mass spectrometry: achievements, problems, prospects"

Durrant, S.F.

JOURNAL OF ANALYTICAL ATOMIC SPECTROMETRY 14[9], 1385-1403, 1999

Número de citações na Web of Science:183

[E002-1999] "Estimation of the optical constants and the thickness of thin films using unconstrained optimization"

Birgin, E.G.; Chambouleyron, I.; Martinez, J.M.

The problem of estimating the thickness and the optical constants of thin Alms using transmission data only is very challenging from the mathematical point of view and has a technological and an economic importance. In many cases it represents a very ill-conditioned inverse problem with many local-nonglobal solutions. In a recent publication we proposed nonlinear programming models for solving this problem. Well-known software for linearly constrained optimization was used with success for this purpose,

In this paper we introduce an unconstrained formulation of the nonlinear programming model and we solve the estimation problem using a method based on repeated calls to a recently introduced unconstrained minimization algorithm, Numerical experiments on computer-generated Alms show that the new procedure is reliable.

JOURNAL OF COMPUTATIONAL PHYSICS 151[2], 862-880, 1999

Número de citações na Web of Science:95

[E003-1999] “Magnetic hysteresis based on dipolar interactions in granular magnetic systems”

Allia, P.; Coisson, M.; Knobel, M.; Tiberto, P.; Vinai, F.

The magnetic hysteresis of granular magnetic systems is investigated in the high-temperature limit (T much greater than blocking temperature of magnetic nanoparticles). Measurements of magnetization curves have been performed at room temperature on various samples of granular bimetallic alloys of the family $\text{Cu}(100-x)\text{Co}(x)$ ($x = 5-20$ at. %) obtained in ribbon form by planar flow casting in a controlled atmosphere, and submitted to different thermal treatments. The loop amplitude and shape, which are functions of sample composition and thermal history, are studied taking advantage of a novel method of graphical representation, particularly apt to emphasize the features of thin, elongated loops. The hysteresis is explained in terms of the effect of magnetic interactions of the dipolar type among magnetic-metal particles, acting to hinder the response of the system of moments to isothermal changes of the applied field. Such a property is accounted for in a mean-field scheme, by introducing a memory term in the argument of the Langevin function which describes the anhyseretic behavior of an assembly of noninteracting superparamagnetic particles. The rms field arising from the cumulative effect of dipolar interactions is linked by the theory to a measurable quantity, the reduced remanence of a major symmetric hysteresis loop. The theory self-consistence and adequacy have been properly tested at room temperature on all examined systems. The agreement with experimental results is always striking, indicating that at high temperatures the magnetic hysteresis of granular systems is dominated by interparticle, rather than single-particle, effects. Dipolar interactions seem to fully determine the magnetic hysteresis in the high-temperature limit for low Co content (x less than or equal to 10). For higher concentrations of magnetic metal, the experimental results indicate that additional hysteric mechanisms have to be introduced.

PHYSICAL REVIEW B 60[17], 12207-12218, 1999

Número de citações na Web of Science:87

[E004-1999] “Atmospheric neutrino observations and flavor changing interactions”

Gonzalez-Garcia, M.C.; Guzzo, M.M.; Krastev, P.I.; Nunokawa, H.; Peres, O.L.G.; Pleitez, V.; Valle, J.W.F.; Funchal, R.Z.

Flavor changing (FC) neutrino-matter interactions can account for the zenith-angle-dependent deficit of atmospheric neutrinos observed in the SuperKamiokande experiment, without directly invoking either neutrino mass or mixing. We find that FC $\nu(\mu)$ -matter interactions provide a good fit to the observed zenith angle distributions, comparable in quality to the neutrino oscillation hypothesis. The required FC interactions arise naturally in many attractive extensions of the standard model.

PHYSICAL REVIEW LETTERS 82[16], 3202-3205, 1999

Número de citações na Web of Science:87

[E005-1999] “Magnetic ordering effects in the Raman spectra of $\text{La}_{1-x}\text{Mn}_x\text{O}_3$ ”

Granado, E.; Garcia, A.; Sanjurjo, J.A.; Rettori, C.; Torriani, I.; Prado, F.; Sanchez, R.D.; Caneiro, A.; Oseroff, S.B.

Temperature-dependent Raman spectra of polycrystalline $\text{La}_{1-x}\text{Mn}_x\text{O}_3$ samples, referred to as $\text{LaMnO}_3+\delta$ for convenience, were correlated to their structural and magnetic properties for different δ . For δ less than or equal to 0.05, a softening of the similar to 610 cm^{-1} Raman mode is observed below the magnetic ordering temperature. This softening is reduced as δ increases from 0.00 to 0.05. This behavior is not associated with lattice anomalies, and is interpreted in terms of a spin-phonon coupling caused by a phonon modulation of the superexchange integral. A quantitative analysis of this effect is presented.

PHYSICAL REVIEW B 60[17], 11879-11882, 1999

Número de citações na Web of Science:85

[E006-1999] “Structural properties and Raman modes of zinc blende InN epitaxial layers”

Tabata, A.; Lima, A.P.; Teles, L.K.; Scolfaro, L.M.R.; Leite, J.R.; Lemos, V.; Schottker, B.; Frey, T.; Schikora, D.; Lischka, K.

Abstract: We report on x-ray diffraction and micro-Raman scattering studies on zinc blende InN epitaxial films. The samples were grown by molecular beam epitaxy on $\text{GaAs}(001)$ substrates using a InAs layer as a buffer. The transverse-optical (TO) and longitudinal-optical phonon frequencies at Γ of $c\text{-InN}$ are determined and compared to the corresponding values for $c\text{-GaN}$. Ab initio self-consistent calculations are carried out for the $c\text{-InN}$ $c\text{-GaN}$ lattice parameters and TO phonon frequencies. A good agreement between theory and experiment is found.

APPLIED PHYSICS LETTERS 74[3], 362-364, 1999

Número de citações na Web of Science:71

[E007-1999] “Metal-insulator transition in a disordered two-dimensional electron gas in GaAs-AlGaAs at zero magnetic field”

Ribeiro, E.; Jaggi, R.D.; Heinzl, T.; Ensslin, K.; Medeiros-Ribeiro, G.; Petroff, P.M.

A metal-insulator transition in two-dimensional electron gases at $B = 0$ is found in Ga[Al]As heterostructures, where a high density of self-assembled InAs quantum dots is incorporated just 3 nm below the heterointerface. The transition occurs at resistances around h/e^2 and critical carrier densities of $1.2 \times 10^{11} \text{ cm}^{-2}$. Effects of electron-electron interactions are expected to be rather weak in our samples, while disorder plays a crucial role.

PHYSICAL REVIEW LETTERS 82[5], 996-99, 1999

Número de citações na Web of Science:69

[E008-1999] “Active-active and active-sterile neutrino oscillation solutions to the atmospheric neutrino anomaly”

Gonzalez-Garcia, M.C.; Nunokawa, H.; Peres, O.L.G.; Valle, J.W.F.

We perform a fit to the full data set corresponding to 33.0 kyr of data of the Super-Kamiokande experiment as well as to all other experiments in order to compare the two most likely solutions to the atmospheric neutrino anomaly in terms of oscillations in the $\nu(\mu) \rightarrow \nu(\tau)$ and $\nu(\mu) \rightarrow \nu(s)$ channels.

Trabalhos mais citados - 2000

[E001-2000] "Signature of atomic structure in the quantum conductance of gold nanowires"

Rodrigues, V.; Fuhrer, T.; Ugarte, D.

We have used high resolution transmission electron microscopy to determine the structure of gold nanowires generated by mechanical stretching. Just before rupture, the contacts adopt only three possible atomic configurations, whose occurrence probabilities and quantized conductance were subsequently estimated. These predictions have shown a remarkable agreement with conductance measurements from a break junction operating in ultrahigh vacuum, corroborating the derived correlation between nanowire atomic structure and conductance behavior.

PHYSICAL REVIEW LETTERS 85[19], 4124-4127, 2000

Número de citações na Web of Science:253

[E002-2000] "Ferromagnetic- and superconducting-like behavior of graphite"

Kopelevich, Y.; Esquinazi, P.; Torres, J.H.S.; Moehlecke, S.

We have identified ferromagnetic- and superconducting-like magnetization hysteresis loops in highly oriented pyrolytic graphite samples below and above room temperature. We also found that both behaviors are very sensitive to low-temperature. We also found that both behaviors are very sensitive to low-temperature as compared to the sample synthesis temperature heat treatment. The possible contribution of magnetic impurities and why these do not appear to be the reason for the observed phenomena is discussed.

JOURNAL OF LOW TEMPERATURE PHYSICS 119[5-6], 691-702, 2000

Número de citações na Web of Science:154

[E003-2000] "Status of the MSW solutions of the solar neutrino problem"

Gonzalez-Garcia, M.C.; de Holanda, P.C.; Pena-Garay, C.; Valle, J.W.F.

We present an updated global analysis of two-flavour MSW solutions to the solar neutrino problem. We perform a fit to the full data set corresponding to the 825-day Super-Kamiokande data sample as well as to chlorine, GALLEX and SAGE experiments. In our analysis we use all measured total event rates as well as all Super-Kamiokande data on the zenith angle dependence, energy spectrum and seasonal variation of the events. We compare the quality of the solutions of the solar neutrino anomaly in terms of conversions of $\nu(e)$ into active or sterile neutrinos. For the case of conversions into active neutrinos we find that, although the data on the total event rates favours the Small Mixing Angle (SMA) solution, once the full data set is included both SMA and Large Mixing Angle (LMA) solutions give an equally good Fit to the data. We find that the best-fit points for the combined analysis are $\Delta m^2 = 3.6 \times 10^{-5} \text{ eV}^2$ and $\sin^2 2\theta = 0.79$ with $\chi^2(\text{min}) = 35.4/30$ d.o.f. and $\Delta m^2 = 5.1 \times 10^{-6} \text{ eV}^2$ and $\sin^2 2\theta = 5.5 \times 10^{-3}$ with $\chi^2(\text{min}) = 37.4/30$ dof. In contrast with the earlier 504-day study of Bahcall-Krastev-Smirnov our results indicate that the LMA solution is not only allowed, but slightly preferred. On the other hand, we show that seasonal effects, although small, may still leach 11% in the lower part of the LMA region, without conflict with the negative hints of a day-night variation (6% is due to the eccentricity of the Earth's orbit).

Using state-of-the-art atmospheric neutrino fluxes we have determined the allowed regions of oscillation parameters for both channels. We find that the Δm^2 values for the active-sterile oscillations (both for positive and negative Δm^2) are higher than for the $\nu(\mu) \rightarrow \nu(\tau)$ case, and that the increased Super-Kamiokande sample slightly favours $\nu(\mu) \rightarrow \nu(\tau)$ oscillations over oscillations into a sterile species $\nu(s)$, $\nu(\mu) \rightarrow \nu(s)$, and disfavours $\nu(\mu) \rightarrow \nu(e)$. We also give the zenith angle distributions predicted for the best fit points in each of the possible oscillation channels. Finally we compare our determinations of the atmospheric neutrino oscillation parameters with the expected sensitivities of future long-baseline experiments K2K, MINOS, ICARUS, OPERA and NOE.

NUCLEAR PHYSICS B 543[1-2], 3-19, 1999

Número de citações na Web of Science:66

[E009-1999] "Optimized free-energy evaluation using a single reversible-scaling simulation"

de Koning, M.; Antonelli, A.; Yip, S.

We present a method, for highly efficient free-energy calculations by means of molecular dynamics and Monte Carlo simulations, which is an optimized combination of coupling parameter and adiabatic switching formalisms. This approach involves dynamical reversible scaling of the potential energy function of a system of interest, and allows accurate determination of its free energy over a wide temperature interval from a single simulation. The method is demonstrated in two applications: crystalline Si at zero pressure and a fee nearest-neighbor antiferromagnetic Ising model.

PHYSICAL REVIEW LETTERS 83[20], 3973-3977, 1999

Número de citações na Web of Science:62

[E010-1999] "Coefficient of thermal expansion and elastic modulus of thin films"

de Lima, M.M.; Lacerda, R.G.; Vilcarrero, J.; Marques, F.C.

The coefficient of thermal expansion (CTE), biaxial modulus, and stress of some amorphous semiconductors (a-Si:H, a-C:H, a-Ge:H, and a-GeC(x):H) and metallic (Ag and Al) thin films were studied. The thermal expansion and the biaxial modulus were measured by the thermally induced bending technique. The stress of the metallic films, deposited by thermal evaporation (Ag and Al), is tensile, while that of the amorphous films deposited by sputtering (a-Si:H, a-Ge:H, and a-GeC(x):H) and by glow discharge (a-C:H) is compressive. We observed that the coefficient of thermal expansion of the tetrahedral amorphous thin films prepared in this work, as well as that of the films reported in literature, depend on the network strain. The CTE of tensile films is smaller than that of their corresponding crystalline semiconductors, but it is higher for compressive films. On the other hand, we found out that the elastic biaxial modulus of the amorphous and metallic films is systematically smaller than that of their crystalline counterparts. This behavior stands for other films reported in the literature that were prepared by different techniques and deposition conditions. These differences were attributed to the reduction of the coordination number and to the presence of defects, such as voids and dangling bonds, in amorphous films. On the other hand, columnar structure and microcrystallinity account for the reduced elasticity of the metallic films.

JOURNAL OF APPLIED PHYSICS 86[9], 4936-4942, 1999

Número de citações na Web of Science:59

In particular the best-fit LMA solution predicts a seasonal effect of 8.5%. For conversions into sterile neutrinos only the SMA solution is possible with best-fit point $\Delta m(2) = 5.0 \times 10^{-6}$ eV(2) and $\sin(2)\theta = 3. \times 10^{-3}$ and $\chi(\min)(2) = 40.2/30$ d.o.f. We also consider departures of the Standard Solar Model (SSM) of Bahcall and Pinsonneault 1998 (BP98) by allowing arbitrary B-8 and hep fluxes. These modifications do not alter significantly the oscillation parameters. The best fit is obtained for $B-8/B-8(SSM) = 0.61$ and $hep/hep(SSM) = 12$ for the SMA solution both for conversions into active or sterile neutrinos and $B-8/B-8(SSM)=1.37$ and $hep/hep(SSM) = 38$ for the LMA solution.

NUCLEAR PHYSICS B 573[1-2], 3-26, 2000

Número de citações na Web of Science:136

[E004-2000] "Excitonic absorption in a quantum dot"

Hawrylak, P.; Narvaez, G.A.; Bayer, M.; Forchel, A.

The excitonic absorption spectrum of a single quantum dot is investigated theoretically and experimentally. The spectrum is determined by an interacting electron-valence-hole complex. We show that the mixing of quantum configurations by two-body interactions leads to distinct absorption spectra controlled by the number of confined electronic shells. The theoretical results are compared with results of photoluminescence excitation spectroscopy on a series of single self-assembled $\text{In}_{0.60}\text{Ga}_{0.40}\text{As}$ quantum dots.

PHYSICAL REVIEW LETTERS 85[2], 389-392, 2000

Número de citações na Web of Science:108

[E005-2000] "Asymmetric polysulfone and polyethersulfone membranes: effects of thermodynamic conditions during formation on their performance"

Barth, C.; Goncalves, M.C.; Pires, A.T.N.; Roeder, J.; Wolf, B.A.

Membranes of polysulfone (PSU) and polyethersulfone (PES) were prepared from ternary and quaternary mixtures containing N,N-dimethylformamide (DMF) as solvent, water as non-solvent, and acetone (AC) as additive. The conditions for phase inversion and the desired phase separation mechanisms were selected on the basis of the phase behavior determined for the solvent/non-solvent/polymer systems. The influences of the composition of the casting solution, of the support, and of film thickness on structure and permeation properties of the membranes were analyzed by scanning electron microscopy (SEM) plus flux and separation experiments. The mechanisms of phase inversion that should prevail under the different conditions according to the measured phase diagrams were corroborated by means of light scattering experiments.

JOURNAL OF MEMBRANE SCIENCE 169[2], 287-299, 2000

Número de citações na Web of Science:105

[E006-2000] "Evidence for phase-separated quantum dots in cubic InGaN layers from resonant Raman scattering"

Lemos, V.; Silveira, E.; Leite, J.R.; Tabata, A.; Trentin, R.; Scolfaro, L.M.R.; Frey, T.; As, D.J.; Schikora, D.; Lischka, K.

The emission of light in the blue-green region from cubic $\text{In}_x\text{Ga}_{1-x}\text{N}$ alloys grown by molecular beam epitaxy is observed at room temperature and 30 K. By using selective resonant Raman spectroscopy (RRS) we demonstrate that the emission;

is due to quantum confinement effects taking place in phase-separated In-rich quantum dots formed in the layers. RRS data show that the In content of the dots fluctuates across the volume of the layers. We find that dot size and alloy fluctuation determine the emission wavelengths.

PHYSICAL REVIEW LETTERS 84[16], 3666-3669, 2000

Número de citações na Web of Science:80

[E007-2000] "Surface and electronic structure of titanium dioxide photocatalysts"

Bilmes, S.A.; Mandelbaum, P.; Alvarez, F.; Victoria, N.M.

TiO₂ films prepared by sol-gel route are active photocatalysts for the oxidation of organics in photoelectrochemical cells. The as-grown films for photocatalysis applications and those exposed to Ar⁺ or H⁺ ion bombardment are characterized by different spectroscopic methods, such as X-ray diffraction (XRD), atomic force microscopy (AFM), UV-vis transmittance, photothermal deflection spectroscopy (PDS) and X-ray photoelectron spectroscopy (XPS), as well as by conductance. This material has defects associated with oxygen vacancies produced during the sample preparation which support nondissociative adsorption of O₂ when films are exposed to air. Charge transfer from reduced Ti species to adsorbed dioxygen leads to Ti-O₂(-) surface complexes that are partially removed by heating at 200 degreesC, and fully removed after 30 min ion bombardment. By comparison with the relatively well-understood structural defects of bombarded TiO₂ we arise to a quite complete structural model of the as grown material which corresponds to an amorphous semiconductor possessing relative low disorder and density of states as compared with a pure amorphous material. These TiO₂ films are modeled as low size crystalline domain embedded in an amorphous matrix whose electronic structure exhibit exponential band tails and a narrow band close to the conduction band. The latter is fully or partially occupied depending on the presence of adsorbed electron scavengers such as dioxygen.

JOURNAL OF PHYSICAL CHEMISTRY B 104[42], 9851-9858, 2000

Número de citações na Web of Science:66

[E008-2000] "Status of the solution to the solar neutrino problem based on nonstandard neutrino interactions"

Bergmann, S.; Guzzo, M.M.; de Holanda, P.C.; Krastev, P.I.; Nunokawa, H.

We analyze the current status of the solution to the solar neutrino problem based both on (a) nonstandard flavor-changing neutrino interactions (FCNI) and (b) nonuniversal flavor diagonal neutrino interactions (FDNI). We find that FCNI and FDNI with matter in the Sun as well as in the Earth provide a good fit not only to the total rate measured by all solar neutrino experiments but also to the day-night and seasonal variations of the event rate, as well as the recoil electron energy spectrum measured by the SuperKamiokande Collaboration. This solution does not require massive neutrinos and neutrino mixing in vacuum. Stringent experimental constraints on FCNI from bounds on lepton flavor violating decays and on FDNI from limits on lepton universality violation rule out $\nu(e) \rightarrow \nu(\mu)$ transitions induced by new physics as a solution to the solar neutrino problem. However, a solution involving $\nu(e) \rightarrow \nu(\tau)$ transitions is viable and could be tested independently by the upcoming B factories if flavor violating tan decays would be observed at a rate close to the present upper bounds.

PHYSICAL REVIEW D 62[7], 073001, 2000

Número de citações na Web of Science:64

[E009-2000] “Measuring leptonic CP violation by low energy neutrino oscillation experiments”

Minakata, H.; Nunokawa, H.

We uncover an interesting phenomenon that neutrino flavor transformation in slowly varying matter density imitates almost exactly that of vacuum neutrino oscillation under suitably chosen experimental parameters. It allows us to have relatively large CP violating measure $\Delta P = P(\nu(\mu) \rightarrow \nu(e)) - P(\langle \nu \rangle \rightarrow \langle \nu \rangle)$ over $\bar{\nu}(\mu) \rightarrow \langle \nu \rangle$ over $\bar{\nu}(e)$ which is essentially free from matter effect contamination. We utilize this phenomenon to design a low-energy long-baseline neutrino oscillation experiment to measure the leptonic CP violating phase.

PHYSICS LETTERS B 495[3-4], 369-377, 2000

Número de citações na Web of Science:60

[E010-2000] “Magnetic microwires as macrospins in a long-range dipole-dipole interaction”

Sampaio, L.C.; Sinnecker, E.H.C.P.; Cernicchiaro, G.R.C.; Knobel, M.; Vazquez, M.; Velazquez, J.

The long-range dipole-dipole interaction in an array of ferromagnetic microwires is studied through magnetic hysteresis measurements and Monte Carlo simulation. The experimental study has been performed on glass-coated amorphous Fe_{77.5}Si_{7.5}B₁₅ microwire with diameter of 5 μ m and lengths from 5 to 60 mm. Hysteresis loops performed at room temperature for an array of N microwires (N = 2, 3, 3, and 5) exhibit jumps and plateaus on the demagnetization, each step correspondent to the magnetization reversal of an individual wire. A model has been constructed taking into account the fact that the magnetization reversal is nucleated at the ends of each wire, under the influence of a dipolar field due to all other wires. Measurements for two wires allowed us to conclude that the dipolar field (or constant coupling) is independent of distance, at least for an array of a few wires. With the exception of three wires, where frustration seems to be present, the predicted reversal fields of our model are in good agreement with measurements. In order to study the role played by the number of wires on the demagnetization process, we calculate hysteresis loops for a large number of wires through the Monte Carlo method.

PHYSICAL REVIEW B 61[13], 8976-8983, 2000

Número de citações na Web of Science:58

Trabalhos mais citados - 2001

[E001-2001] “Magnetic carbon (Retracted Article. See vol 440, pg 707, 2006)”

Makarova, T.L.; Sundqvist, B.; Hohne, R.; Esquinazi, P.; Kopelevich, Y.; Scharff, P.; Davydov, V.A.; Kashevarova, L.S.; Rakhmanina, A.V.

The discovery of nanostructured forms of molecular carbon has led to renewed interest in the varied properties of this element. Both graphite and C(60) can be electron-doped by alkali metals(1) to become superconducting; transition temperatures of up to 52 K have been attained by field-induced hole-doping of C(60) (ref. 2). Recent experiments(3,4) and theoretical studies(5,6) have suggested that electronic instabilities in pure graphite may give rise to superconducting and ferromagnetic properties, even at room temperature. Here we report the serendipitous discovery of strong magnetic signals in rhombohedral C(60).

Our intention was to search for superconductivity in polymerized C(60); however, it appears that our high-pressure, high-temperature polymerization process results in a magnetically ordered state. The material exhibits features typical of ferromagnets: saturation magnetization, large hysteresis and attachment to a magnet at room temperature. The temperature dependences of the saturation and remanent magnetization indicate a Curie temperature near 500 K.

NATURE 413[6857], 716-718, 2001

Número de citações na Web of Science:380

[E002-2001] “Prospect of creating a composite Fermi-Bose superfluid”

Timmermans, E.; Furuya, K.; Milonni, P.W.; Kerman, A.K.

We show that composite Fermi-Bose superfluids can be created in cold-atom traps by employing a Feshbach resonance or coherent photoassociation. The bosonic molecular condensate created in this way implies a new fermion pairing mechanism associated with the exchange of fermion pairs between the molecular condensate and an atomic fermion superfluid. We predict macroscopically coherent, Josephson-Like oscillations of the atomic and molecular populations in response to a sudden change of the molecular energy, and suggest that these oscillations will provide an experimental signature of the pairing.

PHYSICS LETTERS A 285[3-4], 228-233, 2001

Número de citações na Web of Science:272

[E003-2001] “How do gold nanowires break?”

da Silva, E.Z.; da Silva, A.J.R.; Fazio, A.

Suspended gold nanowires have recently been made in an ultrahigh vacuum and were imaged by electron microscopy. Using realistic molecular dynamics simulation, we study the mechanisms of formation, evolution, and breaking of these atomically thin Au nanowires under stress. We show how defects induce the formation of constrictions that eventually will form the one-atom chains. We find that these chains, before breaking, are five atoms long, which is in excellent agreement with experimental results. After the nanowire's rupture, we analyze the structure of the Au tip, which we believe will be universally present due to its highly symmetric nature.

PHYSICAL REVIEW LETTERS 87[25], 256102, 2001

Número de citações na Web of Science:173

[E004-2001] “Theory of magnetic anisotropy in III1-xMnxV ferromagnets”

Abolfath, M.; Jungwirth, T.; Brum, J.; MacDonald, A.H.

We present a theory of magnetic anisotropy in III1-xMnxV-diluted magnetic semiconductors with carrier-induced ferromagnetism. The theory is based on four- and six-band envelope function models for the valence-band holes and a mean-field treatment of their exchange interactions with Mn²⁺ ions. We find that easy-axis reorientations can occur as a function of temperature, carrier density p, and strain. The magnetic anisotropy in strain-free samples is predicted to have a p^{5/3} hole-density dependence at small p, a p⁻¹ dependence at large p, and remarkably large values at intermediate densities. An explicit expression, valid at small p, is given for the uniaxial contribution to the magnetic anisotropy due to unrelaxed epitaxial growth lattice-matching strains.

Results of our numerical simulations are in agreement with magnetic anisotropy measurements on samples with both compressive and tensile strains. We predict that decreasing the hole density in current samples will lower the ferromagnetic transition temperature, but will increase the magnetic anisotropy energy and the coercivity.

PHYSICAL REVIEW B 63[5], 054418, 2001

Número de citações na Web of Science:158

[E005-2001] “Granular Cu-Co alloys as interacting superparamagnets”

Allia, P.; Coisson, M.; Tiberto, P.; Vinai, F.; Knobel, M.; Novak, M.A.; Nunes, W.C.

The anhysteretic magnetization of the granular metallic alloy Cu(90)Co(10) is experimentally studied over a wide temperature range (2-700 K). The measurements definitely exclude that this alloy is a simple superparamagnet, even in the high-temperature limit, although some features of granular systems [such as the typical Langevin-like form of the anhysteretic magnetization curves $M(H)$] are often taken as evidence of superparamagnetism. A phenomenological theory is proposed, explicitly considering that particle moments interact through long-ranged dipolar random forces, whose effect is pictured in terms of a temperature T^* , adding to the actual temperature T in the denominator of the Langevin function argument. This simple formula explains all features of the experimental $M(H)$ curves. The theory indicates that the actual magnetic moments on interacting Co particles are systematically larger than those obtained fitting the magnetic data to a conventional Langevin function. The Cu(90)Co(10) granular alloy is therefore identified as an “interacting superparamagnet” ISR The ISP regime appears as separating the high-temperature, conventional superparamagnetic phase from the low-temperature, blocked-particle regime. In this way, a magnetic-regime diagram can be drawn for each granular system. The competition between single-particle and collective blocking mechanisms is briefly analyzed. The proposed interpretation is thought to be applicable to other fine particle systems; its main features and intrinsic limits are discussed.

PHYSICAL REVIEW B 64[14], 144420, 2001

Número de citações na Web of Science:140

[E006-2001] “Exploring neutrino mixing with low energy superbeams”

Minakata, H.; Nunokawa, H.

We explore the features of neutrino oscillation which are relevant for measurements of the leptonic CP violating phase δ and the sign of Δm_{13}^2 in experiments with low-energy conventional superbeams. Toward the goal, we introduce a new powerful tool called the “CP trajectory diagram in bi-probability space” which allows us to represent pictorially the three effects, the effects of (a) genuine CP violation due to the $\sin \delta$ term, (b) CP conserving $\cos \delta$ term, and (c) fake CP violation due to earth matter, separately in a single diagram. By using the diagram, we observe that there is a two-fold ambiguity in the determination of δ which is related with the sign of Δm_{13}^2 . Possible ways of resolving the ambiguity are discussed. In particular, we point out that an in situ simultaneous measurement of δ and the sign of Δm_{13}^2 can be carried out at distances of about 700 km, or at the Phase II of the JHF experiment provided that $\sin \delta \cdot \Delta m_{13}^2 < 0$, both with a megaton class water Cherenkov detector.

JOURNAL OF HIGH ENERGY PHYSICS 10[001], 2001

Número de citações na Web of Science:127

[E007-2001] “Anisotropic superconducting properties of aligned MgB2 crystallites”

de Lima, O.F.; Ribeiro, R.A.; Avila, M.A.; Cardoso, C.A.; Coelho, A.A.

Samples of aligned MgB₂ crystallites have been prepared, allowing for the first time the direct identification of an upper critical field anisotropy $H_{c2}(ab)/H_{c2}(c) = \xi(ab)/\xi(c)$ similar or equal to 1.7, with $\xi(o,ab)$ similar or equal to 70 Angstrom, $\xi(o,c) = 40$ Angstrom, and a mass anisotropy ratio $m(ab)/m(c)$ similar or equal to 0.3. A ferromagnetic background signal was identified, possibly related to the raw materials purity.

PHYSICAL REVIEW LETTERS 86[26], 5974-5977, 2001

Número de citações na Web of Science:109

[E008-2001] “Real-time imaging of atomistic process in one-atom-thick metal junctions”

Rodrigues, V.; Ugarte, D.

We present an in situ and time resolved high-resolution transmission electron microscopy study of the atomistic process during the last elongation stages of gold nanojunctions. In particular, we concentrate on suspended chains of atoms, which have shown to be remarkably stable, although they present rather long bonds (3.0-3.6 Angstrom). One-atom-thick junctions are robust, but their attachment points move rather easily on the metal surface, allowing the accommodation of apex movements or rotations.

PHYSICAL REVIEW B 63[7], 073405, 2001

Número de citações na Web of Science:109

[E009-2001] “Semiclassical approximations in phase space with coherent states”

Baranger, M.; de Aguiar, M.A.M.; Keck, F.; Korsch, H.J.; Schellhaass, B.

We present a complete derivation of the semiclassical limit of the coherent-state propagator in one dimension, starting from path integrals in phase space. We show that the arbitrariness in the path integral representation, which follows from the overcompleteness of the coherent states, results in many different semiclassical limits. We explicitly derive two possible semiclassical formulae for the propagator, we suggest a third one, and we discuss their relationships. We also derive an initial-value representation for the semiclassical propagator, based on an initial Gaussian wavepacket. It turns out to be related to, but different from, Heller’s thawed Gaussian approximation. It is very different from the Herman-Kluk formula, which is not a correct semiclassical limit. We point out errors in two derivations of the latter. Finally we show how the semiclassical coherent-state propagators lead to WKB-type quantization rules and to approximations for the Husimi distributions of stationary states.

JOURNAL OF PHYSICS A-MATHEMATICAL AND GENERAL, 34[36], 7227-7286, 2001

Número de citações na Web of Science:105

[E010-2001] “(3+1)-spectrum of neutrino masses: a chance for LSND?”

Peres, O.L.G.; Smirnov, A.Y.

If active to active neutrino transitions are dominant modes of the atmospheric ($\nu(\mu) \rightarrow \nu(\tau)$) and the solar neutrino oscillations ($\nu e \rightarrow \nu(\mu)/\nu(\tau)$), as is indicated by recent data, the favoured scheme which accommodates the LSND result - the so-called (2 + 2)-scheme - should be discarded. We introduce the parameters $\eta(\text{atm})(s)$ and $\eta(\text{sun})(s)$ which quantify an involvement of the sterile component in the solar and atmospheric neutrino oscillations. The (2 + 2)-scheme predicts $\eta(\text{atm})(s) + \eta(\text{sun})(s) = 1$ and the experimental proof of deviation from this equality will discriminate the scheme. In this connection the (3 + 1)-scheme is revisited in which the fourth (predominantly sterile) neutrino is isolated from a block of three flavour neutrinos by the mass gap $\Delta m(\text{LSND})(2)$ similar to $(0.4-10) \text{ eV}(2)$. We find that in the (3 + 1)-scheme the LSND result can be reconciled with existing bounds on $\nu(e)(-)$ and $\nu(\mu)$ -disappearance at 95-99% C.L. The generic prediction of the scheme is the $\nu(e)$ and $\nu(\mu)$ -disappearance probabilities at the level of present experimental bounds. The possibility to strengthen the bound on $\nu(\mu)$ -disappearance in the KEK - front detector experiment is studied. We consider phenomenology of the (3 + 1)-scheme, in particular, its implications for the atmospheric neutrinos, neutrinoless double beta decay searches, supernova neutrinos and primordial nucleosynthesis.

NUCLEAR PHYSICS B 599[1-2], 3-29, 2001

Número de citações na Web of Science:96

Trabalhos mais citados - 2002

[E001-2002] "Multiple ionization of atom clusters by intense soft X-rays from a free-electron laser"

Wabnitz, H.; Bittner, L.; de Castro, A.R.B.; Dohrmann, R.; Gurtler, P.; Laarmann, T.; Laasch, W.; Schulz, J.; Swiderski, A.; von Haefen, K.; Moller, T.; Faatz, B.; Fateev, A.; Feldhaus, J.; Gerth, C.; Hahn, U.; Saldin, E.; Schneidmiller, E.; Sytchev, K.; Tiedtke, K.; Treusch, R.; Yurkov, M.

Intense radiation from lasers has opened up many new areas of research in physics and chemistry, and has revolutionized optical technology. So far, most work in the field of nonlinear processes has been restricted to infrared, visible and ultraviolet light(1), although progress in the development of X-ray lasers has been made recently(2). With the advent of a free-electron laser in the soft-X-ray regime below 100 nm wavelength(3), a new light source is now available for experiments with intense, short-wavelength radiation that could be used to obtain deeper insights into the structure of matter. Other free-electron sources with even shorter wavelengths are planned for the future. Here we present initial results from a study of the interaction of soft X-ray radiation, generated by a free-electron laser, with Xe atoms and clusters. We find that, whereas Xe atoms become only singly ionized by the absorption of single photons, absorption in clusters is strongly enhanced. On average, each atom in large clusters absorbs up to 400 eV, corresponding to 30 photons. We suggest that the clusters are heated up and electrons are emitted after acquiring sufficient energy. The clusters finally disintegrate completely by Coulomb explosion.

NATURE 420[6915], 482-485, 2002

Número de citações na Web of Science:287

[E002-2002] "Giant magnetoimpedance: concepts and recent progress"

Knobel, M.; Pirota, K.R.

The giant magnetoimpedance effect (GMI) consists in drastic changes of the complex impedance of soft magnetic materials upon the application of an external magnetic field. The GMI effect is strongly dependent on the frequency of the applied current and the magnetic anisotropies present in the material, among other factors, which spawn a number of interesting new magnetic phenomena. In this context, one can roughly separate the research on GMI into approximately three aspects: (i) theory; (ii) applications and (iii) as a tool to investigate other magnetic parameters. In this work, an updated review of all these aspects is given.

JOURNAL OF MAGNETISM AND MAGNETIC MATERIALS 242, 33-40, Part 1, 2002

Número de citações na Web of Science:110

[E003-2002] "Quantum conductance in silver nanowires: Correlation between atomic structure and transport properties"

Rodrigues, V.; Bettini, J.; Rocha, A.R.; Rego, L.G.C.; Ugarte, D.

We have analyzed the atomic arrangements and quantum conductance of silver nanowires generated by mechanical elongation. The surface properties of Ag induce unexpected structural properties, such as, for example, predominance of high aspect-ratio rodlike wires. The structural behavior was used to understand the Ag quantum conductance data and the proposed correlation was confirmed by means of theoretical calculations. These results emphasize that the conductance of metal point contacts is determined by the preferred atomic structures, and that atomistic descriptions are essential to interpret the quantum transport behavior of metal nanostructures.

PHYSICAL REVIEW B 65[15], 153402, 2002

Número de citações na Web of Science:103

[E004-2002] "Thermoremanence and zero-field-cooled/field-cooled magnetization study of Co-x(SiO2)(1-x) granular films"

Denardin, J.C.; Brandl, A.L.; Knobel, M.; Panissod, P.; Pakhomov, A.B.; Liu, H.; Zhang, X.X.

A systematic study of Co(SiO₂) granular films by means of transmission electron microscopy (ITEM), dc and ac initial magnetic susceptibility, and thermoremanent magnetization (TRM) is presented. The experimental results are compared with simulations of zero-field-cooled (ZFC) and field-cooled (FC) magnetization and TRM curves obtained using a simple model of noninteracting nanoparticles. The Simulated ZFC/FC curves, using the actual parameters obtained from the TEM images, show a different behavior than the experimental magnetic data. The effect of the dipolar interaction among particles introduces a self-averaging effect over a correlation length Λ , which results in a larger average "magnetic" size of the apparent particles together with a narrower size distribution. The analysis of the ZFC/FC curves in the framework of independent "particle clusters" of volume Λ^3 , involving about 25 real particles, explains very well the observed difference between the experimental data for the median blocking temperature [T-B] and their distribution width with respect to the ones expected from the structural observations by TEM. The experimental TRM curves also differ from those obtained from the theoretical model, starting to decrease at a lower temperature than expected from the model, also indicating the strong influence of dipole-dipole interactions.

PHYSICAL REVIEW B 65[6], 064422, 2002

Número de citações na Web of Science:87

[E005-2002] "Origin of anomalously long interatomic distances in suspended gold chains"

Legoas, S.B.; Galvao, D.S.; Rodrigues, V.; Ugarte, D.

The discovery of long bonds in gold atom chains has represented a challenge for physical interpretation. In fact, interatomic distances frequently attain 3.0-3.6 Angstrom values, and distances as large as 5.0 Angstrom may be occasionally observed. Here we studied gold chains by transmission electron microscopy and performed theoretical calculations using cluster ab initio density functional formalism. We show that the insertion of two carbon atoms is required to account for the longest bonds, while distances above 3 Angstrom may be due to a mixture of clean and one C atom contaminated bonds.

PHYSICAL REVIEW LETTERS 88[7], 076105, 2002

Número de citações na Web of Science:77

[E006-2002] "Crystal structure of recombinant human interleukin-22"

Nagem, R.A.P.; Colau, D.; Dumoutier, L.; Renauld, J.C.; Ogata, C.; Polikarpov, I.

Interleukin-22 (IL-10-related T cell-derived inducible factor/IL-TIF/IL-22) is a novel cytokine belonging to the IL-10 family. Recombinant human IL-22 (hIL-22) was found to activate the signal transducers and activators of transcription factors I and 3 as well as acute phase reactants in several hepatoma cell lines, suggesting its involvement in the inflammatory response. The crystallographic structure of recombinant hIL-22 has been solved at 2.0 Angstrom resolution using the SIRAS method. Contrary to IL-10, the hIL-22 dimer does not present an interpenetration of the secondary-structure elements belonging to the two distinct polypeptide chains but results from interface interactions between monomers. Structural differences between these two cytokines, revealed by the crystallographic studies, clearly indicate that, while a homodimer of IL-10 is required for signaling, hIL-22 most probably interacts with its receptor as a monomer.

STRUCTURE 10[8], 1051-1062, 2002

Número de citações na Web of Science:60

[E007-2002] "Hybrid simulations of extensive air showers"

Alvarez-Muniz, J.; Engel, R.; Gaisser, T.K.; Ortiz, J.A.; Stanev, T.

We present a fast one dimensional hybrid method to efficiently simulate extensive air showers up to the highest observed energies. Based on precalculated pion showers and a bootstrap technique, our method predicts the average shower profile, the number of muons at detector level above several energy thresholds as well as the fluctuations of the electromagnetic and hadronic components of the shower. We study the main characteristics of proton-induced air showers up to ultra high energy, comparing the predictions of three different hadronic interaction models: SIBYLL 1.7, SIBYLL 2.1 and QGSJET98. The influence of the hadronic interaction models on the shower evolution, in particular the elongation rate, is discussed and the applicability of analytical approximations is investigated.

PHYSICAL REVIEW D 66[3], 033011, 2002

Número de citações na Web of Science:52

[E008-2002] "Status of a hybrid three-neutrino interpretation of neutrino data"

Guzzo, M.M.; de Holanda, P.C.; Maltoni, M.; Nunokawa, H.; Tortola, M.A.; Valle, J.W.F.

We re-analyse the non-standard interaction (NSI) solutions to the solar neutrino problem in the light of the latest solar as well as atmospheric neutrino data. The latter require oscillations (OSC), while the former do not. Within such a three-neutrino framework the solar and atmospheric neutrino sectors are connected not only by the neutrino mixing angle θ_{13} constrained by reactor and atmospheric data, but also by the flavour-changing (FC) and non-universal (NU) parameters accounting for the solar data. Since the NSI solution is energy-independent the spectrum is undistorted, so that the global analysis observables are the solar neutrino rates in all experiments as well as the Super-Kamiokande day-night measurements. We find that the NSI description of solar data is slightly better than that of the OSC solution and that the allowed NSI regions are determined mainly by the rate analysis. By using a few simplified ansatzes for the NSI interactions we explicitly demonstrate that the NSI values indicated by the solar data analysis are fully acceptable also for the atmospheric data.

NUCLEAR PHYSICS B 629[1-3], 479-490, 2002

Número de citações na Web of Science:47

[E009-2002] "Field-induced metal-insulator transition in the c-axis resistivity of graphite"

Kempa, H.; Esquinazi, P.; Kopelevich, Y.

We show that the resistivities perpendicular $\rho(c)$ and parallel $\rho(a)$ to the basal planes of different graphite samples show similar magnetic-field-driven metal-insulator transitions at a field $B(c)$ similar to 0.1 T applied parallel to the c axis. Our results demonstrate the universality of the recently found scaling in $\rho(a)$ of graphite and indicate that the metalliclike temperature dependence of $\rho(c)$ is directly correlated to that of $\rho(a)$. The similar magnetoresistance found for both resistivities, the violation of Kohler's rule, and the field-induced transition indicate that the semiclassical transport theory is inadequate to understand the transport properties of graphite.

PHYSICAL REVIEW B 65[24], 241101, 2002

Número de citações na Web of Science:46

[E010-2002] "Controlled molecular alignment in phthalocyanine thin films on stepped sapphire surfaces"

Osso, J.O.; Schreiber, F.; Kruppa, V.; Dosch, H.; Garriga, M.; Alonso, M.I.; Cerdeira, F.

We report a detailed study of the growth and structure of thin films of copper hexadecafluorophthalocyanine (F16CuPc) on sapphire. These films show very good out of plane order and have X-ray rocking widths of around 0.02 degrees. If prepared under suitable conditions of A-plane sapphire substrates, the molecules align without significant azimuthal dispersion. Growth on MgO (001) and oxidized silicon wafers resulted in a comparable out-of-plane structure, but showed no azimuthal order. We find that the azimuthal alignment on sapphire is induced by the step edges along the c-axis of the sapphire, which serve as templates for the growth. For growth at different substrate temperatures, we find a monotonic change of the molecular out-of-plane tilt angle, as obtained from Raman scattering, which is accompanied by a change of the out-of-plane lattice parameter.

ADVANCED FUNCTIONAL MATERIALS 12[6-7], 455-460, 2002

Número de citações na Web of Science:42

Trabalhos mais citados em 2003

[E001-2003] "Possible Fulde-Ferrell-Larkin-Ovchinnikov superconducting state in CeCoIn₅"

Bianchi, A (Bianchi, A); Movshovich, R (Movshovich, R); Capan, C (Capan, C); Pagliuso, PG (Pagliuso, PG); Sarrao, JL (Sarrao, JL)

We report specific heat measurements of the heavy fermion superconductor CeCoIn₅ in the vicinity of the superconducting critical field H_{c2} , with magnetic fields in the [110], [100], and [001] directions, and at temperatures down to 50 mK. The superconducting phase transition changes from second to first order for fields above 10 T for H_{parallel} to [110] and H_{parallel} to [100]. In the same range of magnetic fields, we observe a second specific heat anomaly within the superconducting state. We interpret this anomaly as a signature of a Fulde-Ferrell-Larkin-Ovchinnikov (FFLO) inhomogeneous superconducting state. We obtain similar results for H_{parallel} to [001], with the FFLO state occupying a smaller part of the phase diagram.

PHYSICAL REVIEW LETTERS 91[18], 187004, 2003

Número de citações na Web of Science: 298

[E002-2003] "Molecular-dynamics simulations of carbon nanotubes as gigahertz oscillators"

Legoas, S.B.; Coluci, V.R.; Braga, S.F.; Coura, P.Z.; Dantas, S.O.; Galvao, D.S.

Recently, Zheng and Jiang [Phys. Rev. Lett. 88, 045503 (2002)] have proposed that multiwalled carbon nanotubes could be the basis for a new generation of nano-oscillators in the several gigahertz range. In this Letter, we present the first molecular dynamics simulation for these systems. Different nanotube types were considered in order to verify the reliability of such devices as gigahertz oscillators. Our results show that these nano-oscillators are dynamically stable when the radii difference values between inner and outer tubes are of similar to 3.4 Angstrom. Frequencies as large as 38 GHz were observed, and the calculated force values are in good agreement with recent experimental investigations.

PHYSICAL REVIEW LETTERS 90[5], 055504, 2003

Número de citações na Web of Science: 224

[E003-2003] "Avoided antiferromagnetic order and quantum critical point in CeCoIn₅"

Bianchi, A.; Movshovich, R.; Vekhter, I.; Pagliuso, P.G.; Sarrao, J.L.

We measured the specific heat and resistivity of heavy fermion CeCoIn₅ between the superconducting critical field $H_{c2}=5$ T and 9 T, with the field in the [001] direction, and at temperatures down to 50 mK. At 5 T the data show a non-Fermi liquid (NFL) behavior down to the lowest temperatures. At the field above 8 T the data exhibit a crossover from the Fermi liquid to a non-Fermi liquid behavior. We analyzed the scaling properties of the specific heat and compared both the resistivity and the specific heat with the predictions of a spin-fluctuation theory. Our analysis leads us to suggest that the NFL behavior is due to incipient antiferromagnetism (AFM) in CeCoIn₅ with the quantum critical point in the vicinity of H_{c2} . Below H_{c2} the AFM phase which competes with the paramagnetic ground state is superseded by the superconducting transition.

PHYSICAL REVIEW LETTERS 91[25], 257001, 2003

Número de citações na Web of Science: 181

[E004-2003] "Reentrant metallic behavior of graphite in the quantum limit"

Kopelevich, Y.; Torres, J.H.S.; da Silva, R.R.; Mrowka, F.; Kempa, H.; Esquinazi, P.

Magnetotransport measurements performed on several well-characterized highly oriented pyrolytic graphite and single crystalline Kish graphite samples reveal a reentrant metallic behavior in the basal-plane resistance at high magnetic fields, when only the lowest Landau levels are occupied. The results suggest that the quantum Hall effect and Landau-level-quantization-induced superconducting correlations are relevant to understand the metalliclike state(s) in graphite in the quantum limit.

PHYSICAL REVIEW LETTERS 90[15], 156402, 2003

Número de citações na Web of Science: 96

[E005-2003] "Spin glass behavior in RuSr₂Gd_{1.5}Ce_{0.5}Cu₂O_{10-delta}"

Cardoso, C.A.; Araujo-Moreira, F.M.; Awana, V.P.S.; Takayama-Muromachi, E.; de Lima, O.F.; Yamauchi, H.; Karppinen, M.

The dynamics of the magnetic properties of polycrystalline RuSr₂Gd_{1.5}Ce_{0.5}Cu₂O_{10-delta} (Ru-1222) have been studied by ac susceptibility and dc magnetization measurements, including relaxation and ageing studies. Ru-1222 is a reported magnetosuperconductor with Ru spins magnetic ordering at temperatures near 100 K and superconductivity in Cu-O-2 planes below T_c similar to 40 K. The exact nature of Ru spins magnetic ordering is still being debated, and no conclusion has been reached yet. In this work, a frequency-dependent cusp was observed in $\chi''(ac)$ vs T measurements, which is interpreted as a spin glass transition. The change in the cusp position with frequency follows the Vogel-Fulcher law, which is commonly accepted to describe a spin-glass with magnetically interacting clusters. Such an interpretation is supported by thermomagnetic magnetization (TRM) measurements at $T=60$ K. TRM relaxations are well described by a stretched exponential relation, and present significant aging effects.

PHYSICAL REVIEW B 67[2], 020407, 2003

Número de citações na Web of Science: 73

[E006-2003] "LMA MSW solution of the solar neutrino problem and first KamLAND results"

de Holanda, P.C.; Smirnov, A.Y.

The first KamLAND results are shown to be in very good agreement with the predictions made on the basis of the solar neutrino data and the LMA realization of the MSW mechanism. We perform a combined analysis of the KamLAND (rate, spectrum) and the solar neutrino data with a free boron neutrino flux $f(B)$. The best fit values of neutrino parameters are $\Delta m^2 = 7.3 \times 10^{-5}$ eV², $\tan^2 \theta = 0.41$ and $f(B) = 1.05$ with the 1sigma intervals: $\Delta m^2 = (6.2-8.4) \times 10^{-5}$ eV², $\tan^2 \theta = 0.33-0.54$. We find the 3sigma upper bounds: $\Delta m^2 < 2.8 \times 10^{-4}$ eV² and $\tan^2 \theta < 0.84$, and the lower bound $\Delta m^2 > 4 \times 10^{-5}$ eV². At 99% CL the KamLAND spectral result splits the LMA region into two parts with the preferred one at $\Delta m^2 < 10^{-4}$ eV². The higher Δm^2 region is accepted at about the 2 sigma level. We show that effects of non-zero 13-mixing, $\sin^2 \theta_{13} \leq 0.04$, are small, leading to a slight improvement of the fit in the higher Δm^2 region. At the best fit point we predict for SNO: $CC/NC = 0.33(-0.03)(+0.05)$ and $A(DN)(SNO) = 2.8 \pm 0.8\%$ (68% CL), and $A(DN)(SNO) < 9\%$ at the 3 sigma level. Further improvements in the determination of the oscillation parameters are discussed and implications of the solar neutrino and KamLAND results are considered.

JOURNAL OF COSMOLOGY AND ASTROPARTICLE PHYSICS 2, 001, 2003

Número de citações na Web of Science:70

[E007-2003] “Effect of impurities in the large Au-Au distances in gold nanowires”

Novaes, F.D.; da Silva, A.J.R.; da Silva, E.Z.; Fazzio, A.

Experimentally obtained atomically thin gold nanowires have presented exceedingly large Au-Au interatomic distances before they break. Since no theoretical calculations of pure gold nanowires have been able to produce such large distances, we have investigated, through ab initio calculations, how impurities could affect them. We have studied the effect of H, B, C, N, O, and S impurities on the nanowire electronic and structural properties, in particular how they affect the maximum Au-Au bond length. We find that the most likely candidates to explain the distances in the range of 3.6 Angstrom and 4.8 Angstrom are H and S impurity atoms, respectively.

PHYSICAL REVIEW LETTERS 90[3], 036101, 2003

Número de citações na Web of Science:59

[E008-2003] “Optical tweezers for measuring red blood cell elasticity: application to the study of drug response in sickle cell disease”

Brandao, M.M.; Fontes, A.; Barjas-Castro, M.L.; Barbosa, L.C.; Costa, F.F.; Cesar, C.L.; Saad, S.T.O.

The deformability of erythrocytes is a critical determinant of blood flow in microcirculation. By capturing red blood cells (RBC) with optical tweezers and dragging them through a viscous fluid we were able to measure their overall elasticity. We measured, and compared, the RBC deformability of 15 homozygous patients (HbSS) including five patients taking hydroxyurea (HU) for at least 6 months (HbSS/HU), 10 subjects with sickle cell trait (HbAS) and 35 normal controls. Our results showed that the RBC deformability was significantly lower in haemoglobin S (HbS) subjects (HbSS and HbAS), except for HbSS/HU cells, whose deformability was similar to the normal controls. Our data showed that the laser optical tweezers technique is able to detect differences in HbS RBC from subjects taking HU, and to differentiate RBC from normal controls and HbAS, indicating that this is a very sensitive method and can be applied for detection of drug-response in sickle cell disease.

EUROPEAN JOURNAL OF HAEMATOLOGY 70[4], 207-211, 2003

Número de citações na Web of Science:55

[E009-2003] “Magnetism in photopolymerized fullerenes”

Makarova, T.L.; Han, K.H.; Esquinazi, P.; da Silva, R.R.; Kopelevich, Y.; Zakharova, I.B.; Sundqvist, B.

The phototransformation of bulk C-60 and laser- and electron-beam treatment of C-60 films in air changes their magnetic properties. Nonlinear magnetization is observed only for samples irradiated in the presence of oxygen, while, in the case of pressure-polymerized C-60, oxygen adversely affects the magnetic properties. The contrasting roles of oxygen in these processes are discussed. Magnetic force microscopy shows that laser- and electron-beam irradiation of fullerene films produces magnetic images which are highly correlated with the topographic images.

CARBON 41[8], 1575-1584, 2003

Número de citações na Web of Science:42

[E010-2003] “High resolution photoemission study of CdSe and CdSe/ZnS core-shell nanocrystals”

Borchert, H.; Talapin, D.V.; McGinley, C.; Adam, S.; Lobo, A.; de Castro, A.R.B.; Moller, T.; Weller, H.

Colloidally prepared CdSe and CdSe/ZnS core-shell nanocrystals passivated with trioctylphosphine/trioctylphosphine oxide and hexadecylamine have been studied by photoelectron spectroscopy with tuneable synchrotron radiation. High-resolution spectra of the Se 3d level in CdSe nanocrystals indicate the bonding of organic ligands not only to surface Cd but also to surface Se atoms. The investigation of the CdSe/ZnS core-shell nanocrystals allows us to determine the average thickness of the ZnS shell and to study the interface between the two semiconductor nanomaterials. The photoemission spectra indicate a rather well ordered interface. No evidence for interfacial bonds other than Cd-S and Se-Zn is found.

JOURNAL OF CHEMICAL PHYSICS 119[3], 1800-1807, 2003

Número de citações na Web of Science:41

Trabalhos mais citados - 2004

[E001-2004] “Properties and performance of the prototype instrument for the Pierre Auger Observatory”

Abraham, J.; Aglietta, M.; Aguirre, I.C.; Albrow, M.; Allard, D.; Allekotte, I.; Allison, P.; Chinellato, J.A.; Escobar, C.O.; Kemp, E.; Shibuya, E.; et al.

Auger Collaboration

Construction of the first stage of the Pierre Auger Observatory has begun. The aim of the Observatory is to collect unprecedented information about cosmic rays above 10(18) eV. The first phase of the project, the construction and operation of a prototype system, known as the engineering array, has now been completed. It has allowed all of the sub-systems that will be used in the full instrument to be tested under field conditions. In this paper, the properties and performance of these sub-systems are described and their success illustrated with descriptions of some of the events recorded thus far.

NUCLEAR INSTRUMENTS & METHODS IN PHYSICS RESEARCH SECTION A-ACCELERATORS SPECTROMETERS DETECTORS AND ASSOCIATED EQUIPMENT 523[1-2], 50-95, 2004

Número de citações na Web of Science:372

[E002-2004] “Pressure-induced colossal magnetocaloric effect in MnAs”

Gama, S.; Coelho, A.A.; de Campos, A.; Carvalho, A.M.G.; Gandra, F.C.G.; von Ranke, P.J.; de Oliveira, N.A.

To present day, the maximum magnetocaloric effect (MCE) at room temperature for a magnetic field change of 5 T is 40 J/(kg K) for MnAs. In this Letter we present colossal MCE measurements on MnAs under pressure, reaching values up to 267 J/(kg K), far greater than the magnetic limit arising from the assumption of magnetic field independence of the lattice and electronic entropy contributions. The origin of the effect is the contribution to the entropy variation coming from the lattice through the magnetoelastic coupling.

PHYSICAL REVIEW LETTERS 93[23], 237202, 2004

Número de citações na Web of Science:132

[E003-2004] “Phase analysis of quantum oscillations in graphite”

Luk'yanchuk, I.A.; Kopelevich, Y.

The quantum de Haas-van Alphen (dHvA) and Shubnikov-de Haas oscillations measured in graphite were decomposed by pass-band filtering onto contributions from three different groups of carriers. Generalizing the theory of dHvA oscillations for 2D carriers with an arbitrary spectrum and by detecting the oscillation frequencies using a method of two-dimensional phase-frequency analysis which we developed, we identified these carriers as (i) minority holes having a 2D parabolic massive spectrum $p(\perp)$ (perpendicular to) $2/2m(\perp)$, (ii) massive majority electrons with a 3D spectrum and (iii) majority holes with a 2D Dirac-like spectrum $+/-v_p(\perp)$ which seems to be responsible for the unusual strongly-correlated electronic phenomena in graphite.

PHYSICAL REVIEW LETTERS 93[16], 166402, 2004

Número de citações na Web of Science:105

[E004-2004] “Atmospheric neutrinos: LMA oscillations, U-e3 induced interference and CP-violation”

Peres, O.L.G.; Smirnov, A.Y.

We consider oscillations of the low energy (sub-GeV sample) atmospheric neutrinos in the three neutrino context. We present the semi-analytic study of the neutrino evolution and calculate characteristics of the e-like events (total number, energy spectra and zenith angle distributions) in the presence of oscillations. At low energies there are three different contributions to the number of events: the LMA contribution (from $\nu(e)$ -oscillations driven by the solar oscillation parameters), the U-e3-contribution proportional to $s(13)(2)$, and the U-e3-induced interference of the two amplitudes driven by the solar oscillation parameters. The interference term is sensitive to the CP-violation phase. We describe in details properties of these contributions. We find that the LMA, the interference and U-e3 contributions can reach 5-6%, 2-3% and 1-2% correspondingly. An existence of the significant (> 3 -5%) excess of the e-like events in the sub-GeV sample and the absence of the excess in the multi-GeV range testifies for deviation of the 2-3 mixing from maximum. We consider a possibility to measure the deviation as well as the CP-violation phase in future atmospheric neutrino studies.

NUCLEAR PHYSICS B 680[1-3], 479-509, 2004

Número de citações na Web of Science:87

[E005-2004] “Structure and dynamics of carbon nanoscrolls”

Braga, S.F.; Coluci, V.R.; Legoas, S.B.; Giro, R.; Galvao, D.S.; Baughman, R.H.

Carbon nanotube scrolls (CNSs) provide an interesting form of carbon that ideally consists of a single sheet of graphite that is spiral wrapped to form a nanotube. We here use molecular dynamics simulations to investigate CNS formation, stability, and the structural effects due to charge injection. CNS formation is seen to automatically occur when a critical overlap between sheet layers is achieved for the partially curled sheet. We find that charge injection causes unwinding of the CNSs, which might be important for the application of CNSs as nanomechanical actuators.

NANO LETTERS 4[5], 881-884, 2004

Número de citações na Web of Science:79

[E006-2004] “Theoretical study of the formation, evolution, and breaking of gold nanowires”

da Silva, E.Z.; Novaes, F.D.; da Silva, A.J.R.; Fazzio, A.

Real time imaging experiments with metal nanowires (NWs), in particular gold under stress, that show their formation, evolution, and breaking, were obtained with high resolution electron microscopy. In order to understand these results, we use density functional theory (DFT) based methods to simulate the evolution of Au NWs. First we use a tight-binding molecular dynamics (TBMD) method to understand the mechanisms of formation of very thin gold NWs. We present realistic simulations for the breaking of these NWs, whose main features are very similar to the experimental results. We show how defects lead to the formation of one-atom constrictions in the Au NW, which evolves into a one-atom-thick necklace chain. Similarly to the experimental results, we obtain that these necklaces can get as long as five-atoms from apex to apex. Before breaking, we obtain relatively large Au-Au bond distances, of the order of 3.0-3.1 Angstrom. A further pull of the wire causes a sudden increase of one of the bond distances, indicating the breaking of the NW. To get some more insight into the electronic structure aspects of this problem, we considered several of our tight-binding structures before breaking and studied them in detail using an ab initio method based on the DFT. By pulling the wire quasi-statically in this case, we also observed the breaking of the wire at similar distances as in the TBMD. This result was independent of the exchange-correlation potential used-either the local density approximation (LDA) or the generalized gradient approximation (GGA). The pulling force before rupture was obtained as 2.4 nN for the LDA, and 1.9 nN for the GGA. Finally, we also present a detailed analysis of the electronic structure properties for the Au neck atoms, such as the density of states and charge densities, for some configurations before the rupture.

PHYSICAL REVIEW B 69[11], 115411, 2004

Número de citações na Web of Science:77

[E007-2004] “Aniline polymerization into montmorillonite clay: A spectroscopic investigation of the intercalated conduct-ling polymer”

do Nascimento, G.M.; Constantino, V.R.L.; Landers, R.; Temperini, M.L.A.

The polymerization of aniline intercalated into montmorillonite clay was monitored by in situ UV-vis-NIR and resonance Raman spectroscopies and in situ small-angle X-ray scattering. In the initial stages of the polymerization, it is observed the PANI-ES polaronic band at 750 nm in the UV-vis-NIR spectrum and also the characteristic PANI-ES resonance Raman spectrum (excited at 632.8 nm), which indicate that the head-to-tail coupling reactions between anilinium radical cations are occurring. Nevertheless, the resonance Raman spectrum excited at 488.0 nm presents bands at 1211, 1370, 1455, and 1608 cm^{-1} , assigned to the benzidine dication species, which suggests that tail-to-tail coupling reactions are also occurring. In the final stages of polymerization, the presence of electronic absorption bands at 670 and 620 nm indicates the formation of new chromophoric species, which is also confirmed by its peculiar resonance Raman spectrum at 632.8 nm wavelength. The in situ SAXS results show that, during the anilinium polymerization in aqueous clay suspension, the interlayer spacing is ca. 19 Angstrom. XRD diffraction pattern and SEM images of the powder PANI-MMT nanocomposites indicate that the polymerization occurs mainly between the clay layers, and the basal spacing is ca. 13.2 Angstrom. While the IR spectra of nanocomposites show only bands due to PANI-ES-like segments, resonance Raman and nitrogen XANES techniques lead to the presence of PANI-ES-like chains, benzidine segments, azo bonds, and phenazine-like rings in the structure of the confined conducting polymers. The XPS technique detects only PANI-ES segments of the polymeric structure, suggesting that on the external surface and/

or on the edge of clay crystal they are predominant in the chains.

MACROMOLECULES 37[25], 9373-9385, 2004

Número de citações na Web of Science:71

[E008-2004] “Anisotropy of thermal conductivity and possible signature of the Fulde-Ferrell-Larkin-Ovchinnikov state in CeCoIn5”

Capan, C.; Bianchi, A.; Movshovich, R.; Christianson, A.D.; Malinowski, A.; Hundley, M.F.; Lacerda, A.; Pagliuso, P.G.; Sarrao, J.L.

We have measured the thermal conductivity of the heavy-fermion superconductor CeCoIn5 in the vicinity of the upper critical field, with the magnetic field perpendicular to the c axis. Thermal conductivity displays a discontinuous jump at the superconducting phase boundary below critical temperature $T(0)$ approximate to 1 K, indicating a change from a second- to first-order transition and confirming the recent results of specific heat measurements on CeCoIn5. In addition, the thermal conductivity data as a function of field display a kink at a field H_k below the superconducting critical field, which closely coincides with the recently discovered anomaly in specific heat, tentatively identified with the appearance of the spatially inhomogeneous Fulde-Ferrell-Larkin-Ovchinnikov (FFLO) superconducting state. Our results indicate that the thermal conductivity is enhanced within the FFLO state, and call for further theoretical investigations of the order parameter's real-space structure (and, in particular, the structure of vortices) and of the thermal transport within the inhomogeneous FFLO state.

PHYSICAL REVIEW B 70[13], 134513, 2004

Número de citações na Web of Science:69

[E009-2004] “Gigahertz nanomechanical oscillators based on carbon nanotubes”

Legoas, S.B.; Coluci, V.R.; Braga, S.F.; Coura, P.Z.; Dantas, S.; Galvao, D.S.

We report molecular dynamics studies of carbon nanotubes as mechanical gigahertz oscillators. Our results show that different oscillatory regimes exist but that sustained oscillations are possible only when the radii difference values of the inner and outer tubes are similar to 3.4 Angstrom. Frequencies as large as 87 GHz were obtained. Calculated force and frequency values are in good agreement with estimated data from recent experimental investigations.

NANOTECHNOLOGY 15[4], S184-S189, 2004

Número de citações na Web of Science:63

[E010-2004] “Indication of unusual pentagonal structures in atomic-size Cu nanowires”

Gonzalez, J.C.; Rodrigues, V.; Bettini, J.; Rego, L.G.C.; Rocha, A.R.; Coura, P.Z.; Dantas, S.O.; Sato, F.; Galvao, D.S.; Ugarte, D.

We present a study of the structural and quantum conductance properties of atomic-size copper nanowires generated by mechanical stretching. The atomistic evolution was derived from time-resolved electron microscopy observations and molecular dynamics simulations. We have analyzed the quantum transport behavior by means of conductance measurements and theoretical calculations. The results suggest the formation of an unusual and highly stable pentagonal Cu nanowire with a diameter of similar to 0.45 nm and similar to 4.5 conductance quanta.

PHYSICAL REVIEW LETTERS 93[12], 126103, 2004

Número de citações na Web of Science:62

Trabalhos mais citados - 2005

[E001-2005] “Experimental and theoretical challenges in the search for the quark-gluon plasma: The STAR Collaboration's critical assessment of the evidence from RHIC collisions”

Adams, J.; Aggarwal, M.M.; Ahammed, Z.; Amonett, J.; Takahashi, J.

STAR Collaboration

We review the most important experimental results from the first three years of nucleus-nucleus collision studies at RHIC, with emphasis on results from the STAR experiment, and we assess their interpretation and comparison to theory. The theory-experiment comparison suggests that central Au + Au collisions at RHIC produce dense, rapidly thermalizing matter characterized by: (1) initial energy densities above the critical values predicted by lattice QCD for establishment of a quark-gluon plasma (QGP); (2) nearly ideal fluid flow, marked by constituent interactions of very short mean free path, established most probably at a stage preceding hadron formation; and (3) opacity to jets. Many of the observations are consistent with models incorporating QGP formation in the early collision stages, and have not found ready explanation in a hadronic framework. However, the measurements themselves do not yet establish unequivocal evidence for a transition to this new form of matter. The theoretical treatment of the collision evolution, despite impressive successes, invokes a suite of distinct models, degrees of freedom and assumptions of as yet unknown quantitative consequence. We pose a set of important open questions, and suggest additional measurements, at least some of which should be addressed in order to establish a compelling basis to conclude definitively that thermalized, deconfined quark-gluon matter has been produced at RHIC.

NUCLEAR PHYSICS A 757[1-2], 102-183, 2005

Número de citações na Web of Science:1152

[E002-2005] “Event-wise (Pt) fluctuations in Au-Au collisions at root sNN=130 GeV”

Adams, J.; Adler, C.; Aggarwal, M.M.; Ahammed, Z.; Amonett, J.; Anderson, B.D.; Takahashi, J.; et al.

We present the first large-acceptance measurement of event-wise mean transverse momentum $\langle p(t) \rangle$ fluctuations for Au-Au collisions at nucleon-nucleon center-of-momentum collision energy $\sqrt{s(NN)} = 130$ GeV. The observed nonstatistical $\langle p(t) \rangle$ fluctuations substantially exceed in magnitude fluctuations expected from the finite number of particles produced in a typical collision. The r.m.s. fractional width excess of the event-wise $\langle p(t) \rangle$ distribution is $13.7 \pm 0.1(\text{stat}) \pm 1.3(\text{syst})\%$ relative to a statistical reference, for the 15% most-central collisions and for charged hadrons within pseudorapidity range $|\eta| < 1.2$ azimuth, and $0.15 \leq p(t) \leq 2$ GeV/c. The width excess varies smoothly but nonmonotonically with collision centrality and does not display rapid changes with centrality which might indicate the presence of critical fluctuations. The reported $\langle p(t) \rangle$ fluctuation excess is qualitatively larger than those observed at lower energies and differs markedly from theoretical expectations. Contributions to $\langle p(t) \rangle$ fluctuations from semihard parton scattering in the initial state and dissipation in the bulk colored medium are discussed.

PHYSICAL REVIEW C 71[6], 064906, 2005

Número de citações na Web of Science:178

[E003-2005] “Pion interferometry in Au+Au collisions at root s(NN)=200 GeV”

Adams, J.; Aggarwal, M.M.; Ahammed, Z.; Amonett, J.; Anderson, B.D.; Takahashi, J.

STAR Collaboration

We present a systematic analysis of two-pion interferometry in Au+Au collisions at $\sqrt{s(NN)}=200$ GeV using the STAR detector at Relativistic Heavy Ion Collider. We extract the Hanbury-Brown and Twiss radii and study their multiplicity, transverse momentum, and azimuthal angle dependence. The Gaussianness of the correlation function is studied. Estimates of the geometrical and dynamical structure of the freeze-out source are extracted by fits with blast-wave parametrizations. The expansion of the source and its relation with the initial energy density distribution is studied.

PHYSICAL REVIEW C 71[4], 044906, 2005

Número de citações na Web of Science:178

[E004-2005] “Quantum teleportation of an arbitrary two-qubit state and its relation to multipartite entanglement”

Rigolin, G.

We explicitly show a protocol in which an arbitrary two qubit state $|\phi\rangle = a|00\rangle + b|01\rangle + c|10\rangle + d|11\rangle$ is faithfully and deterministically teleported from Alice to Bob. We construct the 16 orthogonal generalized Bell states that can be used to teleport the two qubits. The local operations Bob must perform on his qubits in order to recover the teleported state are also constructed. They are restricted only to single-qubit gates. This means that a controlled-NOT gate is not necessary to complete the protocol. A generalization where N qubits are teleported is also shown. We define a generalized magic basis, which possesses interesting properties. These properties help us to suggest a generalized concurrence from which we construct a measure of entanglement that has a clear physical interpretation: A multipartite state has maximum entanglement if it is a genuine quantum teleportation channel.

PHYSICAL REVIEW A 71[3], 032303, Part A, 2005

Número de citações na Web of Science:121

[E005-2005] “phi meson production in Au + Au and p + p collisions at root S-NN=200 GeV”

Adams, J.; Adler, C.; Aggarwal, M.M.; Ahammed, Z.; Amonett, J.; Anderson, B.D.; Arkhipkin, D.; Takahashi, J.; et al.

STAR Collaboration

We report the STAR measurement of phi meson production in Au + Au and p + p collisions at $\sqrt{s(NN)} = 200$ GeV. Using the event mixing technique, the phi spectra and yields are obtained at mid-rapidity for five centrality bins in Au + Au collisions and for non-singly-diffractive p + p collisions. It is found that the phi transverse momentum distributions from Au + Au collisions are better fitted with a single-exponential while the p + p spectrum is better described by a double-exponential distribution. The measured nuclear modification factors indicate that phi production in central Au + Au collisions is suppressed relative to peripheral collisions when scaled by the number of binary collisions ($\langle N_{\text{bin}} \rangle$). The systematics of $\langle p(T) \rangle$ versus centrality and the constant ϕ/K^- ratio versus beam species, centrality, and collision energy rule out kaon coalescence as the dominant mechanism for phi production.

PHYSICS LETTERS B 612[3-4], 181-189, 2005

Número de citações na Web of Science:105

[E006-2005] “Pion, kaon, proton and anti-proton transverse momentum distributions from p+p and d+Au collisions at root(NN)-N-S=200GeV”

Adams, J.; Aggarwal, M.M.; Ahammed, Z.; Amonett, J.; Takahashi, J.; et al.

STAR Collaboration

Identified mid-rapidity particle spectra of $\pi^{+/-}$, $K^{+/-}$, and $p(\bar{p})$ over bar) from 200 GeV p + p and d + Au collisions are reported. A time-of-flight detector based on multi-gap resistive plate chamber technology is used for particle identification. The particle-species dependence of the Cronin effect is observed to be significantly smaller than that at lower energies. The ratio of the nuclear modification factor (R_{dAu}) between protons ($p + (\bar{p})$ over bar) and charged hadrons (h) in the transverse momentum range $1.2 < p(T) < 3.0$ GeV/c is measured to be $1.19 \pm 0.05(\text{stat}) \pm 0.03(\text{syst})$ in minimum-bias collisions and shows little centrality dependence. The yield ratio of $(p + (\bar{p})$ over bar)/ h in minimum-bias d + Au collisions is found to be a factor of 2 lower than that in Au + Au collisions, indicating that the Cronin effect alone is not enough to account for the relative baryon enhancement observed in heavy ion collisions at RHIC.

PHYSICS LETTERS B 616[1-2], 8-16, 2005

Número de citações na Web of Science:84

[E007-2005] “High efficiency transfer of quantum information and multiparticle entanglement generation in translation-invariant quantum chains”

Plenio, M.B.; Semiao, F.L.

We demonstrate that a translation-invariant chain of interacting quantum systems can be used for high efficiency transfer of quantum entanglement and the generation of multiparticle entanglement over large distances and between arbitrary sites without the requirement of precise spatial or temporal control. The scheme is largely insensitive to disorder and random coupling strengths in the chain. We discuss harmonic oscillator systems both in the case of arbitrary Gaussian states and in situations when at most one excitation is in the system. The latter case, which we prove to be equivalent to an xy-spin chain, may be used to generate genuine multiparticle entanglement. Such a ‘quantum data bus’ may prove useful in future solid state architectures for quantum information processing.

NEW JOURNAL OF PHYSICS 7, 73, 2005

Número de citações na Web of Science:75

[E008-2005] “K(892)(*) resonance production in Au+Au and p+p collisions at root s(NN)=200 GeV”

Adams, J.; Aggarwal, M.M.; Ahammed, Z.; Amonett, J.; Anderson, B.D.; Takahashi, J.; et al.

The short-lived $K(892)^*$ resonance provides an efficient tool to probe properties of the hot and dense medium produced in relativistic heavy-ion collisions. We report measurements of K^* in $\sqrt{s(NN)}=200$ GeV Au+Au and p+p collisions reconstructed via its hadronic decay channels $K(892)^*(0) \rightarrow K \pi$ and $K(892)^*(+/-) \rightarrow K(S)0 \pi^{+/-}$ using the STAR detector at the Relativistic Heavy Ion Collider at Brookhaven National Laboratory. The $K^*(0)$ mass has been studied as a function of $p(T)$ in minimum bias p+p and central Au+Au collisions. The $K^* p(T)$ spectra for minimum bias p+p interactions and for Au+Au collisions in different centralities are presented. The K^*/K yield ratios for all centralities in Au+Au collisions are found to be significantly lower than the ratio in minimum bias p+p collisions, indicating the importance of hadronic interactions between chemical and kinetic freeze-outs. A significant nonzero $K^*(0)$ elliptic flow (v_2) is observed in

Au+Au collisions and is compared to the K-S(0) and Lambda v(2). The nuclear modification factor of K* at intermediate p(T) is similar to that of K-S(0) but different from Lambda. This establishes a baryon-meson effect over a mass effect in the particle production at intermediate p(T) ($2 < p(T) \leq 4$ GeV/c).

PHYSICAL REVIEW C 71[6], 064902, 2005

Número de citações na Web of Science:74

[E009-2005] “Disorder-driven non-Fermi liquid behaviour of correlated electrons”

Miranda, E.; Dobrosavljevic, V.

Systematic deviations from standard Fermi-liquid behaviour have been widely observed and documented in several classes of strongly correlated metals. For many of these systems, mounting evidence is emerging that the anomalous behaviour is most likely triggered by the interplay of quenched disorder and strong electronic correlations. In this review, we present a broad overview of such disorder-driven non-Fermi liquid behaviour, and discuss various examples where the anomalies have been studied in detail. We describe both their phenomenological aspects as observed in experiment, and the current theoretical scenarios that attempt to unravel their microscopic origin.

REPORTS ON PROGRESS IN PHYSICS 68 10[2337-2408], 2005

Número de citações na Web of Science:74

[E010-2005] “Confirmation of the doubly charmed baryon Epsilon+(cc)(3520) via its decay to pD(+)K(-)”

Ocherashvili, A.; Moinester, M.A.; Russ, J.; Escobar, C.O.; et al.

SELEX Collaboration

We observe a signal for the doubly charmed baryon Xi(cc)(+) in the decay mode Xi(cc)(+) -> pD(+)K(-) to complement the previous cc reported decay Xi(cc)(+) -> Lambda(c)(+)K(-)pi(+) in data from SELEX, the charm hadroproduction experiment at Fermilab. In this new decay mode we observe an excess of 5.62 events over a combinatoric background estimated by event mixing to be 1.38 +/- 0.13 events. The mixed background has Gaussian statistics, giving a signal significance of 4.8 sigma. The Poisson probability that a background fluctuation can produce the apparent signal is less than 6.4 x 10(-4). The observed mass of this state is 3518 +/- 3 MeV/c(2), consistent with the published result. Averaging the two results gives a mass of 3518.7 +/- 1.7 MeV/c(2). The observation of this new weak decay mode confirms the previous SELEX suggestion that this state is a double charm baryon. The relative branching ratio for these two modes is 0.36 +/- 0.21.

PHYSICS LETTERS B 628[1-2], 18-24, 2005

Número de citações na Web of Science:72

Trabalhos mais citados - 2006

[E001-2006] “Observation of muon neutrino disappearance with the MINOS detectors in the NuMI neutrino beam”

Michael, D.G.; Adamson, P.; Alexopoulos, T.; Escobar, C.O.; et al.

MINOS Collaboration

This Letter reports results from the MINOS experiment based on its initial exposure to neutrinos from the Fermilab NuMI beam. The rates and energy spectra of charged current nu(mu) interactions are compared in two detectors located along the beam axis at distances of 1 and 735 km.

With 1.27x10(20) 120 GeV protons incident on the NuMI target, 215 events with energies below 30 GeV are observed at the Far Detector, compared to an expectation of 336 +/- 14 events. The data are consistent with nu(mu) disappearance via oscillations with vertical bar Delta m(32)(2)vertical bar=2.74(-0.26)(+0.44)x10(-3) eV(2) and sin(2)(2 theta(23))> 0.87 (68% C.L.).

PHYSICAL REVIEW LETTERS 97[19], 191801, 2006

Número de citações na Web of Science:286

[E002-2006] “First direct observation of Dirac fermions in graphite”

Zhou, S.Y.; Gweon, G.H.; Graf, J.; Fedorov, A.V.; Spataru, C.D.; Diehl, R.D.; Kopelevich, Y.; Lee, D.H.; Louie, S.G.; Lanzara, A.

Originating from relativistic quantum field theory, Dirac fermions have been invoked recently to explain various peculiar phenomena in condensed-matter physics, including the novel quantum Hall effect in graphene(1,2), the magnetic-field-driven metal - insulator-like transition in graphite(3,4), superconductivity in He-3 (ref. 5) and the exotic pseudogap phase of high-temperature superconductors(6,7). Despite their proposed key role in those systems, direct experimental evidence of Dirac fermions has been limited. Here, we report the first direct observation of relativistic Dirac fermions with linear dispersion near the Brillouin zone (BZ) corner H, which coexist with quasiparticles that have a parabolic dispersion near another BZ corner K. In addition, we also report a large electron pocket that we attribute to defect-induced localized states. Thus, graphite presents a system in which massless Dirac fermions, quasiparticles with finite effective mass and defect states all contribute to the low-energy electronic dynamics.

NATURE PHYSICS 2[9], 595-599, 2006

Número de citações na Web of Science:252

[E003-2006] “Identified hadron spectra at large transverse momentum in p-p and d+Au collisions at,root(NN)-N-S=200 GeV”

Adams, J.; Aggarwal, M.M.; Ahammed, Z.; Amonett, J.; Anderson, B.D.; Anderson, M.; Takahashi, J.; et al.

STAR Collaboration

We present the transverse momentum (PT) spectra for identified charged pions, protons and anti-protons from p + p and d + Au collisions at root sNN = 200 GeV. The spectra are measured around midrapidity (vertical bar y vertical bar < 0.5) over the range of 0.3 < PT < 10 GeV/c with particle identification from the ionization energy loss and its relativistic rise in the time projection chamber and time-of-flight in STAR. The charged pion and proton + anti-proton spectra at high PT in p + p and d + Au collisions are in good agreement with a phenomenological model (EPOS) and with next-to-leading order perturbative quantum chromodynamic (NLO pQCD) calculations with a specific fragmentation scheme and factorization scale. We found that all proton, anti-proton and charged pion spectra in p + p collisions follow x(T)-scaling for the momentum range where particle production is dominated by hard processes (p(T) greater than or similar to 2 GeV/c). The nuclear modification factor around midrapidity is found to be greater than unity for charged pions and to be even larger for protons at 2 < PT < 5 GeV/c.

PHYSICS LETTERS B 637[3], 161-169, 2006

Número de citações na Web of Science:151

[E004-2006] “Direct observation of dijets in central Au plus Au collisions at root s(NN)=200 GeV”

Adams, J.; Aggarwal, M.M.; Ahammed, Z.; Amonett, J.; Anderson, B.D.; Anderson, M.; Takahashi, J.; et al.

STAR Collaboration

The STAR Collaboration at the Relativistic Heavy Ion Collider reports measurements of azimuthal correlations of high transverse momentum ($p(T)$) charged hadrons in Au+Au collisions at higher $p(T)$ than reported previously. As $p(T)$ is increased, a narrow, back-to-back peak emerges above the decreasing background, providing a clear dijet signal for all collision centralities studied. Using these correlations, we perform a systematic study of dijet production and suppression in nuclear collisions, providing new constraints on the mechanisms underlying partonic energy loss in dense matter.

PHYSICAL REVIEW LETTERS 97[16], 162301, 2006

Número de citações na Web of Science:117

[E005-2006] “Minijet deformation and charge-independent angular correlations on momentum subspace (η , ϕ) in Au-Au collisions at $\sqrt{s_{NN}}=130$ GeV”

Adams, J (Adams, J.); Aggarwal, MM (Aggarwal, M. M.); Ahammed, Z (Ahammed, Z.); Amonett, J (Amonett, J.); Anderson, BD (Anderson, B. D.); Anderson, M.; Takahashi, J.; et al.

STAR Collaboration

Measurements of two-particle correlations on angular difference variables $\eta(1)-\eta(2)$ (pseudorapidity) and $\phi(1)-\phi(2)$ (azimuth) are presented for all primary charged hadrons with transverse momentum $0.15 \leq p(t) \leq 2$ GeV/c and vertical bar η vertical bar ≤ 1.3 from Au-Au collisions at $\sqrt{s_{NN}}=130$ GeV. Large-amplitude correlations are observed over a broad range in relative angles where distinct structures appear on the same-side and away-side (i.e., relative azimuth less than $\pi/2$ or greater than $\pi/2$). The principal correlation structures include that associated with elliptic flow plus a strong, same-side peak. It is hypothesized that the latter results from correlated hadrons associated with semi-hard parton scattering in the early stage of the heavy-ion collision which produces a jet-like correlation peak at small relative angles. The width of the jet-like peak on $\eta(1)-\eta(2)$ increases by a factor 2.3 from peripheral to central collisions, suggesting strong coupling of semi-hard scattered partons to a longitudinally-expanding medium. The new methods of jet analysis introduced here provide access to scattered partons at low transverse momentum well below the kinematic range where perturbative quantum chromodynamics and standard fragmentation models are applicable.

PHYSICAL REVIEW C 73[6], 064907, 2006

Número de citações na Web of Science:117

[E006-2006] “Forward neutral pion production in p+p and d+Au collisions at $\sqrt{s_{NN}}=200$ GeV”

Adams, J.; Aggarwal, M.M.; Ahammed, Z.; Amonett, J.; Anderson, B.D.; Takahashi, J.; et al.

Measurements of the production of forward $\pi(0)$ mesons from p+p and d+Au collisions at $\sqrt{s_{NN}} = 200$ GeV are reported. The p+p yield generally agrees with next-to-leading order perturbative QCD calculations. The d+Au yield per binary collision is suppressed as η increases, decreasing to similar to 30% of the p+p yield at $\langle \eta \rangle = 4.00$, well below shadowing expectations. Exploratory measurements of azimuthal correlations of the forward $\pi(0)$ with charged hadrons at η approximate to 0 show a recoil peak in p+p that is suppressed in d+Au at low pion energy. These observations are qualitatively consistent with a saturation picture of the low-x gluon structure of heavy nuclei.

PHYSICAL REVIEW LETTERS 97[15], 152302, 2006

Número de citações na Web of Science:104

[E007-2006] “Identified baryon and meson distributions at large transverse momenta from Au plus Au collisions at $\sqrt{s_{NN}}=200$ GeV”

Abelev, B.I.; Aggarwal, M.M.; Ahammed, Z.; Anderson, B.D.; Anderson, M.; Arkhipkin, D.; Takahashi, J.; et al.

Transverse momentum spectra of $\pi(+/-)$, p, and (p) over bar p up to 12 GeV/c at midrapidity in centrality selected Au + Au collisions at $\sqrt{s_{NN}} = 200$ GeV are presented. In central Au + Au collisions, both $\pi(+/-)$ and $p(p)$ over bar show significant suppression with respect to binary scaling at $p(T)$ greater than or similar to 4 GeV/c. Protons and antiprotons are less suppressed than $\pi(+/-)$, in the range 1.5 less than or similar to $p(T)$ less than or similar to 6 GeV/c. The $\pi(-)/\pi(+)$ and (p) over bar / p ratios show at most a weak pT dependence and no significant centrality dependence. The p/π ratios in central Au + Au collisions approach the values in p + p and d + Au collisions at $p(T)$ greater than or similar to 5 GeV/c. The results at high $p(T)$ indicate that the partonic sources of $\pi(+/-)$, p, and (p) over bar have similar energy loss when traversing the nuclear medium.

PHYSICAL REVIEW LETTERS 97[15], 152301, 2006

Número de citações na Web of Science:94

[E008-2006] “Longitudinal double-spin asymmetry and cross section for inclusive jet production in polarized proton collisions at $\sqrt{s}=200$ GeV”

Abelev, B.I.

We report a measurement of the longitudinal double-spin asymmetry A_{LL} and the differential cross section for inclusive midrapidity jet production in polarized proton collisions at $\sqrt{s}=200$ GeV. The cross section data cover transverse momenta $5 < p(T) < 50$ GeV/c and agree with next-to-leading order perturbative QCD evaluations. The A_{LL} data cover $5 < p(T) < 17$ GeV/c and disfavor at 98% C.L. maximal positive gluon polarization in the polarized nucleon.

PHYSICAL REVIEW LETTERS 97[25], 252001, 2006

Número de citações na Web of Science:94

[E009-2006] “Strange baryon resonance production in $\sqrt{s_{NN}}=200$ GeV p+p and Au+Au collisions”

Abelev, B. I.; Aggarwal, M. M.; Ahammed, Z.; Amonett, J.; Anderson, B. D.; Anderson, M.; Takahashi, J.; et al.

STAR Collaboration

We report the measurements of $\Sigma(1385)$ and $\Lambda(1520)$ production in p+p and Au+Au collisions at $\sqrt{s_{NN}}=200$ GeV from the STAR Collaboration. The yields and the $p(T)$ spectra are presented and discussed in terms of chemical and thermal freeze-out conditions and compared to model predictions. Thermal and microscopic models do not adequately describe the yields of all the resonances produced in central Au+Au collisions. Our results indicate that there may be a time span between chemical and thermal freeze-out during which elastic hadronic interactions occur.

PHYSICAL REVIEW LETTERS 97[13], 132301, 2006

Número de citações na Web of Science:94

[E010-2006] "Extended squaraine dyes with large two-photon absorption cross-sections"

Chung, S.J.; Zheng, S.J.; Odani, T.; Beverina, L.; Fu, J.; Padilha, L.A.; Biesso, A.; Hales, J.M.; Zhan, X.W.; Schmidt, K.; Ye, A.J.; Zojer, E.; Barlow, S.; Hagan, D.J.; Van Stryland, E.W.; Yi, Y.P.; Shuai, Z.G.; Pagani, G.A.; Bredas, J.L.; Perry, J.W.; Marder, S.R.

JOURNAL OF THE AMERICAN CHEMICAL SOCIETY 128[45], 14444-14445, 2006

Número de citações na Web of Science:89

Trabalhos mais citados - 2007

[E001-2007] "Correlation of the highest-energy cosmic rays with nearby extragalactic objects"

Abraham, J.; Abreu, P.; Aglietta, M.; Aguirre, C.; Chinellato, J. A.; Escobar, C. O.; Fauth, A. C.; Kemp, E.; Takahashi, J.; et al.

Pierre Auger Collaboration

Using data collected at the Pierre Auger Observatory during the past 3.7 years, we demonstrated a correlation between the arrival directions of cosmic rays with energy above 6×10^{19} electron volts and the positions of active galactic nuclei (AGN) lying within similar to 75 megaparsecs. We rejected the hypothesis of an isotropic distribution of these cosmic rays with at least a 99% confidence level from a prescribed a priori test. The correlation we observed is compatible with the hypothesis that the highest-energy particles originate from nearby extragalactic sources whose flux has not been substantially reduced by interaction with the cosmic background radiation. AGN or objects having a similar spatial distribution are possible sources.

SCIENCE 318[5852], 938-943, 2007

Número de citações na Web of Science:339

[E002-2007] "Transverse momentum and centrality dependence of High-p(T) nonphotonic electron suppression in Au plus Au collisions at root(NN)=200 GeV"

Abelev, B. I.; Aggarwal, M. M.; Ahammed, Z.; Anderson, B. D.; Arkhipkin, D.; Averichev, G. S.; Takahashi, J.; et al.

STAR Collaboration

The STAR collaboration at the BNL Relativistic Heavy-Ion Collider (RHIC) reports measurements of the inclusive yield of nonphotonic electrons, which arise dominantly from semileptonic decays of heavy flavor mesons, over a broad range of transverse momenta ($1.2 < p(T) < 10$ GeV/c) in p+p, d+Au, and Au+Au collisions at root s(NN)=200 GeV. The nonphotonic electron yield exhibits an unexpectedly large suppression in central Au+Au collisions at high p(T), suggesting substantial heavy-quark energy loss at RHIC. The centrality and p(T) dependences of the suppression provide constraints on theoretical models of suppression.

PHYSICAL REVIEW LETTERS 98[19], 192301, 2007

Número de citações na Web of Science:207

[E003-2007] "Theory of neutrinos: a white paper"

Mohapatra, R. N.; Antusch, S.; Babu, K. S.; Barenboim, G.; Chen, M. C.; de Gouvea, A.; de Holanda, P.; Dutta, B.; Grossman, Y.; Joshipura, A.; Kayser, B.; Kersten, J.; Keum, Y.Y.; King, S.F.; Langacker, P.; Lindner, M.; Loinaz, W.; Masina, I.; Mocioiu, I.; Mohanty, S.; Murayama, H.; Pascoli, S.; Petcov, S.T.; Pilaftsis, A.; Ramond, P.; Ratz, M.; Rodejohann, W.; Shrock, R.; Takeuchi, T.; Underwood, T.; Wolfenstein, L.

This paper is a review of the present status of neutrino mass physics, which grew out of an APS sponsored study of neutrinos in 2004. After a discussion of the present knowledge of neutrino masses and mixing and some popular ways to probe the new physics implied by recent data, it summarizes what can be learned about neutrino interactions as well as the nature of new physics beyond the Standard Model from the various proposed neutrino experiments. The intriguing possibility that neutrino mass physics may be at the heart of our understanding of a long standing puzzle of cosmology, i.e. the origin of matter-antimatter asymmetry is also discussed.

REPORTS ON PROGRESS IN PHYSICS 70[11], 1757-1867, 2007

Número de citações na Web of Science:149

[E004-2007] "Non-random coextinctions in phylogenetically structured mutualistic networks"

Rezende, E.L.; Lavabre, J.E.; Guimaraes, P.R.; Jordano, P.; Bascompte, J.

The interactions between plants and their animal pollinators and seed dispersers have moulded much of Earth's biodiversity(1-3). Recently, it has been shown that these mutually beneficial interactions form complex networks with a well-defined architecture that may contribute to biodiversity persistence(4-8). Little is known, however, about which ecological and evolutionary processes generate these network patterns(3,9). Here we use phylogenetic methods(10,11) to show that the phylogenetic relationships of species predict the number of interactions they exhibit in more than one-third of the networks, and the identity of the species with which they interact in about half of the networks. As a consequence of the phylogenetic effects on interaction patterns, simulated extinction events tend to trigger coextinction cascades of related species. This results in a non-random pruning of the evolutionary tree(12,13) and a more pronounced loss of taxonomic diversity than expected in the absence of a phylogenetic signal. Our results emphasize how the simultaneous consideration of phylogenetic information and network architecture can contribute to our understanding of the structure and fate of species-rich communities.

NATURE 448[7156], 925-U6, 2007

Número de citações na Web of Science:100

[E005-2007] "Strange particle production in p+p collisions at root s=200 GeV"

Abelev, B.I.; Adams, J.; Aggarwal, M.M.; Ahammed, Z.; Amonett, J.; Anderson, B.D.; Takahashi, J.; et al. et al.

STAR Collaboration

We present strange particle spectra and yields measured at midrapidity in root s = 200 GeV proton-proton (p + p) collisions at the BNL Relativistic Heavy Ion Collider (RHIC). We find that the previously observed universal transverse mass ($m(T) = \sqrt{p_T^2 + m(0)^2}$) scaling of hadron production in p + p collisions seems to break down at higher m(T) and that there is a difference in the shape of the m(T) spectrum between baryons and mesons. We observe midrapidity antibaryon to baryon ratios near unity for Lambda and Xi baryons and no dependence of the ratio on transverse momentum, indicating that our data do not yet reach the quark-jet dominated region. We show the dependence of the mean transverse momentum $\langle p(T) \rangle$ on measured charged particle multiplicity and on particle mass and infer that these trends are consistent with gluon-jet dominated particle production. The data are compared with previous measurements made at the CERN Super Proton Synchrotron and Intersecting Storage Rings and in Fermilab experiments and with leading-order and next-to-leading-order string fragmentation model predictions.

We infer from these comparisons that the spectral shapes and particle yields from p + p collisions at RHIC energies have large contributions from gluon jets rather than from quark jets.

PHYSICAL REVIEW C 75[6], 064901, 2007

Número de citações na Web of Science:80

[E006-2007] “Scaling properties of hyperon production in Au+Au collisions at root s(NN)=200 GeV”

Adams, J.; Aggarwal, M. M.; Ahammed, Z.; Amonett, J.; Anderson, B. D.; Anderson, M.; Takahashi, J.; et al.

STAR Collaboration

We present the scaling properties of Λ , Ξ , and Ω in midrapidity Au+Au collisions at the Brookhaven National Laboratory Relativistic Heavy Ion Collider at root s(NN)=200 GeV. The yield of multistrange baryons per participant nucleon increases from peripheral to central collisions more rapidly than that of Λ , indicating an increase of the strange-quark density of the matter produced. The strange phase-space occupancy factor $\gamma(s)$ approaches unity for the most central collisions. Moreover, the nuclear modification factors of p , Λ , and Ξ are consistent with each other for $2 < p(T) < 5$ GeV/c in agreement with a scenario of hadron formation from constituent quark degrees of freedom.

PHYSICAL REVIEW LETTERS 98[6], 062301, 2007

Número de citações na Web of Science:71

[E007-2007] “Field enhancement within an optical fibre with a subwavelength air core”

Wiederhecker, G. S.; Cordeiro, C. M. B.; Couny, F.; Benabid, F.; Maier, S.A.; Knight, J.C.; Cruz, C. H. B.; Fragnito, H. L.

Tightly confined light enables a variety of applications ranging from nonlinear light management to atomic manipulation. Photonic-crystal fibres (PCFs) can provide strong guidance in very small cores while simultaneously offering long interaction lengths(1). However, light confinement in waveguides is usually ultimately limited by diffraction(2,3), which tends to spread light away from the waveguiding core, despite its higher refractive index. It was recently demonstrated that such spreading fields can be trapped by a nanometre-scale slot inside a strongly guiding silicon-on-insulator (SOI) waveguide(4,5). In this letter we demonstrate the concentration of optical energy within a subwavelength-scale air hole running down the length of a PCF core. The core resembles a submicrometre-diameter tube with a bore diameter of 200 nm or less. The high intensity in an air hole, coupled with long interaction lengths, promises a new class of experiments in light-matter interaction and nonlinear fibre optics.

NATURE PHOTONICS 1[2], 115-118, 2007

Número de citações na Web of Science:69

[E008-2007] “Measurement of neutrino velocity with the MINOS detectors and NuMI neutrino beam”

Adamson, P.; Andreopoulos, C.; Arms, K. E.; Armstrong, R.; Auty, D. J.; Avvakumov, S.; Escobar, C. O.; et al.

The velocity of a similar to 3 GeV neutrino beam is measured by comparing detection times at the near and far detectors of the MINOS experiment, separated by 734 km. A total of 473 far detector neutrino events was used to measure $(\nu - c)/c = 5.1 \pm 2.9 \times 10^{-5}$ (at 68% C.L.). By correlating the measured energies of 258 charged-current neutrino events to their arrival times at the far detector,

a limit is imposed on the neutrino mass of $m(\nu) < 50 \text{ MeV}/c^2$ (99% C.L.).

PHYSICAL REVIEW D 76[7], 072005, 2007

Número de citações na Web of Science:61

[E009-2007] “Mass, quark-number, and root s(NN) dependence of the second and fourth flow harmonics in ultrarelativistic nucleus-nucleus collisions”

Abelev, B. I.; Aggarwal, M. M.; Ahammed, Z.; Anderson, B. D.; Arkhipkin, D.; Averichev, G.S.; Takahashi, J.; et al.

STAR Collaboration

We present STAR measurements of the azimuthal anisotropy parameter $v(2)$ for pions, kaons, protons, Λ , Ξ , and Ω over $\bar{v}(2)$ (Ξ over \bar{v} , and Ω over \bar{v} , along with $v(4)$ for pions, kaons, protons, and Λ over \bar{v} at midrapidity for Au+Au collisions at root s(NN)=62.4 and 200 GeV. The $v(2)(p(T))$ values for all hadron species at 62.4 GeV are similar to those observed in 130 and 200 GeV collisions. For observed kinematic ranges, $v(2)$ values at 62.4, 130, and 200 GeV are as little as 10-15% larger than those in Pb+Pb collisions at root s(NN)=17.3 GeV. At intermediate transverse momentum ($p(T)$ from 1.5-5 GeV/c), the 62.4 GeV $v(2)(p(T))$ and $v(4)(p(T))$ values are consistent with the quark-number scaling first observed at 200 GeV. A four-particle cumulant analysis is used to assess the nonflow contributions to pions and protons and some indications are found for a smaller nonflow contribution to protons than pions. Baryon $v(2)$ is larger than antibaryon $v(2)$ at 62.4 and 200 GeV, perhaps indicating either that the initial spatial net-baryon distribution is anisotropic, that the mechanism leading to transport of baryon number from beam- to midrapidity enhances $v(2)$ or that antibaryon and baryon annihilation is larger in the in-plane direction.

PHYSICAL REVIEW C 75[5], 054906, 2007

Número de citações na Web of Science:58

[E010-2007] “Divacancies in graphene and carbon nanotubes”

Amorim, R.G.; Fazzio, A.; Antonelli, A.; Novaes, F.D.; da Silva, A.J.R.

Divacancies are among the most important defects that alter the charge transport properties of single-walled carbon nanotubes (SWNT), and we here study, using ab initio calculations, their properties. Two structures were investigated, one that has two pentagons side by side with an octagon (585) and another composed of three pentagons and three heptagons (555777). We investigate their stability as a function of tube diameter, and calculate their charge transport properties. The 585 defect is less stable in graphene due to two broken bonds in the pentagons. We estimate that the 555777 becomes more stable than the 585 for a diameter of about 40 angstrom (53 angstrom) for an armchair (zigzag) SWNTs, indicating that they will prevail in large diameter multiwalled carbon nanotubes and graphene ribbons.

NANO LETTERS 7[8], 2459-2462, 2007

Número de citações na Web of Science:57

Trabalhos mais citados - 2008

[E001-2008] “Correlation of the highest-energy cosmic rays with the positions of nearby active galactic nuclei”

Abraham, J.; Abreu, P.; Aglietta, M.; Aguirre, C.; Allard, D.; Allekotte, I.; Allen, J.; Allison, P.; Chinellato, J. A.; Dobrigkeit, C.; Escobar, C. O.; Fauth, A. C.; Kemp, E.; Selmi-Dei, D.P.; Takahashi, J.; et al.

Data collected by the Pierre Auger Observatory provide evidence for anisotropy in the arrival directions of the cosmic rays with the highest-energies, which are correlated with the positions of relatively nearby active galactic nuclei (AGN) [Pierre Auger Collaboration, Science 318 (2007) 938]. The correlation has maximum significance for cosmic rays with energy greater than similar to 6×10^{19} eV and AGN at a distance less than similar to 75 Mpc. We have confirmed the anisotropy at a confidence level of more than 99% through a test with parameters specified a priori, using an independent data set. The observed correlation is compatible with the hypothesis that cosmic rays with the highest-energies originate from extra-galactic sources close enough so that their flux is not significantly attenuated by interaction with the cosmic background radiation (the Greisen-Zatsepin-Kuz'min effect). The angular scale of the correlation observed is a few degrees, which suggests a predominantly light composition unless the magnetic fields are very weak outside the thin disk of our galaxy. Our present data do not identify AGN as the sources of cosmic rays unambiguously, and other candidate sources which are distributed as nearby AGN are not ruled out. We discuss the prospect of unequivocal identification of individual sources of the highest-energy cosmic rays within a few years of continued operation of the Pierre Auger Observatory.

ASTROPARTICLE PHYSICS 29[3], 188-204, 2008

Número de citações na Web of Science:215

[E002-2008] "Observation of the suppression of the flux of cosmic rays above 4×10^{19} eV"

Abraham, J.; Abreu, P.; Aglietta, M.; Aguirre, C.; Allard, D.; Allekotte, I.; Allen, J.; Allison, P. Chinellato, J. A.; Escobar, C. O.; Fauth, A. C.; Kemp, E.; Muller, M. A.; Selmi-Dei, D.P.; Takahashi, J.; et al.

The energy spectrum of cosmic rays above 2.5×10^{18} eV, derived from 20 000 events recorded at the Pierre Auger Observatory, is described. The spectral index γ of the particle flux, J proportional to $E^{-\gamma}$, at energies between 4×10^{18} eV and 4×10^{19} eV is $2.69 \pm 0.02(\text{stat}) \pm 0.06(\text{syst})$, steepening to $4.2 \pm 0.4(\text{stat}) \pm 0.06(\text{syst})$ at higher energies. The hypothesis of a single power law is rejected with a significance greater than 6 standard deviations. The data are consistent with the prediction by Greisen and by Zatsepin and Kuz'min.

PHYSICAL REVIEW LETTERS 101[6], 061101, 2008

Número de citações na Web of Science:213

[E003-2008] "Measurement of neutrino oscillations with the MINOS detectors in the NuMI beam"

Adamson, P.; Andreopoulos, C.; Arms, K.E.; Armstrong, R.; Auty, D. J.; Ayres, D. S.; Escobar, C.O.; et al.

MINOS Collaboration

This Letter reports new results from the MINOS experiment based on a two-year exposure to muon neutrinos from the Fermilab NuMI beam. Our data are consistent with quantum-mechanical oscillations of neutrino flavor with mass splitting $\Delta m^2 = (2.43 \pm 0.13) \times 10^{-3} \text{ eV}^2$ (68% C.L.) and mixing angle $\sin^2(2\theta) > 0.90$ (90% C.L.). Our data disfavor two alternative explanations for the disappearance of neutrinos in flight: namely, neutrino decays into lighter particles and quantum decoherence of neutrinos, at the 3.7 and 5.7 standard-deviation levels, respectively.

PHYSICAL REVIEW LETTERS 101[13], 131802, 2008

Número de citações na Web of Science:172

[E004-2008] "A consistent metric for nestedness analysis in ecological systems: reconciling concept and measurement"

Almeida-Neto, M.; Guimaraes, P.; Guimaraes, P.R.; Loyola, R.D.; Ulrich, W.

Nestedness has been widely reported for both metacommunities and networks of interacting species. Even though the concept of this ecological pattern has been well-defined, there are several metrics by which it can be quantified. We noted that current metrics do not correctly quantify two major properties of nestedness: (1) whether marginal totals (i.e. fills) differ among columns and/or among rows, and (2) whether the presences (1's) in less-filled columns and rows coincide, respectively, with those found in the more-filled columns and rows. We propose a new metric directly based on these properties and compare its behavior with that of the most used metrics, using a set of model matrices ranging from highly-nested to alternative structures in which no nestedness should be detected. We also used an empirical dataset to explore possible biases generated by the metrics as well as to evaluate correlations between metrics. We found that nestedness has been quantified by metrics that inappropriately detect this pattern, even for matrices in which there is no nestedness. In addition, the most used metrics are prone to type I statistical errors while our new metric has better statistical properties and consistently rejects a nested pattern for different types of random matrices. The analysis of the empirical data showed that two nestedness metrics, matrix temperature and the discrepancy measure, tend to overestimate the degrees of nestedness in metacommunities. We emphasize and discuss some implications of these biases for the theoretical understanding of the processes shaping species interaction networks and metacommunity structure.

OIKOS 117[8], 1227-1239, 2008

Número de citações na Web of Science:124

[E005-2008] "Centrality dependence of charged hadron and strange hadron elliptic flow from root s(NN)=200 GeV Au+Au collisions"

Abelev, B. I.; Aggarwal, M.M.; Ahammed, Z.; Anderson, B. D.; Arkhipkin, D.; Averichev, G.S.; Takahashi, J.;

STAR Collaboration

We present STAR results on the elliptic flow v_2 of charged hadrons, strange and multistrange particles from $\sqrt{s(NN)} = 200$ GeV Au+Au collisions at the BNL Relativistic Heavy Ion Collider (RHIC). The detailed study of the centrality dependence of v_2 over a broad transverse momentum range is presented. Comparisons of different analysis methods are made in order to estimate systematic uncertainties. To discuss the nonflow effect, we have performed the first analysis of v_2 with the Lee-Yang zero method for $K_S(0)$ and Λ . In the relatively low PT region, $P-T \leq 2$ GeV/c, a scaling with $m(T) - m$ is observed for identified hadrons in each centrality bin studied. However, we do not observe $v_2(p(T))$ scaled by the participant eccentricity to be independent of centrality. At higher PT, $2 \leq PT \leq 6$ GeV/c, v_2 scales with quark number for all hadrons studied. For the multistrange hadron Ω , which does not suffer appreciable hadronic interactions, the values of v_2 are consistent with both $m(T) - m$ scaling at low $p(T)$ and number-of-quark scaling at intermediate $p(T)$. As a function of collision centrality, an increase of $p(T)$ -integrated v_2 scaled by the participant eccentricity has been observed, indicating a stronger collective flow in more central Au+Au collisions.

PHYSICAL REVIEW C 77[5], 054901, 2008

Número de citações na Web of Science:98

[E006-2008] “Over 4000 nm bandwidth of mid-IR supercontinuum generation in sub-centimeter segments of highly nonlinear tellurite PCFs”

Domachuk, P.; Wolchover, N. A.; Cronin-Golomb, M.; Wang, A.; George, A. K.; Cordeiro, C. M. B.; Knight, J. C.; Omenetto, F. G.

We report broad bandwidth, mid-IR supercontinuum generation using a sub-cm (8 mm) length of highly nonlinear tellurite microstructured photonic crystal fiber (PCF). We pump the fiber at telecommunication wavelengths by using 1550 nm, 100 fs pulses of energy $E=1.9$ nJ. When coupled in the PCF, these pulses result in a supercontinuum (SC) bandwidth of 4080 nm extending from 789 to 4870 nm measured at 20 dBm below the peak spectral power. This bandwidth is comparable or in excess of previously reported spectra for other nonlinear glass fiber formulations despite the significantly shorter fiber length. In addition, besides offering a convenient pump wavelength, short fiber lengths enable smoother SC spectra, lower dispersion, and reduced material absorption at longer wavelengths making the use of this PCF particularly interesting.

OPTICS EXPRESS 16[10], 7161-7168, 2008

Número de citações na Web of Science:93

[E007-2008] “Upper limit on the cosmic-ray photon flux above 10(19) eV using the surface detector of the Pierre Auger Observatory”

Abraham, J.; Abreu, P.; Aglietta, M.; Aguirre, C.; Allard, D.; Allekotte, I.; Chinellato, J. A.; de Mello, W. J. M.; Dobrigkeit, C.; Escobar, C.O.; Kemp, E.; Takahashi, J.; et al.

A method is developed to search for air showers initiated by photons using data recorded by the surface detector of the Auger Observatory. The approach is based on observables sensitive to the longitudinal shower development, the signal risetime and the curvature of the shower front. Applying this method to the data, tipper limits on the flux of photons of 3.8×10^{-3} , 2.5×10^{-3} , and 2.2×10^{-3} $\text{km}^{-2} \text{sr}^{-1} \text{yr}^{-1}$ above 10(19) eV, 2×10^{19} eV, and 4×10^{19} eV are derived, with corresponding limits on the fraction of photons being 2.0%, 5.1%, and 31% (all limits at 95% c.l.). These photon limits disfavor certain exotic models of sources of cosmic rays. The results also show that the approach adopted by the Auger Observatory to calibrate the shower energy is not strongly biased by a contamination from photons.

ASTROPARTICLE PHYSICS 29[4], 243-256, 2008

Número de citações na Web of Science:90

[E008-2008] “Study of muon neutrino disappearance using the Fermilab Main Injector neutrino beam”

Adamson, P.; Andreopoulos, C.; Arms, K. E.; Armstrong, R.; Auty, D. J.; Avvakumov, S.; Escobar, C. O.; et al.

Minos Collaboration

We report the results of a search for $\nu(\mu)$ disappearance by the Main Injector Neutrino Oscillation Search [D. G. Michael (MINOS), Phys. Rev. Lett. 97, 191801 (2006)]. The experiment uses two detectors separated by 734 km to observe a beam of neutrinos created by the Neutrinos at the Main Injector facility at Fermi National Accelerator Laboratory. The data were collected in the first 282 days of beam operations and correspond to an exposure of 1.27×10^{20} protons on target. Based on measurements in the Near Detector, in the absence of neutrino oscillations we expected 336 ± 14 $\nu(\mu)$ charged-current interactions at the Far Detector but observed 215. This deficit of events corresponds to a significance of 5.2 standard deviations. The deficit is energy dependent and is consistent with two-flavor neutrino oscillations according to $|\Delta m^2| = 2.74(-0.26)(+0.44)$

$\times 10^{-3}$ eV²/c(4) and $\sin^2 \theta > 0.87$ at 68% confidence level.

PHYSICAL REVIEW D 77[7], 072002, 2008

Número de citações na Web of Science:73

[E009-2008] “Sign change of Poisson’s ratio for carbon nanotube sheets”

Hall, L.J.; Coluci, V.R.; Galvao, D.S.; Kozlov, M.E.; Zhang, M.; Dantas, S.O.; Baughman, R.H.

Most materials shrink laterally like a rubber band when stretched, so their Poisson’s ratios are positive. Likewise, most materials contract in all directions when hydrostatically compressed and decrease density when stretched, so they have positive linear compressibilities. We found that the in-plane Poisson’s ratio of carbon nanotube sheets (buckypaper) can be tuned from positive to negative by mixing single-walled and multiwalled nanotubes. Density-normalized sheet toughness, strength, and modulus were substantially increased by this mixing. A simple model predicts the sign and magnitude of Poisson’s ratio for buckypaper from the relative ease of nanofiber bending and stretch, and explains why the Poisson’s ratios of ordinary writing paper are positive and much larger. Theory also explains why the negative in-plane Poisson’s ratio is associated with a large positive Poisson’s ratio for the sheet thickness, and predicts that hydrostatic compression can produce biaxial sheet expansion. This tunability of Poisson’s ratio can be exploited in the design of sheet-derived composites, artificial muscles, gaskets, and chemical and mechanical sensors.

SCIENCE 320[5875], 504-507, 2008

Número de citações na Web of Science:71

[E010-2008] “Upper limit on the diffuse flux of ultrahigh energy tau neutrinos from the Pierre Auger Observatory”

Abraham, J.; Abreu, P.; Aglietta, M.; Aguirre, C.; Allard, D.; Allekotte, I.; Allen, J.; Allison, P.; Chinellato, J. A.; de Mello, W. J. M.; Dobrigkeit, C.; Escobar, C. O.; Fauth, A. C.; Kemp, E.; Muller, M. A.; Selmi-Dei, D.P.; Takahashi, J.; et al.

Pierre Auger Collaboration

The surface detector array of the Pierre Auger Observatory is sensitive to Earth-skimming tau neutrinos that interact in Earth’s crust. Tau leptons from $\nu(\tau)$ charged-current interactions can emerge and decay in the atmosphere to produce a nearly horizontal shower with a significant electromagnetic component. The data collected between 1 January 2004 and 31 August 2007 are used to place an upper limit on the diffuse flux of $\nu(\tau)$ at EeV energies. Assuming an $E(\nu)$ differential energy spectrum the limit set at 90% C. L. is $E(\nu)^2 dN(\nu)/dE(\nu) < 1: 3 \times 10^{-7}$ $\text{GeV cm}^{-2} \text{s}^{-1} \text{sr}^{-1}$ in the energy range 2×10^{17} eV $< E(\nu) < 2 \times 10^{19}$ eV.

PHYSICAL REVIEW LETTERS 100[21], 211101, 2008

Número de citações na Web of Science:67

Trabalhos mais citados - 2009

[E001-2009] “Robustness of quantum discord to sudden death”

Werlang, T.; Souza, S.; Fanchini, F. F.; Villas-Boas, C. J. We calculate the dissipative dynamics of two-qubit quantum discord under Markovian environments. We analyze various dissipative channels such as dephasing, depolarizing, and generalized amplitude damping, assuming independent perturbation, in which each qubit is coupled to its own channel.

Choosing initial conditions that manifest the so-called sudden death of entanglement, we compare the dynamics of entanglement with that of quantum discord. We show that in all cases where entanglement suddenly disappears, quantum discord vanishes only in the asymptotic limit, behaving similarly to individual decoherence of the qubits, even at finite temperatures. Hence, quantum discord is more robust than the entanglement against decoherence so that quantum algorithms based only on quantum discord correlations may be more robust than those based on entanglement.

PHYSICAL REVIEW A 80[2], 024103, 2009

Número de citações na Web of Science:180

[E002-2009] “Systematic measurements of identified particle spectra in pp, d plus Au, and Au plus Au collisions at the STAR detector”

Abelev, B. I.; Aggarwal, M. M.; Ahammed, Z.; Anderson, B. D.; Arkhipkin, D.; Averichev, G. S.; Takahashi, J.; Vasconcelos, G. M. S.; et al.

STAR Collaboration

Identified charged-particle spectra of $\pi^{+/-}$, $K^{+/-}$, p , and \bar{p} over bar at midrapidity ($|\eta| < 0.1$) measured by the dE/dx method in the STAR (solenoidal tracker at the BNL Relativistic Heavy Ion Collider) time projection chamber are reported for pp and d + Au collisions at $\sqrt{s(NN)} = 200$ GeV and for Au + Au collisions at 62.4, 130, and 200 GeV. Average transverse momenta, total particle production, particle yield ratios, strangeness, and baryon production rates are investigated as a function of the collision system and centrality. The transverse momentum spectra are found to be flatter for heavy particles than for light particles in all collision systems; the effect is more prominent for more central collisions. The extracted average transverse momentum of each particle species follows a trend determined by the total charged-particle multiplicity density. The Bjorken energy density estimate is at least several GeV/fm³ for a formation time less than 1 fm/c. A significantly larger net-baryon density and a stronger increase of the net-baryon density with centrality are found in Au + Au collisions at 62.4 GeV than at the two higher energies. Antibaryon production relative to total particle multiplicity is found to be constant over centrality, but increases with the collision energy. Strangeness production relative to total particle multiplicity is similar at the three measured RHIC energies. Relative strangeness production increases quickly with centrality in peripheral Au + Au collisions, to a value about 50% above the pp value, and remains rather constant in more central collisions. Bulk freeze-out properties are extracted from thermal equilibrium model and hydrodynamics-motivated blast-wave model fits to the data. Resonance decays are found to have little effect on the extracted kinetic freeze-out parameters because of the transverse momentum range of our measurements. The extracted chemical freeze-out temperature is constant, independent of collision system or centrality; its value is close to the predicted phase-transition temperature, suggesting that chemical freeze-out happens in the vicinity of hadronization and the chemical freeze-out temperature is universal despite the vastly different initial conditions in the collision systems. The extracted kinetic freeze-out temperature, while similar to the chemical freeze-out temperature in pp, d + Au, and peripheral Au + Au collisions, drops significantly with centrality in Au + Au collisions, whereas the extracted transverse radial flow velocity increases rapidly with centrality. There appears to be a prolonged period of particle elastic scatterings from chemical to kinetic freeze-out in central Au + Au collisions. The bulk properties extracted at chemical and kinetic freeze-out are observed to evolve smoothly over the measured energy range, collision systems, and collision centralities.

PHYSICAL REVIEW C 79[3], 034909, 2009

Número de citações na Web of Science:142

[E003-2009] “Azimuthal Charged-Particle Correlations and Possible Local Strong Parity Violation”

Abelev, B. I.; Aggarwal, M. M.; Ahammed, Z.; Alakhverdyants, A. V.; Anderson, B. D.; de Souza, R. D.; Takahashi, J.; Vasconcelos, G. M. S.; et al.

STAR Collaboration

Parity-odd domains, corresponding to nontrivial topological solutions of the QCD vacuum, might be created during relativistic heavy-ion collisions. These domains are predicted to lead to charge separation of quarks along the system's orbital momentum axis. We investigate a three-particle azimuthal correlator which is a P even observable, but directly sensitive to the charge separation effect. We report measurements of charged hadrons near center-of-mass rapidity with this observable in Au+Au and Cu+Cu collisions at $\sqrt{s(NN)}=200$ GeV using the STAR detector. A signal consistent with several expectations from the theory is detected. We discuss possible contributions from other effects that are not related to parity violation.

PHYSICAL REVIEW LETTERS 103[25], 251601, 2009

Número de citações na Web of Science:96

[E004-2009] “Long range rapidity correlations and jet production in high energy nuclear collisions”

Abelev, B. I.; Aggarwal, M. M.; Ahammed, Z.; Alakhverdyants, A. V.; Anderson, B. D.; de Souza, R. D.; Takahashi, J.; Vasconcelos, G. M. S.; et al.

STAR Collaboration

The STAR Collaboration at the Relativistic Heavy Ion Collider presents a systematic study of high-transverse-momentum charged-di-hadron correlations at small azimuthal pair separation $\Delta\phi$ in d+Au and central Au+Au collisions at $\sqrt{s(NN)}=200$ GeV. Significant correlated yield for pairs with large longitudinal separation $\Delta\eta$ is observed in central Au+Au collisions, in contrast to d+Au collisions. The associated yield distribution in $\Delta\eta \times \Delta\phi$ can be decomposed into a narrow jet-like peak at small angular separation which has a similar shape to that found in d+Au collisions, and a component that is narrow in $\Delta\phi$ and depends only weakly on $\Delta\eta$, the “ridge.” Using two systematically independent determinations of the background normalization and shape, finite ridge yield is found to persist for trigger $p(t) > 6$ GeV/c, indicating that it is correlated with jet production. The transverse-momentum spectrum of hadrons comprising the ridge is found to be similar to that of bulk particle production in the measured range ($2 < p(t) < 4$ GeV/c).

PHYSICAL REVIEW C 80[6], 064912, 2009

Número de citações na Web of Science:74

[E005-2009] “Topology Studies of Hydrodynamics Using Two-Particle Correlation Analysis”

Takahashi, J.; Tavares, B. M.; Qian, W. L.; Andrade, R.; Grassi, F.; Hama, Y.; Kodama, T.; Xu, N.

The effects of fluctuating initial conditions are studied in the context of relativistic heavy ion collisions where a rapidly evolving system is formed. Two-particle correlation analysis is applied to events generated with the NEXSPHERIO hydrodynamic code, starting with fluctuating nonsmooth initial conditions (IC). The results show that the nonsmoothness in the IC survives the hydroevolution and can be seen as topological features of the angular correlation function of the particles emerging from the evolving system.

A long range correlation is observed in the longitudinal direction and in the azimuthal direction a double peak structure is observed in the opposite direction to the trigger particle. This analysis provides clear evidence that these are signatures of the combined effect of tubular structures present in the IC and the proceeding collective dynamics of the hot and dense medium.

PHYSICAL REVIEW LETTERS 103[24], 242301, 2009

Número de citações na Web of Science:73

[E006-2009] “Graphene to graphane: a theoretical study”

Flores, M. Z. S.; Autreto, P. A. S.; Legoas, S. B.; Galvao, D. S.

Graphane is a two-dimensional system consisting of a single layer of fully saturated (sp³) hybridization) carbon atoms. In an ideal graphane structure C-H bonds exhibit an alternating pattern (up and down with relation to the plane defined by the carbon atoms). In this work we have investigated, using ab initio and reactive molecular dynamics simulations, the role of H frustration (breaking the H atoms' up and down alternating pattern) in graphane-like structures. Our results show that a significant percentage of uncorrelated H frustrated domains are formed in the early stages of the hydrogenation process leading to membrane shrinkage and extensive membrane corrugations. These results also suggest that large domains of perfect graphane-like structures are unlikely to be formed, as H frustrated domains are always present.

NANOTECHNOLOGY 20[46], 465704, 2009

Número de citações na Web of Science:65

[E007-2009] “Indications of Conical Emission of Charged Hadrons at the BNL Relativistic Heavy Ion Collider”

Abelev, B. I.; Aggarwal, M. M.; Ahammed, Z.; Anderson, B. D.; Arkhipkin, D.; Averichev, G. S.; de Souza, R. D.; Takahashi, J.; Vasconcelos, G. M. S.; et al.

STAR Collaboration

Three-particle azimuthal correlation measurements with a high transverse momentum trigger particle are reported for pp, d + Au, and Au + Au collisions at $\sqrt{s_{NN}} = 200$ GeV by the STAR experiment. Dijet structures are observed in pp, d + Au and peripheral Au + Au collisions. An additional structure is observed in central Au + Au data, signaling conical emission of correlated charged hadrons. The conical emission angle is found to be $\theta = 1.37 \pm 0.02(\text{stat}) \pm 0.07(\text{syst})$, independent of p perpendicular to

PHYSICAL REVIEW LETTERS 102[5], 052302, 2009

Número de citações na Web of Science:60

[E008-2009] “Limit on the diffuse flux of ultrahigh energy tau neutrinos with the surface detector of the Pierre Auger Observatory”

Abraham, J.; Abreu, P.; Aglietta, M.; Aguirre, C.; Ahn, E. J.; Allard, D.; Allekotte, I.; Allen, J.; Chinellato, J. A.; de Almeida, R. M.; de Mello, W. J. M., Jr.; Dobrigkeit, C.; Escobar, C. O.; Fauth, A. C.; Kemp, E.; Muller, M. A.; Selmi-Dei, D. P.; Peixoto, C. J. T.; et al.

Pierre Auger Collaboration

Data collected at the Pierre Auger Observatory are used to establish an upper limit on the diffuse flux of tau neutrinos in the cosmic radiation. Earth-skimming $\nu(\tau)$ may interact in the Earth's crust and produce a tau lepton by means of charged-current interactions.

The tau lepton may emerge from the Earth and decay in the atmosphere to produce a nearly horizontal shower with a typical signature, a persistent electromagnetic component even at very large atmospheric depths. The search procedure to select events induced by tau decays against the background of normal showers induced by cosmic rays is described. The method used to compute the exposure for a detector continuously growing with time is detailed. Systematic uncertainties in the exposure from the detector, the analysis, and the involved physics are discussed. No tau neutrino candidates have been found. For neutrinos in the energy range $2 \times 10^{17} \text{ eV} < E(\nu) < 2 \times 10^{19} \text{ eV}$, assuming a diffuse spectrum of the form $E(\nu)^{-2}$, data collected between 1 January 2004 and 30 April 2008 yield a 90% confidence-level upper limit of $E(\nu)^2 dN(\nu \tau)/dE(\nu) < 9 \times 10^{-8} \text{ GeV cm}^{-2} \text{ s}^{-1} \text{ sr}^{-1}$.

PHYSICAL REVIEW D 79[10], 102001, 2009

Número de citações na Web of Science:49

[E009-2009] “On the determination of the magnetic entropy change in materials with first-order transitions”

Caron, L.; Ou, Z. Q.; Nguyen, T. T.; Thanh, D. T. C.; Tegus, O.; Bruck, E.

An accurate method to determine the magnetic entropy change in materials with hysteretic first-order transitions is presented, which is needed to estimate their potential for applications. We have investigated the effect of the maximal entropy change derived from magnetization measurements performed in different measurement processes. The results show that the isothermal entropy change can be derived from the Maxwell relations even for samples with large thermal hysteresis. In the temperature region with hysteresis, over estimating the entropy change can be avoided by measuring the isothermal magnetization of the sample after it is cooled from the paramagnetic state to the measurement temperature. In this way the so-called peak effect is not observed as shown here for a few compounds.

JOURNAL OF MAGNETISM AND MAGNETIC MATERIALS 321[21], 3559-3566, 2009

Número de citações na Web of Science:45

[E010-2009] “J/psi production at high transverse momenta in p plus p and Cu plus Cu collisions at root s(NN)=200 GeV”

Abelev, B. I.; Aggarwal, M. M.; Ahammed, Z.; Anderson, B. D.; Arkhipkin, D.; Averichev, G. S.; de Souza, R. D.; Takahashi, J.; Vasconcelos, G. M. S.; et al.

STAR Collaboration

The STAR Collaboration at the Relativistic Heavy Ion Collider presents measurements of J/ψ $e^{+} e^{-}$ at midrapidity and high transverse momentum ($p_T > 5 \text{ GeV}/c$) in p + p and central Cu + Cu collisions at $\sqrt{s_{NN}} = 200 \text{ GeV}$. The inclusive J/ψ production cross section for Cu + Cu collisions is found to be consistent at high $p(T)$ with the binary collision-scaled cross section for p + p collisions. At a confidence level of 97%, this is in contrast to a suppression of J/ψ production observed at lower $p(T)$. Azimuthal correlations of J/ψ with charged hadrons in p + p collisions provide an estimate of the contribution of B-hadron decays to J/ψ production of $13\% \pm 5\%$.

PHYSICAL REVIEW C 80[4], 041902, 2009

Número de citações na Web of Science:38

Trabalhos mais citados - 2010

[E001-2012] “Non-Markovian dynamics of quantum discord”

Fanchini, F. F.; Werlang, T.; Brasil, C. A.; Arruda, L. G. E.; Caldeira, A. O.

We evaluate the quantum discord dynamics of two qubits in independent and common non-Markovian environments. We compare the dynamics of entanglement with that of quantum discord. For independent reservoirs the quantum discord vanishes only at discrete instants whereas the entanglement can disappear during a finite time interval. For a common reservoir, quantum discord and entanglement can behave very differently with sudden birth of the former but not of the latter. Furthermore, in this case the quantum discord dynamics presents sudden changes in the derivative of its time evolution which is evidenced by the presence of kinks in its behavior at discrete instants of time.

PHYSICAL REVIEW A 81[5], 052107, 2010

Número de citações na Web of Science:147

[E002-2010] “Measurement of the Depth of Maximum of Extensive Air Showers above 10(18) eV”

Abraham, J.; Abreu, P.; Aglietta, M.; Ahn, E. J.; Allard, D.; Allekotte, I.; Allen, J.; Alvarez-Muniz, J.; Chinellato, J. A.; de Almeida, R. M.; de Mello Junior, W. J. M.; Dobrigkeit, C.; Escobar, C. O.; Fauth, A. C.; Kemp, E.; Muller, M. A.; Selmi-Dei, D. P.; et al.

We describe the measurement of the depth of maximum, X_{max} , of the longitudinal development of air showers induced by cosmic rays. Almost 4000 events above 10(18) eV observed by the fluorescence detector of the Pierre Auger Observatory in coincidence with at least one surface detector station are selected for the analysis. The average shower maximum was found to evolve with energy at a rate of $(106 \pm 35-21) \text{ g/cm}^2/\text{decade}$ below 10(18.24) ± 0.05 eV, and $d24 \pm 3 \text{ g/cm}^2/\text{ecade}$ above this energy. The measured shower-to-shower fluctuations decrease from about 55 to 26 g/cm^2 . The interpretation of these results in terms of the cosmic ray mass composition is briefly discussed.

PHYSICAL REVIEW LETTERS 104[9], 091101, 2010

Número de citações na Web of Science:122

[E003-2010] “Elliptic Flow of Charged Particles in Pb-Pb Collisions at root s(NN)=2.76 TeV”

Aamodt, K.; Abelev, B.; Quintana, A. A.; Adamova, D.; Adare, A. M.; Aggarwal, M. M.; Chinellato, D. D.; Cosentino, M. R.; Takahashi, J.; et al.

ALICE Collaboration

We report the first measurement of charged particle elliptic flow in Pb-Pb collisions at $\sqrt{s(\text{NN})} = 2.76 \text{ TeV}$ with the ALICE detector at the CERN Large Hadron Collider. The measurement is performed in the central pseudorapidity region ($|\eta| < 0.8$) and transverse momentum range $0.2 < p(t) < 5.0 \text{ GeV}/c$. The elliptic flow signal $v(2)$, measured using the 4-particle correlation method, averaged over transverse momentum and pseudorapidity is $0.087 \pm 0.002(\text{stat}) \pm 0.003(\text{syst})$ in the 40%-50% centrality class. The differential elliptic flow $v(2)(p(t))$ reaches a maximum of 0.2 near $p(t) = 3 \text{ GeV}/c$. Compared to RHIC Au-Au collisions at $\sqrt{s(\text{NN})} = 200 \text{ GeV}$, the elliptic flow increases by about 30%. Some hydrodynamic model predictions which include viscous corrections are in agreement with the observed increase.

PHYSICAL REVIEW LETTERS 105[25], 252302, 2010

Número de citações na Web of Science:102

[E004-2010] “Measurement of the energy spectrum of cosmic rays above 10(18) eV using the Pierre Auger Observatory”

Abraham, J.; Abreu, P.; Aglietta, M.; Ahn, E. J.; Allard, D.; Allen, J.; Alvarez-Muniz, J.; Chinellato, J. A.; de Almeida, R. M.; de Mello Junior, W. J. M.; Dobrigkeit, C.; Escobar, C. O.; Fauth, A. C.; Kemp, E.; Muller, M. A.; Selmi-Dei, D. P.; et al.

Pierre Auger Collaboration

We report a measurement of the flux of cosmic rays with unprecedented precision and Statistics using the Pierre Auger Observatory Based on fluorescence observations in coincidence with at least one Surface detector we derive a spectrum for energies above 10(18) eV We also update the previously published energy spectrum obtained with the surface detector array The two spectra are combined addressing the systematic uncertainties and, in particular, the influence of the energy resolution on the spectral shape The spectrum can be described by a broken power law $E^{-\gamma}$ with index $\gamma = 3.3$ below the ankle which is measured at $\log_{10}(E\text{-ankle}/\text{eV}) = 18.6$ Above the ankle the spectrum is described by a power law with index 2.6 followed by a flux suppression, above about $\log_{10}(E/\text{eV}) = 19.5$, detected with high statistical significance.

PHYSICS LETTERS B 685[4-5], 239-246, 2010

Número de citações na Web of Science:97

[E005-2010] “Charged-particle multiplicity measurement in proton-proton collisions at root s=0.9 and 2.36 TeV with ALICE at LHC”

Aamodt, K.; Abel, N.; Abeysekara, U.; Quintana, A. A.; Abramyan, A.; Adamova, D.; Chinellato, D. D.; Cosentino, M. R.; Takahashi, J.; et al.

ALICE Collaboration

Charged-particle production was studied in proton-proton collisions collected at the LHC with the ALICE detector at centre-of-mass energies 0.9 TeV and 2.36 TeV in the pseudorapidity range $|\eta| < 1.4$. In the central region ($|\eta| < 0.5$), at 0.9 TeV, we measure charged-particle pseudo-rapidity density $dN(\text{ch})/d\eta = 3.02 \pm 0.01(\text{stat.}) \pm 0.05(\text{syst.})$ for inelastic interactions, and $dN(\text{ch})/d\eta = 3.58 \pm 0.01(\text{stat.}) \pm 0.12(\text{syst.})$ for non-single-diffractive interactions. At 2.36 TeV, we find $dN(\text{ch})/d\eta = 3.77 \pm 0.01(\text{stat.}) \pm 0.12(\text{syst.})$ for inelastic, and $dN(\text{ch})/d\eta = 4.43 \pm 0.01(\text{stat.}) \pm 0.17(\text{syst.})$ for non-single-diffractive collisions. The relative increase in charged-particle multiplicity from the lower to higher energy is $24.7\% \pm 0.5(\text{stat.}) \pm 2.8(\text{syst.})\%$ for inelastic and $23.7\% \pm 0.5(\text{stat.}) \pm 1.1(\text{syst.})\%$ for non-single-diffractive interactions. This increase is consistent with that reported by the CMS collaboration for non-single-diffractive events and larger than that found by a number of commonly used models. The multiplicity distribution was measured in different pseudorapidity intervals and studied in terms of KNO variables at both energies. The results are compared to proton-antiproton data and to model predictions.

EUROPEAN PHYSICAL JOURNAL C 68[1-2], 89-108, 2010

Número de citações na Web of Science:86

[E006-2010] “System-reservoir dynamics of quantum and classical correlations”

Maziero, J.; Werlang, T.; Fanchini, F. F.; Celeri, L. C.; Serra, R. M.

We examine the system-reservoir dynamics of classical and quantum correlations in the decoherence phenomenon within a two-qubit composite system interacting with two independent environments.

The most common noise channels (amplitude damping, phase damping, bit flip, bit-phase flip, and phase flip) are analyzed. By analytical and numerical analyses we find that, contrary to what is usually stated in the literature, decoherence may occur without entanglement between the system and the environment. We also show that, in some cases, the bipartite quantum correlation initially present in the system is completely evaporated and not transferred to the environments.

PHYSICAL REVIEW A 81[2], 022116, 2010

Número de citações na Web of Science:82

[E007-2010] “Charged-particle multiplicity measurement in proton-proton collisions at root s=7 TeV with ALICE at LHC”

Aamodt, K.; Abel, N.; Abeyssekara, U.; Abrahantes Q. A.; Abramyan, A.; Adamova, D.; Aggarwal, M. M.; Chinellato, D. D.; Cosentino, M. R.; Takahashi, J.; et al.

The pseudorapidity density and multiplicity distribution of charged particles produced in proton-proton collisions at the LHC, at a centre-of-mass energy $\sqrt{s} = 7$ TeV, were measured in the central pseudorapidity region $|\eta| < 1$. Comparisons are made with previous measurements at $\sqrt{s} = 0.9$ TeV and 2.36 TeV. At $\sqrt{s} = 7$ TeV, for events with at least one charged particle in $|\eta| < 1$, we obtain $dN(\text{ch})/d\eta = 6.01 \pm 0.01(\text{stat.}) - 0.12(\text{+}0.20)$ (syst.). This corresponds to an increase of $57.6\% \pm 0.4\%(\text{stat.}) - 1.8\%(\text{+}3.6)$ (syst.) relative to collisions at 0.9 TeV, significantly higher than calculations from commonly used models. The multiplicity distribution at 7 TeV is described fairly well by the negative binomial distribution.

EUROPEAN PHYSICAL JOURNAL C 68[3-4], 345-354, 2010

Número de citações na Web of Science:73

[E008-2010] “Charged-Particle Multiplicity Density at Midrapidity in Central Pb-Pb Collisions at root s(NN)=2.76 TeV”

Aamodt, K.; Abelev, B.; Quintana, A.A.; Adamova, D.; Adare, A. M.; Aggarwal, M. M.; Chinellato, D. D.; Cosentino, M. R.; Takahashi, J.; et al.

ALICE Collaboration

The first measurement of the charged-particle multiplicity density at midrapidity in Pb-Pb collisions at a center-of-mass energy per nucleon pair $\sqrt{s(\text{NN})} = 2.76$ TeV is presented. For an event sample corresponding to the most central 5% of the hadronic cross section, the pseudorapidity density of primary charged particles at midrapidity is $1584 \pm 4(\text{stat}) \pm 76(\text{syst})$, which corresponds to $8.3 \pm 0.4(\text{syst})$ per participating nucleon pair. This represents an increase of about a factor 1.9 relative to pp collisions at similar collision energies, and about a factor 2.2 to central Au-Au collisions at $\sqrt{s(\text{NN})} = 0.2$ TeV. This measurement provides the first experimental constraint for models of nucleus-nucleus collisions at LHC energies.

PHYSICAL REVIEW LETTERS 105[25], 252301, 2010

Número de citações na Web of Science:69

[E009-2010] “First proton-proton collisions at the LHC as observed with the ALICE detector: measurement of the charged-particle pseudorapidity density at root s=900 GeV”

Aamodt, K.; Abel, N.; Abeyssekara, U.; Quintana, A.A.; Acero, A.; Adamova, D.; Aggarwal, M.M.; Chinellato, D. D.; Cosentino, M. R.; Valdivieso, G. D.; Tavares, B. M.; Takahashi, J.; et al.

ALICE Collaboration

On 23rd November 2009, during the early commissioning of the CERN Large Hadron Collider (LHC), two counter-rotating proton bunches were circulated for the first time concurrently in the machine, at the LHC injection energy of 450 GeV per beam. Although the proton intensity was very low, with only one pilot bunch per beam, and no systematic attempt was made to optimize the collision optics, all LHC experiments reported a number of collision candidates. In the ALICE experiment, the collision region was centred very well in both the longitudinal and transverse directions and 284 events were recorded in coincidence with the two passing proton bunches. The events were immediately reconstructed and analyzed both online and offline. We have used these events to measure the pseudorapidity density of charged primary particles in the central region. In the range vertical bar eta vertical bar < 0.5, we obtain $dN(\text{ch})/d\eta = 3.10 \pm 0.13(\text{stat.}) \pm 0.22(\text{syst.})$ for all inelastic interactions, and $dN(\text{ch})/d\eta = 3.51 \pm 0.15(\text{stat.}) \pm 0.25(\text{syst.})$ for nonsingle diffractive interactions. These results are consistent with previous measurements in proton-antiproton interactions at the same centre-of-mass energy at the CERN Sp(p)over bar>S collider. They also illustrate the excellent functioning and rapid progress of the LHC accelerator, and of both the hardware and software of the ALICE experiment, in this early start-up phase.

EUROPEAN PHYSICAL JOURNAL C 65[1-2], 111-125, 2010

Número de citações na Web of Science:67

[E010-2010] “Update on the correlation of the highest energy cosmic rays with nearby extragalactic matter”

Abreu, P.; Aglietta, M.; Ahn, E. J.; Allard, D.; Allekotte, I.; Allen, J.; Castillo, J. A.; Chinellato, J. A.; de Almeida, R. M.; de Mello Junior, W. J. M.; Dobrigkeit, C.; Escobar, C. O.; Fauth, A. C.; Kemp, E.; Muller, M. A.; Selmi-Dei, D. P.; et al.

Pierre Auger Collaboration

Data collected by the Pierre Auger Observatory through 31 August 2007 showed evidence for anisotropy in the arrival directions of cosmic rays above the Greisen-Zatsepin-Kuz'min energy threshold, 6×10^{19} eV. The anisotropy was measured by the fraction of arrival directions that are less than 3.1 degrees from the position of an active galactic nucleus within 75 Mpc (using the Veron-Cetty and Veron 12th catalog). An updated measurement of this fraction is reported here using the arrival directions of cosmic rays recorded above the same energy threshold through 31 December 2009. The number of arrival directions has increased from 27 to 69, allowing a more precise measurement. The correlating fraction is $(38(-6)(+7))\%$, compared with 21% expected for isotropic cosmic rays. This is down from the early estimate of $(69(-+11)(13))\%$. The enlarged set of arrival directions is examined also in relation to other populations of nearby extragalactic objects: galaxies in the 2 Microns All Sky Survey and active galactic nuclei detected in hard X-rays by the Swift Burst Alert Telescope. A celestial region around the position of the radiogalaxy Cen A has the largest excess of arrival directions relative to isotropic expectations. The 2-point autocorrelation function is shown for the enlarged set of arrival directions and compared to the isotropic expectation.

ASTROPARTICLE PHYSICS 34[5], 314-326, 2010

Número de citações na Web of Science:64

Trabalhos mais citados - 2011

[E001-2011] “Suppression of charged particle production at large transverse momentum in central Pb-Pb collisions at root s(NN)=2.76 TeV”

Aamodt, K.; Quintana, A. A.; Adamova, D.; Adare, A. M.; Aggarwal, M. M.; Rinella, G. A.; Chinellato, D. D.; Cosentino, M. R.; Takahashi, J.; et al.

ALICE Collaboration

Inclusive transverse momentum spectra of primary charged particles in Pb-Pb collisions at root s(NN) = 2.76 TeV have been measured by the ALICE Collaboration at the LHC. The data are presented for central and peripheral collisions, corresponding to 0-5% and 70-80% of the hadronic Pb-Pb cross section. The measured charged particle spectra in $|\eta| < 0.8$ and $0.3 < p(T) < 20$ GeV/c are compared to the expectation in pp collisions at the same root s(NN), scaled by the number of underlying nucleon-nucleon collisions. The comparison is expressed in terms of the nuclear modification factor R-AA. The result indicates only weak medium effects (R-AA approximate to 0.7) in peripheral collisions. In central collisions, R-AA reaches a minimum of about 0.14 at $p(T) = 6-7$ GeV/c and increases significantly at larger p(T). The measured suppression of high-p(T) particles is stronger than that observed at lower collision energies, indicating that a very dense medium is formed in central Pb-Pb collisions at the LHC.

PHYSICS LETTERS B 696[1-2], 30-39, 2011

Número de citações na Web of Science:114

[E002-2011] “Laser cooling of a nanomechanical oscillator into its quantum ground state”

Chan, J.; Alegre, T.P.M.; Safavi-Naeini, A.H.; Hill, J.T.; Krause, A.; Groblacher, S.; Aspelmeyer, M.; Painter, O.

The simple mechanical oscillator, canonically consisting of a coupled mass-spring system, is used in a wide variety of sensitive measurements, including the detection of weak forces(1) and small masses(2). On the one hand, a classical oscillator has a well-defined amplitude of motion; a quantum oscillator, on the other hand, has a lowest-energy state, or ground state, with a finite-amplitude uncertainty corresponding to zero-point motion. On the macroscopic scale of our everyday experience, owing to interactions with its highly fluctuating thermal environment a mechanical oscillator is filled with many energy quanta and its quantum nature is all but hidden. Recently, in experiments performed at temperatures of a few hundredths of a kelvin, engineered nanomechanical resonators coupled to electrical circuits have been measured to be oscillating in their quantum ground state(3,4). These experiments, in addition to providing a glimpse into the underlying quantum behaviour of mesoscopic systems consisting of billions of atoms, represent the initial steps towards the use of mechanical devices as tools for quantum metrology(5,6) or as a means of coupling hybrid quantum systems(7-9). Here we report the development of a coupled, nanoscale optical and mechanical resonator(10) formed in a silicon microchip, in which radiation pressure from a laser is used to cool the mechanical motion down to its quantum ground state (reaching an average phonon occupancy number of 0.85 ± 0.08). This cooling is realized at an environmental temperature of 20 K, roughly one thousand times larger than in previous experiments and paves the way for optical control of mesoscale mechanical oscillators in the quantum regime.

NATURE 478[7367], 89-92, 2011

Número de citações na Web of Science:95

[E003-2011] “Improved Search for Muon-Neutrino to Electron-Neutrino Oscillations in MINOS”

Adamson, P.; Auty, D. J.; Coelho, J. A. B.; Escobar, C. O.; et al.

We report the results of a search for $\nu(e)$ appearance in a $\nu(\mu)$ beam in the MINOS long-baseline neutrino experiment. With an improved analysis and an increased exposure of 8.2×10^{20} protons on the NuMI target at Fermilab, we find that $2\sin(2)(\theta_{23})\sin(2)(2\theta_{13}) < 0.12(0.20)$ at 90% confidence level for $\delta = 0$ and the normal (inverted) neutrino mass hierarchy, with a best-fit of $2\sin(2)(\theta_{23})\sin(2)(2\theta_{13}) = 0.041(-0.031)(+0.047)(0.079(-0.053)(+0.071))$. The $\theta_{13} = 0$ hypothesis is disfavored by the MINOS data at the 89% confidence level.

PHYSICAL REVIEW LETTERS 107[18], 181802, 2011

Número de citações na Web of Science:89

[E004-2011] “Higher Harmonic Anisotropic Flow Measurements of Charged Particles in Pb-Pb Collisions at root s(NN)=2.76 TeV”

Aamodt, K.; Abelev, B.; Quintana, A.A.; Adamova, D.; Adare, A. M.; Chinellato, D. D.; Cosentino, M. R.; Takahashi, J.; et al.

ALICE Collaboration

We report on the first measurement of the triangular $\nu(3)$, quadrangular $\nu(4)$, and pentagonal $\nu(5)$ charged particle flow in Pb-Pb collisions at root s(NN) = 2.76 TeV measured with the ALICE detector at the CERN Large Hadron Collider. We show that the triangular flow can be described in terms of the initial spatial anisotropy and its fluctuations, which provides strong constraints on its origin. In the most central events, where the elliptic flow $\nu(2)$ and $\nu(3)$ have similar magnitude, a double peaked structure in the two-particle azimuthal correlations is observed, which is often interpreted as a Mach cone response to fast partons. We show that this structure can be naturally explained from the measured anisotropic flow Fourier coefficients.

PHYSICAL REVIEW LETTERS 107[3], 032301, 2011

Número de citações na Web of Science:73

[E005-2011] “Centrality Dependence of the Charged-Particle Multiplicity Density at Midrapidity in Pb-Pb Collisions at root s(NN)=2.76 TeV”

Aamodt, K.; Quintana, A.A.; Adamova, D.; Adare, A. M.; Aggarwal, M. M.; Rinella, G.A.; Chinellato, D. D.; Cosentino, M. R.; Takahashi, J.; et al.

ALICE Collaboration

The centrality dependence of the charged-particle multiplicity density at midrapidity in Pb-Pb collisions at root s(NN) = 2.76 TeV is presented. The charged-particle density normalized per participating nucleon pair increases by about a factor of 2 from peripheral (70%-80%) to central (0%-5%) collisions. The centrality dependence is found to be similar to that observed at lower collision energies. The data are compared with models based on different mechanisms for particle production in nuclear collisions.

PHYSICAL REVIEW LETTERS 106[3], 032301, 2011

Número de citações na Web of Science:57

[E006-2011] “Measurement of the Neutrino Mass Splitting and Flavor Mixing by MINOS”

Adamson, P.; Andreopoulos, C.; Armstrong, R.; Auty, D. J.; Ayres, D. S.; Backhouse, C. Coelho, J. A. B.; Escobar, C. O.; et al.

MINOS Collaboration

Measurements of neutrino oscillations using the disappearance of muon neutrinos from the Fermilab NuMI neutrino beam as observed by the two MINOS detectors are reported. New analysis methods have been applied to an enlarged data sample from an exposure of 7.25×10^{20} protons on target. A fit to neutrino oscillations yields values of Δm^2 vertical bar = $(2.32(-0.08)(+0.12) \times 10^{-3}) \text{ eV}^2$ for the atmospheric mass splitting and $\sin^2(2\theta) > 0.90$ (90% C.L.) for the mixing angle. Pure neutrino decay and quantum decoherence hypotheses are excluded at 7 and 9 standard deviations, respectively.

PHYSICAL REVIEW LETTERS 106[18], 181801, 2011

Número de citações na Web of Science:53

[E007-2011] “Conservation law for distributed entanglement of formation and quantum discord”

Fanchini, F. F.; Cornelio, M. F.; de Oliveira, M. C.; Caldeira, A. O.

We present a direct relation, based upon a monogamic principle, between entanglement of formation (EOF) and quantum discord (QD), showing how they are distributed in an arbitrary tripartite pure system. By extending it to a paradigmatic situation of a bipartite system coupled to an environment, we demonstrate that the EOF and the QD obey conservation relation. By means of this relation we show that in the deterministic quantum computer with one pure qubit the protocol has the ability to rearrange the EOF and the QD, which implies that quantum computation can be understood on a different basis as a coherent dynamics where quantum correlations are distributed between the qubits of the computer. Furthermore, for a tripartite mixed state we show that the balance between distributed EOF and QD results in a stronger version of the strong subadditivity of entropy.

PHYSICAL REVIEW A 84[1], 012313, 2011

Número de citações na Web of Science:46

[E008-2011] “Two-pion Bose-Einstein correlations in central Pb-Pb collisions at $\sqrt{s_{NN}}=2.76 \text{ TeV}$ ”

Aamodt, K.; Quintana, A. A.; Adamova, D.; Adare, A. M.; Aggarwal, M. M.; Chinellato, D. D.; Cosentino, M. R.; Takahashi, J.; et al.

ALICE Collaboration

The first measurement of two-pion Bose-Einstein correlations in central Pb-Pb collisions at $\sqrt{s_{NN}} = 2.76 \text{ TeV}$ at the Large Hadron Collider is presented. We observe a growing trend with energy now not only for the longitudinal and the outward but also for the sideward pion source radius. The pion homogeneity volume and the decoupling time are significantly larger than those measured at RHIC.

PHYSICS LETTERS B 696[4], 328-337, 2011

Número de citações na Web of Science:38

[E009-2011] “Entanglement Irreversibility from Quantum Discord and Quantum Deficit”

Cornelio, M. F.; de Oliveira, M. C.; Fanchini, F. F.

We relate the problem of irreversibility of entanglement with the recently defined measures of quantum correlation-quantum discord and one-way quantum deficit. We show that the entanglement of formation is always strictly larger than the coherent information and the entanglement cost is also larger in most cases. We prove irreversibility of entanglement under local operations and classical communication for a family of entangled states. This family is a generalization of the maximally correlated states for which we also give an analytic expression for the distillable entanglement, the relative entropy of entanglement, the distillable secret key, and the quantum discord.

PHYSICAL REVIEW LETTERS 107[1], 020502, 2011

Número de citações na Web of Science:30

[E010-2011] “First Direct Observation of Muon Antineutrino Disappearance”

Adamson, P.; Andreopoulos, C.; Auty, D. J.; Ayres, D. S.; Backhouse, C.; Coelho, J. A. B.; Escobar, C. O.; et al.

MINOS Collaboration

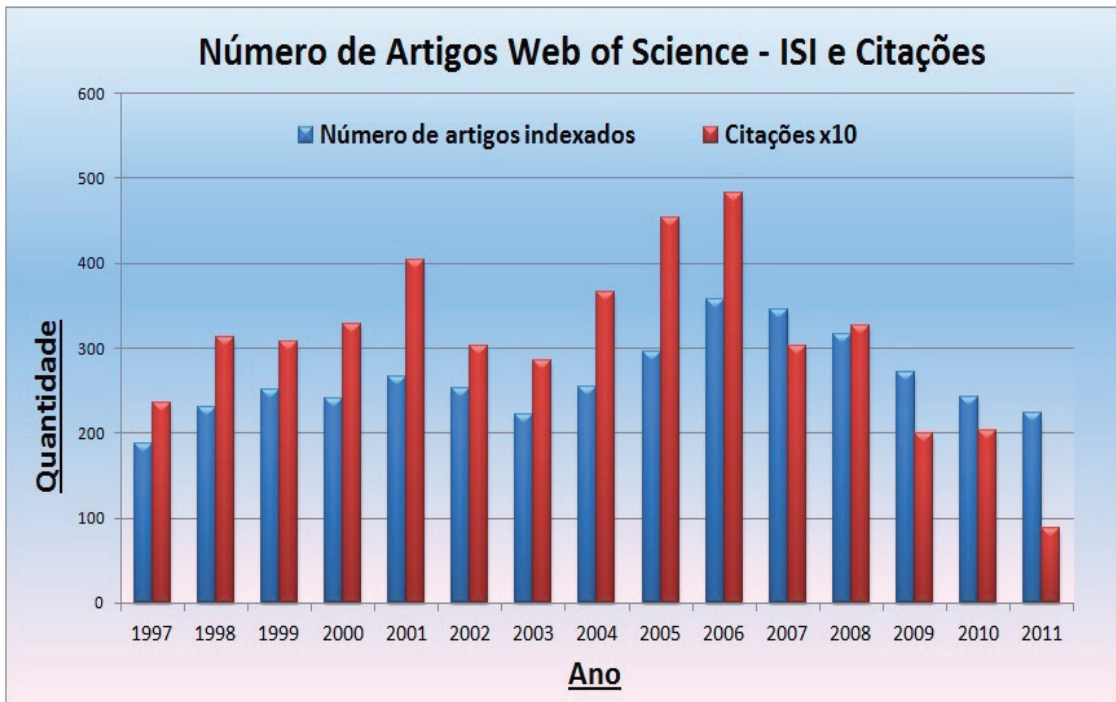
This Letter reports the first direct observation of muon antineutrino disappearance. The MINOS experiment has taken data with an accelerator beam optimized for (ν) over bar (μ) production, accumulating an exposure of 1.71×10^{20} protons on target. In the Far Detector, 97 charged current (ν) over bar (μ) events are observed. The no-oscillation hypothesis predicts 156 events and is excluded at 6.3 sigma. The best fit to oscillation yields Δm^2 over bar (2) vertical bar = $[3.36(-0.40)(+0.46)(\text{stat}) \pm 0.06(\text{sys})] \times 10^{-3} \text{ eV}^2$, $\sin^2(2\theta)$ over bar = $0.86(-0.12)(+0.11)(\text{stat}) \pm 0.01(\text{syst})$. The MINOS $\nu(\mu)$ and (ν) over bar (μ) measurements are consistent at the 2.0% confidence level, assuming identical underlying oscillation parameters.

PHYSICAL REVIEW LETTERS 107[1], 021801, 2011

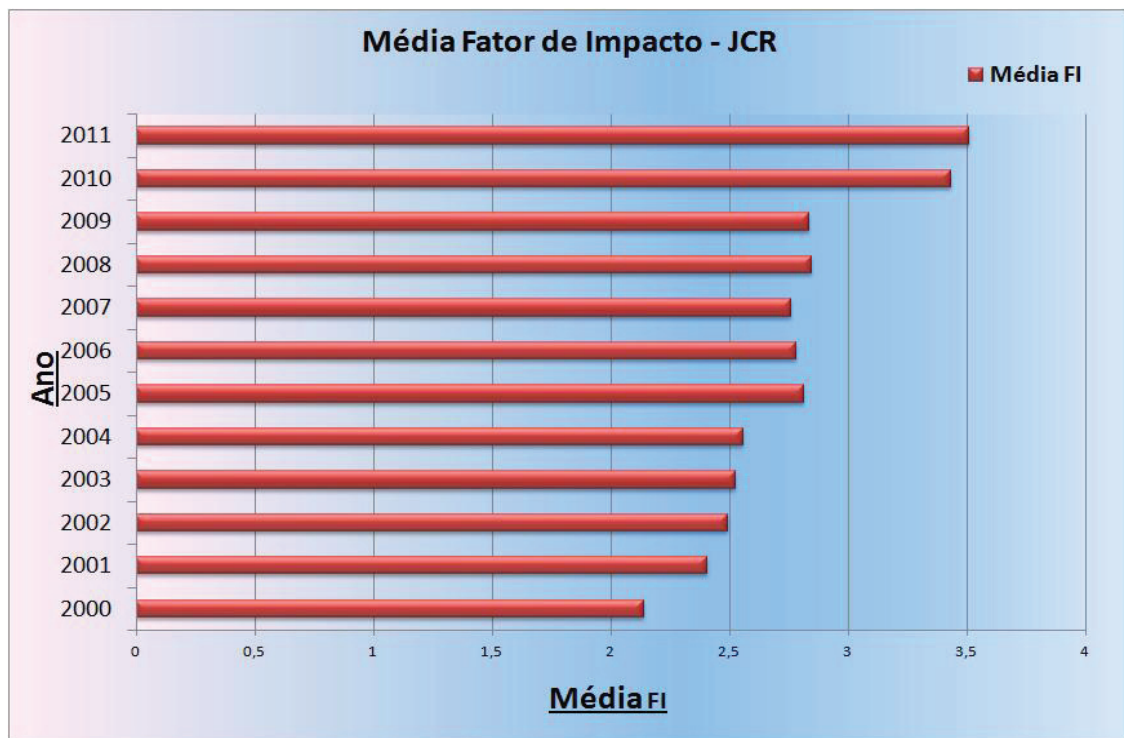
Número de citações na Web of Science:23

Observação: O número de citações se refere às pesquisas realizadas nos meses de setembro e outubro/2012. A base utilizada como fonte para as pesquisas mantém atualização diária e os números mudam constantemente. Dessa forma, considere como referência os meses citados.

Número de Artigos e citações nos últimos 15 anos de publicações IFGW



Média do Fator de Impacto - JCR das publicações IFGW de 2000 à 2011



Abstracta

15 anos informando você!

* Acesse o portal Abstracta <<http://abstracta.ifi.unicamp.br>> e faça seu cadastro como Leitor para receber as novidades de cada novo número publicado.

Abstracta

Instituto de Física

Diretor: Prof. Dr. Daniel Pereira

Diretor Associado: Prof. Dr. Newton Cesario Frateschi

Universidade Estadual de Campinas - UNICAMP

Cidade Universitária Zeferino Vaz

13083-859 - Campinas - SP - Brasil

e-mail: secdir@ifi.unicamp.br

Fone: OXX 19 3521-5300

Publicação

Biblioteca do Instituto de Física Gleb Wataghin
<http://portal.ifi.unicamp.br/biblioteca>

Diretora Técnica: Sandra Maria Carlos Cartaxo
Coordenador da Comissão de Biblioteca: Prof. Dr. André Koch Torres de Assis

Elaboração
Maria Graciele Trevisan (Bibliotecária)
graciele@ifi.unicamp.br

Projeto Gráfico
ÍgneaDesign

Impressão: Gráfica Central - Unicamp